

IMPROVING NDE CAPABILITY THROUGH MULTIPLE
INSPECTION WITH APPLICATION TO GAS TURBINE
ENGINE DISKS

Jann N. Yang
Robert C. Donath
Metals Behavior Branch
Metals and Ceramics Division

June 1983

Final Report for Period February 1982-August 1982

Approved for public release; distribution unlimited.



MATERIALS LABORATORY
AIR FORCE WRIGHT AERONAUTICAL LABORATORIES
AIR FORCE SYSTEMS COMMAND
WRIGHT-PATTERSON AIR FORCE BASE, OHIO 45433

83 08 22 05 9

ADA131762

DTIC FILE COPY

NOTICE

When Government drawings, specifications, or other data are used for any purpose other than in connection with a definitely related Government procurement operation, the United States Government thereby incurs no responsibility nor any obligation whatsoever; and the fact that the government may have formulated, furnished, or in any way supplied the said drawings, specifications, or other data, is not to be regarded by implication or otherwise as in any manner licensing the holder or any other person or corporation, or conveying any rights or permission to manufacture, use, or sell any patented invention that may in any way be related thereto.

This report has been reviewed by the Office of Public Affairs (ASD/PA) and is releasable to the National Technical Information Service (NTIS). At NTIS, it will be available to the general public, including foreign nations.

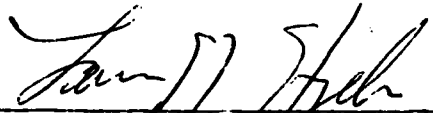
This technical report has been reviewed and is approved for publication.



ROBERT C. DONATH
Metals Behavior Branch
Metals and Ceramics Division



JOHN P. HENDERSON
Chief, Metals Behavior Branch
Metals and Ceramics Division



LAWRENCE N. HJELM, Asst Chief
Metals and Ceramics Division
Materials Laboratory

"If your address has changed, if you wish to be removed from our mailing list, or if the addressee is no longer employed by your organization please notify AFWAL/NLLN, W-PAFB, OH 45433 to help us maintain a current mailing list".

Copies of this report should not be returned unless return is required by security considerations, contractual obligations, or notice on a specific document.

UNCLASSIFIED

SECURITY CLASSIFICATION OF THIS PAGE (When Data Entered)

REPORT DOCUMENTATION PAGE		READ INSTRUCTIONS BEFORE COMPLETING FORM
1. REPORT NUMBER AFWAL-TR-82-4111	2. GOVT ACCESSION NO. AD A13 762	3. RECIPIENT'S CATALOG NUMBER
4. TITLE (and Subtitle) IMPROVING NDE CAPABILITY THROUGH MULTIPLE INSPECTION WITH APPLICATION TO GAS TURBINE ENGINE DISKS		5. TYPE OF REPORT & PERIOD COVERED February - August 1982
7. AUTHOR(s) J.N. Yang and R.C. Donath		6. PERFORMING ORG. REPORT NUMBER
9. PERFORMING ORGANIZATION NAME AND ADDRESS Air Force Wright Aeronautical Laboratories MLLN Wright-Patterson Air Force Base, OH 45433		8. CONTRACT OR GRANT NUMBER(s)
11. CONTROLLING OFFICE NAME AND ADDRESS Materials Laboratory Air Force Wright Aeronautical Laboratories Wright-Patterson Air Force Base, Ohio 45433		10. PROGRAM ELEMENT, PROJECT, TASK AREA & WORK UNIT NUMBERS 2307P102 641225
14. MONITORING AGENCY NAME & ADDRESS (if different from Controlling Office)		12. REPORT DATE June 1983
		13. NUMBER OF PAGES 96
		15. SECURITY CLASS. (of this report) UNCLASSIFIED
		15a. DECLASSIFICATION/DOWNGRADING SCHEDULE
16. DISTRIBUTION STATEMENT (of this Report) Approved for public release; distribution unlimited.		
17. DISTRIBUTION STATEMENT (of the abstract entered in Block 20, if different from Report)		
18. SUPPLEMENTARY NOTES → Current + non-destructive evaluation (NDE) →		
19. KEY WORDS (Continue on reverse side if necessary and identify by block number) Non-destructive evaluation Probability of crack detection NDE reliability Theory of multiple inspections Retirement-for-cause Gas turbine engine NDE reliability for engine disk Multiple inspections for engine disk		
20. ABSTRACT (Continue on reverse side if necessary and identify by block number) Current NDE techniques are not capable of repeatedly producing correct indications when applied to flaws of the same length. As a result, the probability of detection (POD) for all cracks of a given length has been used to define the capability of a particular NDE system in a given environment. Thus the NDE reliability consists of two types of errors: Type I and Type II. → For safety-critical components in airframe structures, Type I error is of major concern. According to the damage tolerant requirement, the inspection limit or the reset		

UNCLASSIFIED

SECURITY CLASSIFICATION OF THIS PAGE(When Data Entered)

crack size a_{NDE} should be the crack length associated with a 90% detection probability and 95% confidence level. On the other hand ~~however~~ the main criterion used for the analysis of the Retirement-For-Cause (RFC) of gas turbine engine components is the minimization of the life cycle cost (LCC). Hence, both Type I and Type II errors are of practical importance.

While it is possible to reduce the Type I error by increasing the value of a_{NDE} or to reduce the Type II error by decreasing the a_{NDE} value, it is impossible to improve one type of error without an adverse effect on the other type of error in a single inspection procedure. There are circumstances in which the critical crack size is so small that the required a_{NDE} value with high levels of detection probability and confidence may not be achieved by an NDE system. It is also conceivable that a given NDE system at the depot level may not be able to reduce the life cycle cost (because of Type II error) such that it may be more economical to just replace the component without an inspection. In order to circumvent those difficulties, the possible application of multiple inspections is studied in the present report.

The objectives of this report are to: (i) formulate and derive mathematically the resulting POD curve for multiple inspection systems; (ii) investigate quantitatively the benefit and advantage of multiple inspection procedures; (iii) establish the direction in which the NDE capability should be improved under certain mission requirements; (iv) establish the strategy and sequence for multiple inspection procedures to reduce either Type I error or Type II errors or both; (v) determine the POD curve for a disk from the POD curve of an NDE system; (vi) determine the inspection reliability of engine disks; and (vii) evaluate the benefit of multiple inspections for engine disks. Using currently available eddy-current NDE capability, it is demonstrated that both Type I error and Type II error can be significantly reduced simultaneously by the use of multiple inspection procedures. Examples are given to illustrate the proposed multiple inspection approach. A significant impact of multiple inspections on the inspection reliability of engine disks is demonstrated.

UNCLASSIFIED

SECURITY CLASSIFICATION OF THIS PAGE(When Data Entered)

FOREWORD

This report was prepared by the Metals Behavior Branch, Metals and Ceramics Division, Materials Laboratory, Air Force Wright Aeronautical Laboratories, Wright-Patterson Air Force Base, Ohio. The research reported herein was conducted under Project No. 2307, "Solid Mechanics," Task 2307P102, "Failure Prediction in Metals." Professor J. N. Yang was engaged as a visiting scientist from the School of Engineering and Applied Science, The George Washington University, Washington, D.C., 20052.

The idea of multiple inspection procedures and its potential payoffs was proposed by Dr. W. H. Reimann. Valuable and helpful discussions with Messrs. T. Cooper and D. M. Forney and with Drs. T. Nicholas and J. Moyzis are gratefully acknowledged.

This report covers research conducted during the period February 1982 to August 1982.

Accession For	
NTIS GRA&I	<input checked="" type="checkbox"/>
DTIC TAB	<input type="checkbox"/>
Unannounced	<input type="checkbox"/>
Justification	
Distribution	
Availability Codes	
Avail and/or	
Dist	Notes
A	



TABLE OF CONTENTS

SECTION	PAGE
I. INTRODUCTION	1
II. THEORY OF MULTIPLE INSPECTIONS	7
1. Union Rule	8
2. Intersection Rule	10
3. Combination Rule for Three Inspections	10
4. Inspection Sequence for Minimum Number and Cost of Inspections	14
5. Correlated Multiple Inspections	15
6. Applications of Independent Inspections	16
7. Type I and Type II Errors	16
8. Distribution of Pre-Inspection Flaw Length	18
III. NUMERICAL EXAMPLES	19
1. Example No. 1	19
2. Example No. 2	23
IV. INSPECTION RELIABILITY OF ENGINE DISKS	34
1. Completely Correlated Crack Length	36
2. Example No. 3	38
a. Exponential POD Function	38
b. Weibull POD Function	41
c. Exponential POD Function with a Lower Bound	43
d. Narrow-Banded Weibull POD Function	45
e. Conclusions	45
3. Totally Uncorrelated Crack Length	47
4. Example No. 4	51
a. Various POD Functions	51
b. Conclusions	56
V. MULTIPLE INSPECTIONS FOR ENGINE DISKS	57
1. Totally Correlated Flaw Length	57
2. Totally Uncorrelated Flaw Length	58
3. Numerical Examples	60
a. Examples for Totally Correlated Flaw Length	60
b. Examples for Totally Uncorrelated Flaw Length	62
4. Concluding Remarks	63

TABLE OF CONTENTS (Concluded)

SECTION	PAGE
VI. INSPECTION RELIABILITY OF ENGINE DISKS USING P&W POD CURVE	65
VII. CONCLUSIONS AND DISCUSSION	77
APPENDIX A: MULTIPLE INSPECTIONS WITH CORRELATED NDE SYSTEMS	81
APPENDIX B: EXPERIMENTAL PROCEDURES FOR ESTABLISHING CONDITIONAL POD CURVE	84
REFERENCES	85

LIST OF ILLUSTRATIONS

FIGURE		PAGE
1	POD Curves for Various NDE Systems.	2
2	Fracture Mechanics Residual Life N_f and Return to Service Interval N_R .	3
3	Type I and Type II Errors; (a) Small a_{NDE} , (b) Large a_{NDE} and (c) Ideal NDE System.	5
4	Rejected Components Shown in Shaded Areas.	8
5	Inspection Procedure for Two NDE Systems with Union Rule.	9
6	Inspection Procedure for Two NDE Systems with Intersection Rule.	11
7	Inspection Procedure for Three NDE Systems with Union-Intersection Rule.	13
8	Eddy Current Inspections of Skin and Stringer Wing Assembly, 60 Inspections Per Fastener Hole (from References 3 and 8).	20
9	Resulting POD Curves Under Multiple Inspections; (a) Union Rule and (b) Union-Intersection Rule.	21
10	Optimized Probability Method - 361 Eddy Current Inspections of Etched Fatigue Cracks in 2219-T87 Aluminum Plates (from Reference 2).	24
11	POD Curves (1 and 2) and Resulting POD Curves Using the Union Rule.	25
12	POD Curves for the Third Inspection System $POD(a;3)$.	28
13(a)	Resulting POD Curves Under Three Inspections Using the Union-Intersection Rule: (a) $POD[a;(1U2)\Omega 3]$, Weibull $POD(a;3)$.	29
13(b)	Resulting POD Curves Under Three Inspections Using the Union-Intersection Rule: (b) $POD[a;(1U2)\Omega 3]$, Straight Line $POD(a;3)$.	29
13(c)	Resulting POD Curves Under Three Inspections Using the Union-Intersection Rule: (c) $POD[a;(1U1)\Omega 3]$, Weibull $POD(a;3)$.	30
13(d)	Resulting POD Curves Under Three Inspections Using the Union-Intersection Rule: (d) $POD[a;(1U1)\Omega 3]$, Straight Line $POD(a;3)$.	30
14	POD Curves for NDE Systems (Curves 1 and 2) and Resulting POD Curve (Curve 3) Under Multiple Inspections.	32

LIST OF ILLUSTRATIONS (Concluded)

FIGURE		PAGE
15	Schematic Distribution of Flaw Length in Bolt Holes; (a) Totally Correlated Crack Length and (b) Totally Uncorrelated Crack Length.	35
16	Exponential POD Curves for the NDE System and Disk.	40
17	Weibull POD Curves for the NDE System and Disk.	42
18	Exponential POD Curves with Lower Bound at 1 mm for the NDE System and Disk.	44
19	Narrow-Banded Weibull POD Curves for the NDE System and Disk.	46
20	Schematic Description of Type I and Type II Errors for Independent Flaw Length.	49
21	Distributions of Pre-inspection Flaw Length for Bolt Hole and Disk; $\lambda = 0.7/\text{mm}$.	51
22	Distribution of Pre-inspection Flaw Length for Bolt Hole and Disk; $\lambda = 1.0/\text{mm}$.	55
23	Procedures for Two Inspections for Disks.	59
24	POD Curve for Second Turbine Disk Radial Cooling Hole.	66
25	Probability Density Functions of Pre-inspection Flaw Length with 100% Coefficient of Variation.	68
26	Lognormal Probability Density Function for Pre-inspection Flaw Length with 50% Coefficient of Variation.	75
27	Procedures for Establishing Conditional POD Curve.	84

LIST OF TABLES

TABLE		PAGE
1	Type I and Type II Errors; $a_{NDE} = 12.4 \text{ mm}$, $P_G = 91.63\%$.	22
2	Type I and Type II Errors; $\beta_1 = 0.46/\text{mm}$, $\beta_2 = 0.198/\text{mm}$, $a_{NDE} = 5 \text{ mm}$, $P_G = 97\%$.	27
3	Type I and Type II Errors; $\beta_1 = 0.46/\text{mm}$, $\beta_2 = 0.46/\text{mm}$, $a_{NDE} = 5 \text{ mm}$, $P_G = 97\%$.	27
4	Type I and Type II Errors; $\beta_1 = 0.46/\text{mm}$, $\beta_2 = 0.46/\text{mm}$, $a_{NDE} = 3.5 \text{ mm}$, $P_G = 91.4\%$.	31
5	Type I and Type II Errors; $\beta_1 = 0.46/\text{mm}$, $\beta_2 = 0.46/\text{mm}$, $a_0 = 1.5 \text{ mm}$, $a_{NDE} = 5 \text{ mm}$.	33
6	Type I and Type II Errors for Disk; Exponential POD Curve with $\beta_1 = 0.46/\text{mm}$.	40
7	Type I and Type II Errors for Disk: Weibull POD Curve with $\alpha_0 = 3.0$, $\beta_0 = 3.79/\text{mm}$.	42
8	Type I and Type II Errors: Exponential POD Curve with Lower Bound at $a_0 = 1 \text{ mm}$, $\beta_1 = 0.46/\text{mm}$.	44
9	Type I and Type II Errors: Narrow-Banded Weibull POD Curve with $\alpha_0 = 8.0$, $\beta_0 = 2.48/\text{mm}$.	46
10	Type I and Type II Errors for Totally Uncorrelated Crack Length; Exponential POD Curve with $\beta_1 = 0.46/\text{mm}$ and $\lambda = 0.7/\text{mm}$.	52
11	Type I and Type II Errors for Totally Uncorrelated Crack Length with $\lambda = 1.0/\text{mm}$.	55
12	Type I and Type II Error for Totally Uncorrelated Crack Length with $\lambda = 1.0/\text{mm}$ and Narrow-Banded Weibull-Type POD Curve for $\alpha_0 = 8.0$ and $\beta_0 = 4.13 \text{ mm}$.	56
13	Type I and Type II Errors for Totally Correlated Crack Length Using Two Inspections; $\lambda = 0.7/\text{mm}$, $\beta_1 = 0.46/\text{mm}$, $\alpha = 8.0$, $\beta = 4.13 \text{ mm}$.	61

LIST OF TABLES (Concluded)

TABLE		PAGE
14	Type I and Type II Errors for Totally Correlated Crack Length Using Two Inspections: $\lambda = 0.7/\text{mm}$, $\alpha_0 = 3.0$, $\beta_0 = 3.79 \text{ mm}$, $\alpha = 8.0$, $\beta = 4.13 \text{ mm}$.	62
15	Type I and Type II Errors for Totally Uncorrelated Crack Length Using Two Inspections; $\lambda = 1.0 \text{ mm}$, $\alpha = 8.0$, $\beta = 4.13 \text{ mm}$.	63
16	Type I and Type II Errors for Disk Using P&W POD Curve and Average Flaw Length 1.429 mils ($\lambda=0.71 \text{ mil}$); Exponential Distribution for Pre-inspection Flaw Length, + Totally Correlated Flaw Length, ++ Totally Independent Flaw Length.	69
17	Type I and Type II Errors for Disk Using P&W POD Curve and Average Flaw Length 2.0 mils ($\lambda=0.2/\text{mil}$); Exponential Distribution for Pre-inspection Flaw Length, + Totally Correlated Flaw Length, ++ Totally Independent Flaw Length.	70
18	Type I and Type II Errors for Disk Using P&W POD Curve and Median Flaw Length 1.045 mils ($\mu=0.019$); Lognormal Distribution for Pre-inspection Flaw Length, + Totally Correlated Flaw Length, ++ Totally Independent Flaw Length.	72
19	Type I and Type II Errors for Disk Using P&W POD Curve and Median Flaw Length 1.57 mils ($\mu=0.1963$); Lognormal Distribution for Pre-inspection Flaw Length, + Totally Correlated Flaw Length, ++ Totally Independent Flaw Length.	73
20	Type I and Type II Errors for Disks Using P&W POD Curve and Median Flaw Length 2.06 mils ($\mu=0.3133$); Lognormal Distribution for Pre-inspection Flaw Length with 50% Dispersion, + Totally Correlated Flaw Length, ++ Totally Independent Flaw Length.	76

SECTION I

INTRODUCTION

Current nondestructive evaluation techniques are not capable of repeatedly producing correct indications when applied to flaws of the same length. The chance of detecting a given crack length depends on many factors, such as the location, orientation and shape of the flaw, materials, inspectors, inspection environments, etc. As a result, the probability of detection (POD) for all cracks of a given length has been used in the literature to define the capability of a particular NDE system in a given environment. Some POD curves are shown in Figure 1 for various laboratory inspection techniques. Many other POD curves can be found, for instance, in References 1 through 3.

In practical applications, a nondestructive inspection limit, a_{NDE} , is usually specified, which is a crack length corresponding to a high detection probability and a high confidence level. For instance, the damage tolerant specification (References 4 and 5) requires that the NDE system should be capable of detecting the specified crack length, a_{NDE} , with a ninety per cent detection probability and a ninety-five per cent confidence level. The fracture mechanics residual life, N_f , is the life for the crack length, a_{NDE} , to propagate to the critical crack length, a_c , under expected usage environments, as shown in Figure 2(a). The return to service interval, denoted by N_R , is equal to N_f divided by a safety factor, S_f , i.e., $N_R = N_f/S_f$. If no crack is detected during inspection, the component is returned to service and the crack length in that component is assumed to be equal to a_{NDE} , as shown in Figure 2(b). Then, in the analysis of that component, the crack length is reset to be equal to a_{NDE} . Therefore, the inspection limit, a_{NDE} , is also referred to as the reset crack length. In the damage tolerant analysis, a safety factor of 2.0 has been used.

It follows from Figure 1 that there are two possible errors that can occur in any inspection situation: failure to give a positive indication in the presence of a crack whose length is greater than a_{NDE} (Type I error), and the giving of a positive indication when the crack

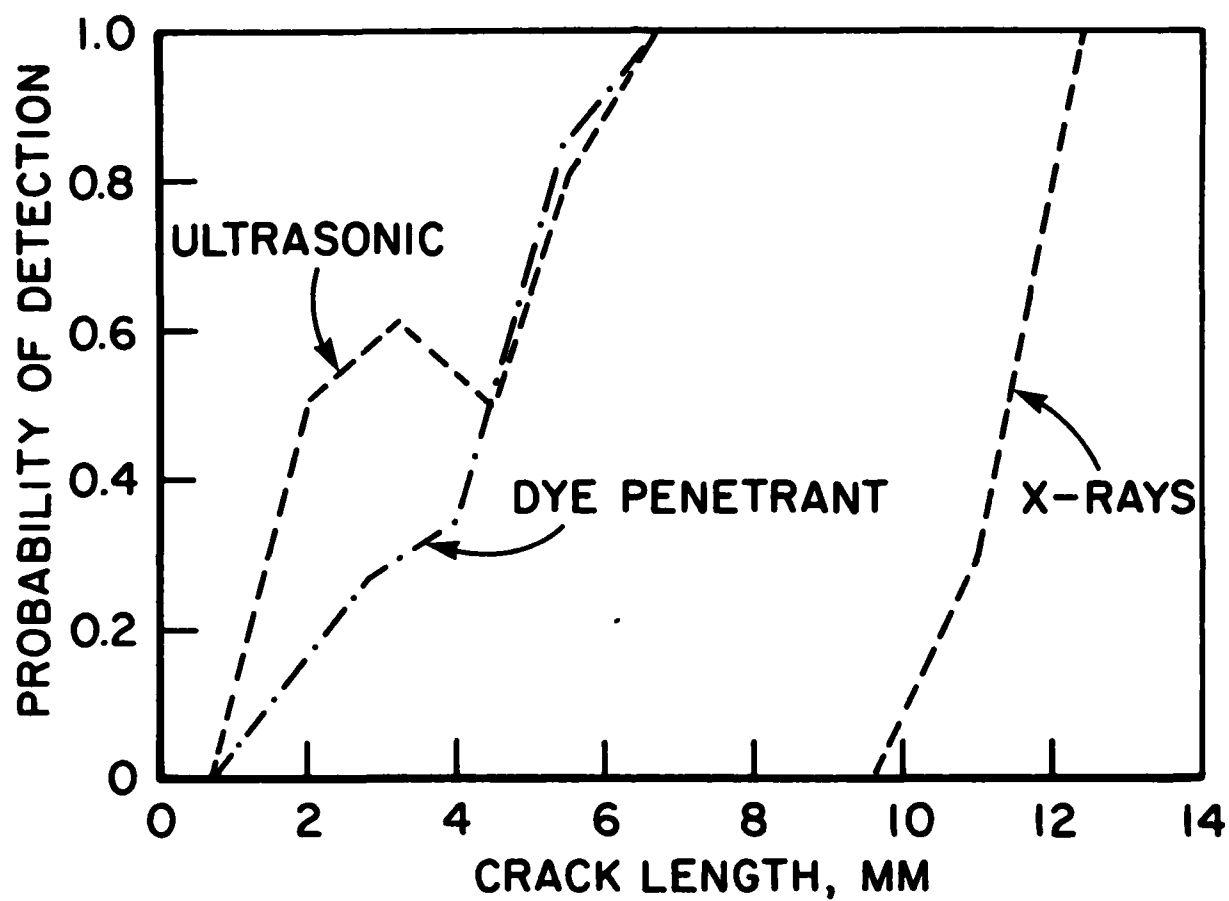


Figure 1. POD Curves for Various NDE Systems.

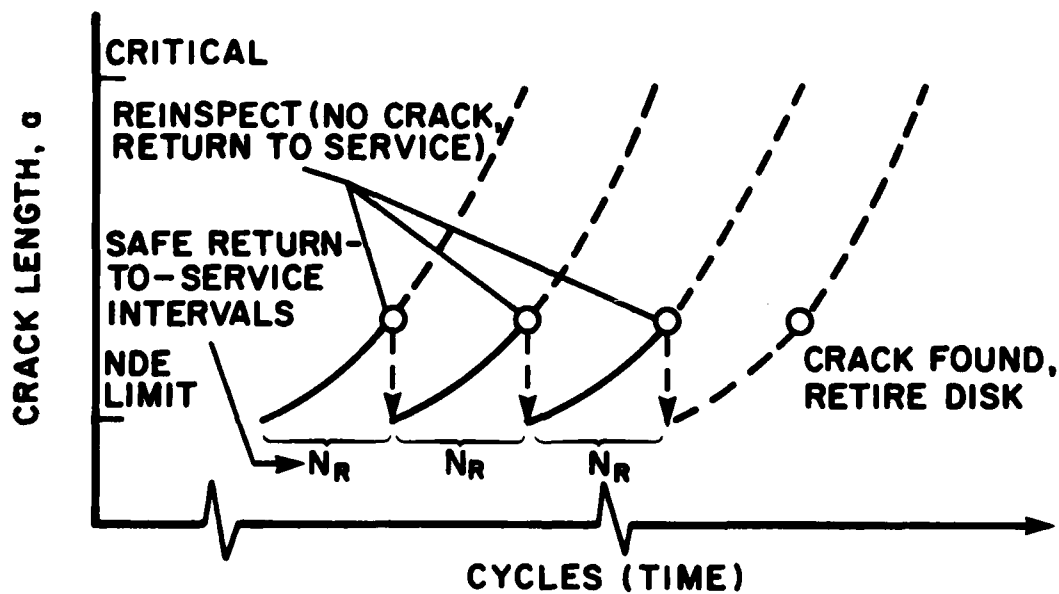
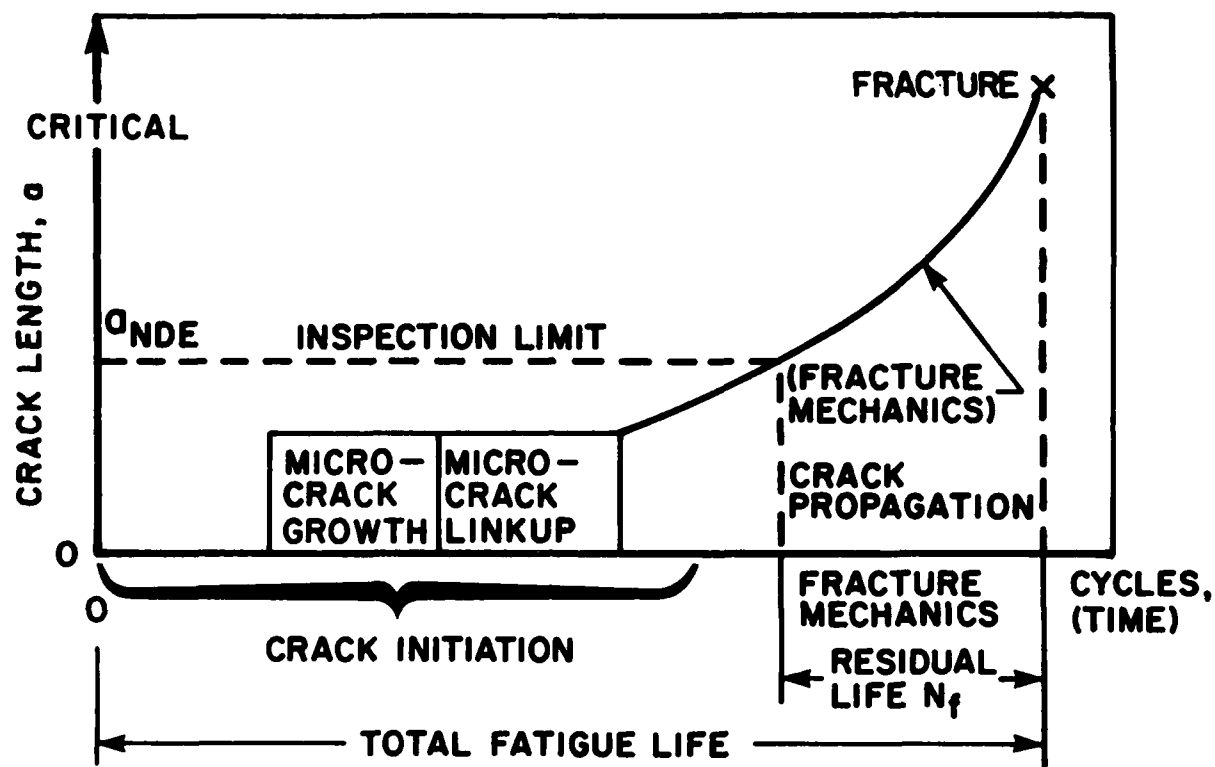


Figure 2. Fracture Mechanics Residual Life N_f and Return to Service Interval N_R .

length is smaller than a_{NDE} (Type II error). For safety critical components in airframe structures, Type I error is of primary concern. In the Retirement-For-Cause (RFC) analysis of gas turbine engine components, however, both Type I and Type II errors are important, because the criterion used in RFC analyses is the minimization of the life cycle cost (LCC) for engine components (References 6 and 7). As a result, the reduction for both types of error is one of the main objectives of the present study.

The Type I error allows the components containing a crack length longer than a_{NDE} to return to service, thus greatly increasing the potential safety hazard. For a given NDE system, the Type I error can be made as small as possible, by choosing a large value for the inspection limit, a_{NDE} . However, as the value of a_{NDE} increases, the return to service interval, N_R , reduces, thus increasing the frequency or cost of inspections. Moreover, while the Type I error can be reduced by increasing the value of a_{NDE} , the Type II error increases accordingly, as shown in Figures 3(a) and 3(b).

The Type II error rejects good components and therefore has an adverse effect on the cost of replacement and the life cycle cost. For a given NDE system with a single inspection, it is impossible to reduce the Type II error without increasing the Type I error, and vice versa.

It is obvious, therefore, that the ideal inspection capability of an NDE system is a unit step function, as shown in Figure 3(c), in which both Type I and Type II errors are zero. Unfortunately, such an ideal NDE system may be far from reality.

There are situations where the required a_{NDE} is so small the NDE system may not be able to detect it with high levels of reliability and confidence. Such a difficulty may be circumvented by the use of multiple inspection procedures. The possible improvements for the inspection reliability of an NDE system, through multiple inspection procedures, will be demonstrated in this report.

The POD curve of an NDE system is dependent upon the specific location and material being inspected. Because an engine disk contains

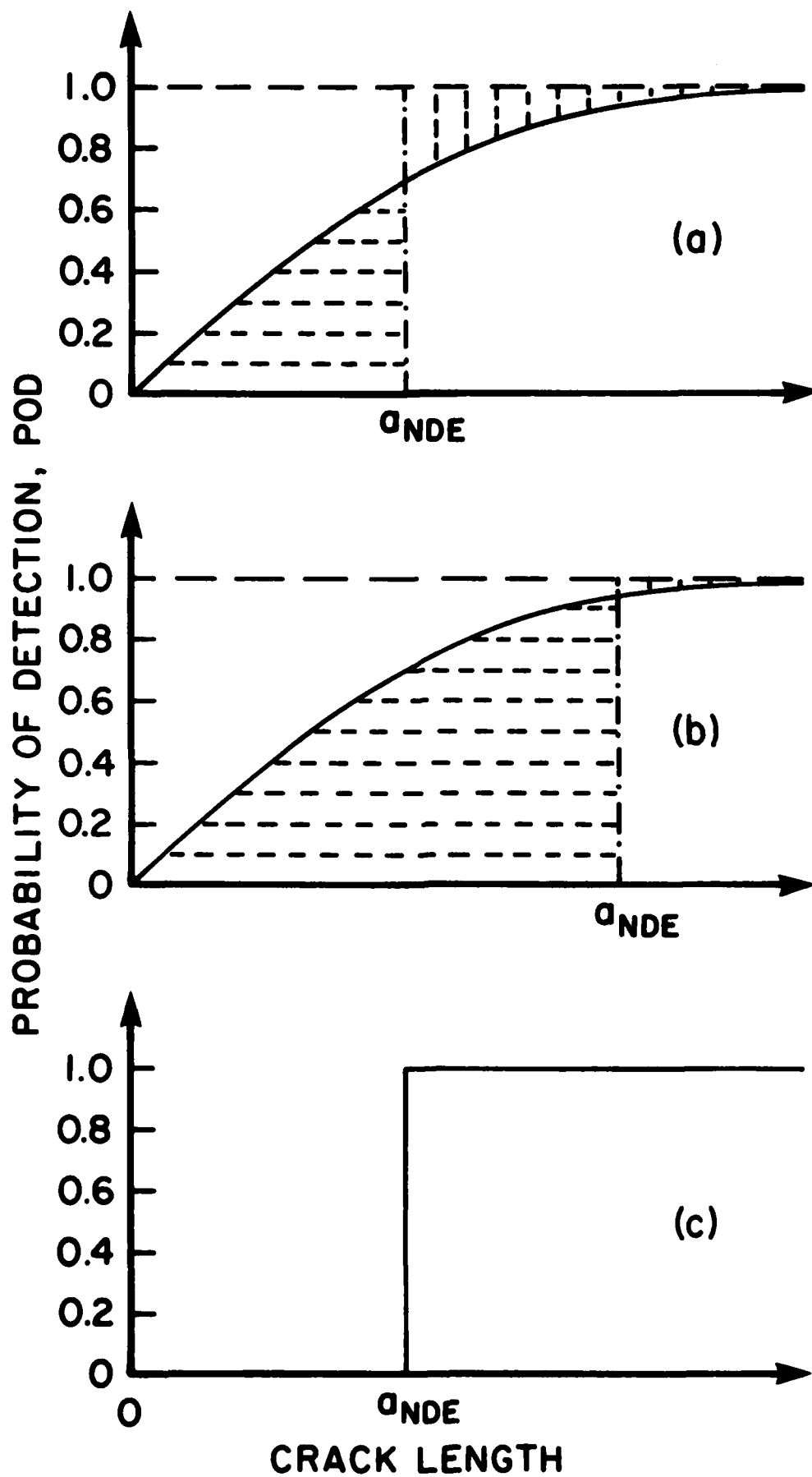


Figure 3. Type I and Type II Errors; (a) Small a_{NDE} , (b) Large a_{NDE} and (c) Ideal NDE System.

a large number of critical locations, each with its own POD curve, such as bolt holes, cooling holes, rim holes, etc., the inspection reliability for a disk differs significantly from that for a hole, since a disk is retired if at least one hole is rejected by the NDE system. An exploratory study for the inspection reliability of engine disks and the effect of multiple inspections is made herein.

The objectives of this study are: (i) to formulate and derive mathematically the resulting POD curve for components under multiple inspections, (ii) to investigate quantitatively the potential benefit of multiple inspection procedures, (iii) to establish the direction in which the capability of an NDE system should be improved, (iv) to establish the strategy and sequence for multiple inspections to reduce either Type I error or Type II error, or both, (v) to determine the POD curve for a disk from the POD of an NDE system, (vi) to determine the inspection reliability of engine disks, and (vii) to evaluate the benefit of multiple inspections for engine disks. Numerical results are presented to demonstrate the potential benefit of the proposed multiple inspection procedures for gas turbine engine disks.

SECTION II

THEORY OF MULTIPLE INSPECTIONS

In the literature, the POD curve for a particular NDE system has been established from repeated inspection data in which the inspector may or may not be the same. Then the inspection data set is analyzed using either the binomial method (e.g., References 1-3) or the method of regression analysis (Reference 8). It should be emphasized, however, that the binomial and regression methods assume explicitly that the result of each inspection using the same NDE system (whether the same inspector or not) is statistically independent of the other (i.e., independent sampling). Thus all the POD curves available in the literature are based on the premise that the results of multiple inspections are statistically independent. Such an assumption may be subject to criticism. However, to be consistent with current practice and to use available POD curves, the assumption will be employed first in the following formulation. The mathematical formulation in which the results of multiple inspections are not statistically independent is given in Appendix A. The issue of dependent and independent multiple inspections along with the application to gas turbine engine components will be discussed later.

The formulation and solution will be established in an appropriate perspective for multiple inspection procedures. With the mathematical solution put into an appropriate setting, one can manipulate various NDE capabilities (or POD curves) to achieve a most economical multiple inspection system in terms of Type I error, Type II error and both.

Let the following POD curves associated with m inspection systems be given;

$POD(a;1)$ = probability of detecting the crack length, a , under No. 1 NDE system

$POD(a;j)$ = probability of detecting the crack length, a , under No. j NDE system; $j=1,2,\dots,m$.

In general, $POD(a;i)$ is different from $POD(a;j)$. However, they may also be identical as a special case. Two basic inspection rules and their combinations are described in the following.

1. UNION RULE

A component (or a critical location) is rejected if it is rejected by either one of the NDE systems employed as shown in Figure 4.

Let $POD(a;1 \cup 2)$ = probability that the crack length, a , is detected by either No. 1 NDE system or No. 2 NDE system or both. Then, based on the assumption that the inspections by both NDE systems are statistically independent, the resulting POD curve for the component is given by

$$POD(a;1 \cup 2) = 1 - [1 - POD(a;1)][1 - POD(a;2)] \quad (1)$$

or

$$POD(a;1 \cup 2) = POD(a;1) + POD(a;2) - POD(a;1)POD(a;2) \quad (2)$$

In a similar fashion, the probability of detection (POD) under m NDE systems, denoted by $P(a; \bigcup_{j=1}^m j)$ is obtained as

$$POD(a; \bigcup_{j=1}^m j) = 1 - \prod_{j=1}^m [1 - POD(a;j)] \quad (3)$$

In general, the application of multiple inspections using the union rule will reduce the Type I error and the inspection limit a_{NDE} , thus improving the structural safety and reliability. However, it may also increase the Type II error; the extent of which depends on the particular functional form of $POD(a;j)$; $j=1,2,\dots,m$. An exceptional case is that if $POD(a;2)$ has a lower bound at a_{NDE} , i.e., $POD(a;2)$ is equal to zero for $a \leq a_{NDE}$, then there is no increase in the Type II error under two inspections. A schematical flow chart for the inspection procedures using two NDE systems and the union rule is shown in Figure 5.

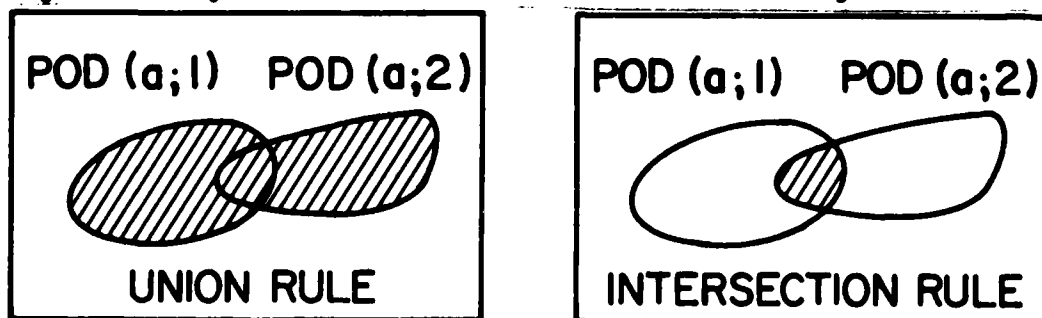


Figure 4. Rejected Components Shown in Shaded Areas.

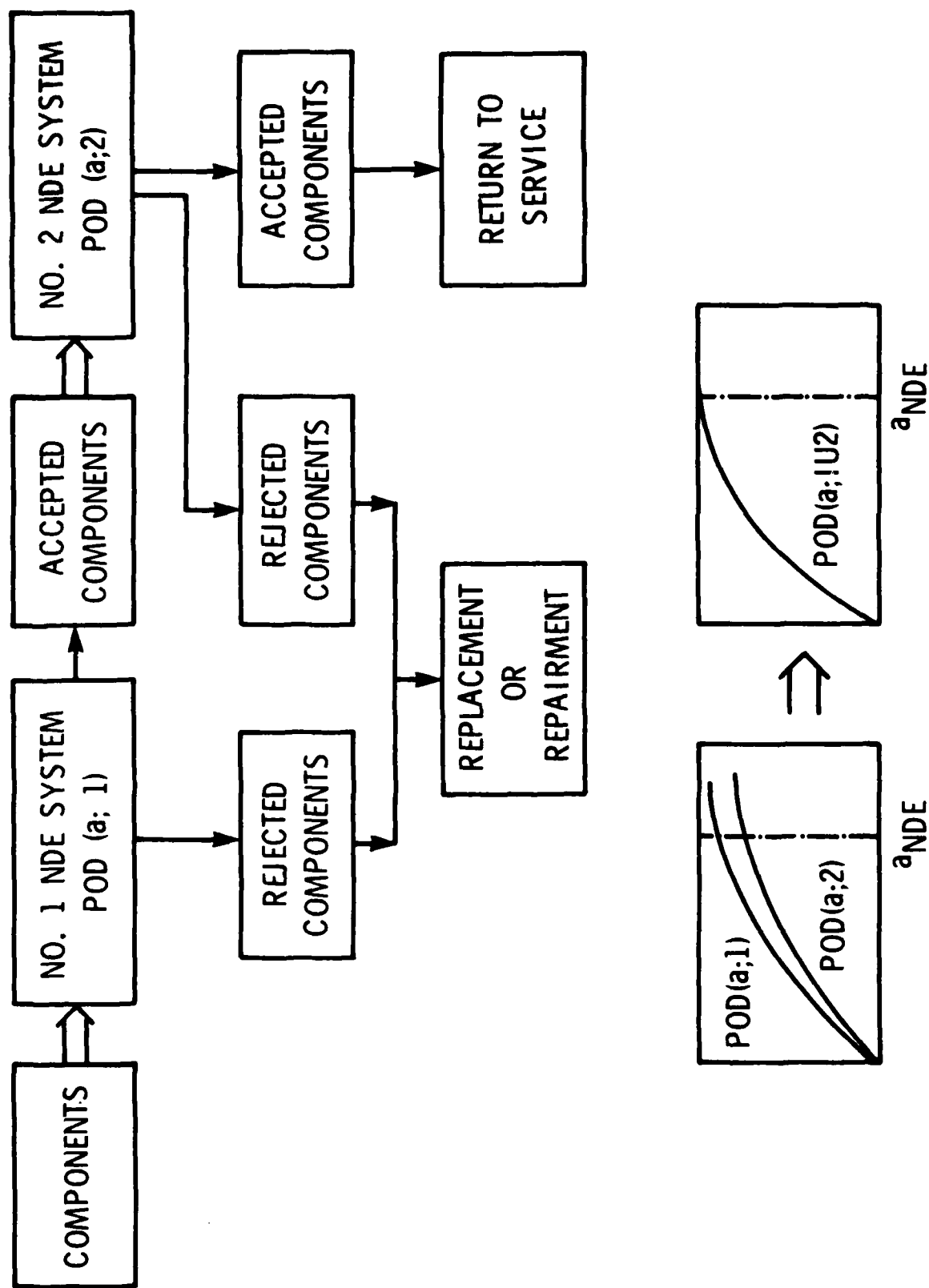


Figure 5. Inspection Procedure for Two NDE Systems with Union Rule

2. INTERSECTION RULE

A component (or a critical location) is rejected if and only if it is rejected by all the NDE systems employed, as shown in Figure 4.

If $POD(a;1\&2)$ denotes the probability of detecting the crack length, a , by both No. 1 and No. 2 NDE systems, then we have

$$POD(a;1\&2) = POD(a;1)POD(a;2) \quad (4)$$

In a similar manner, the probability of detecting the crack length, a , by every one of m NDE systems employed is given by

$$POD(a; \bigcap_{j=1}^m j) = \prod_{j=1}^m POD(a;j) \quad (5)$$

In general, the application of multiple inspections using the intersection rule alone will degrade the NDE capability. It is precisely due to such a property that the Type II error can be reduced. However, caution should be taken such that the degradation for the Type I error will be insignificant. For instance, using two inspection systems, the condition for not having a serious adverse effect on the Type I error is that $POD(a;2)$ should be very close to unity at $a=a_{NDE}$ as will be described later. If $POD(a;2)$ has an upper bound at a_{NDE} , i.e., $POD(a;2)=1$ for $a \geq a_{NDE}$, then the Type I error will not be effected. A flow chart for the inspection procedure using two NDE systems and the intersection rule is shown in Figure 6.

3. COMBINATION RULE FOR THREE INSPECTIONS

As described previously, the application of either the union rule or the intersection rule alone cannot reduce both Type I and Type II errors simultaneously. However, a combined use of both union and intersection rules, along with an appropriate choice of $POD(a;3)$, can result in a simultaneous improvement for both types of error.

Because of practical limitations, such as the facility and inspection cost, we shall describe only a possible combination of union and intersection rules using three inspections as follows.

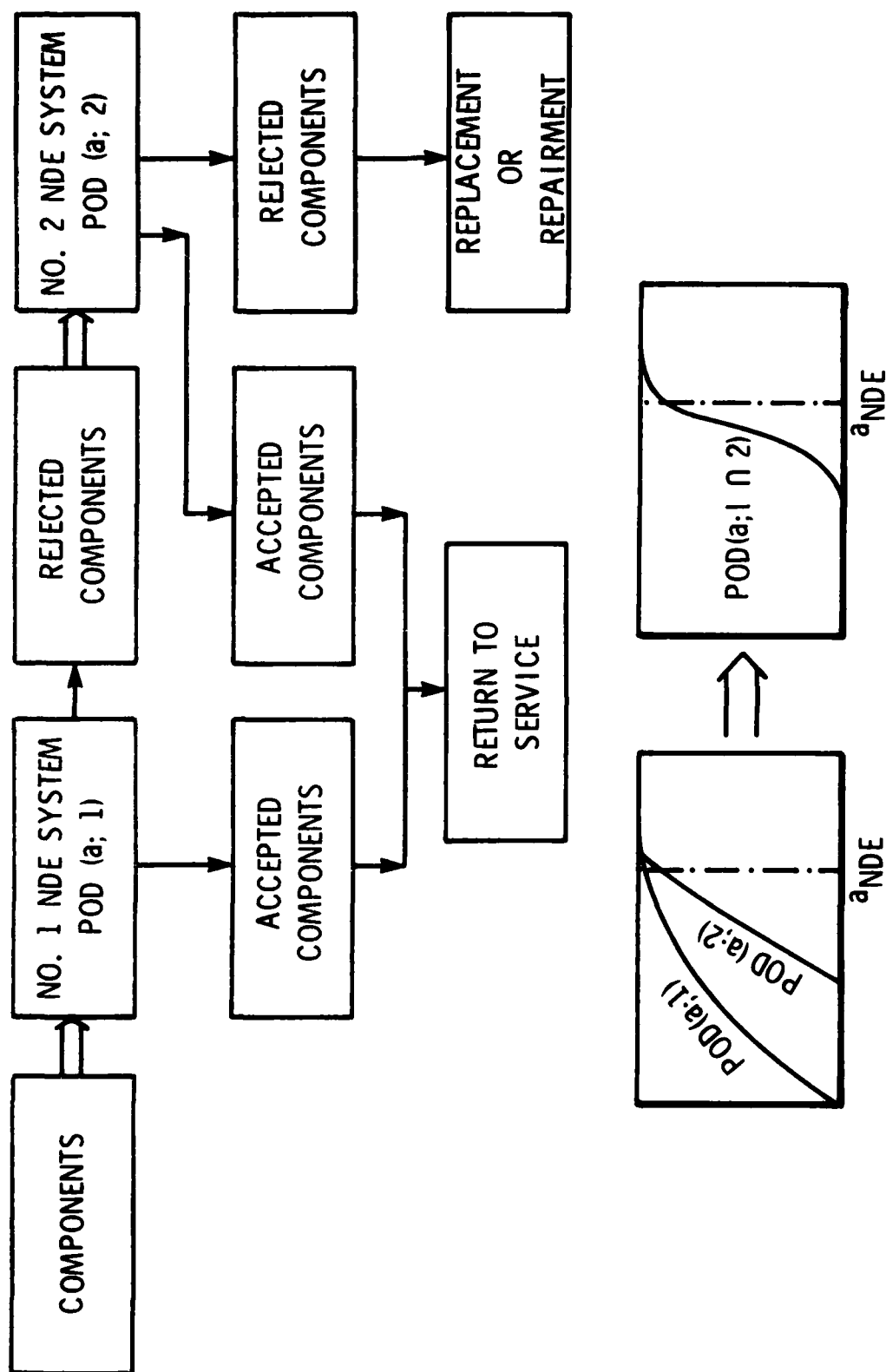


Figure 6. Inspection Procedure for Two NDE Systems with Intersection Rule.

Let $POD[a;(1U2)\cap 3]$ be the probability of detecting the crack length, a , under three inspections, where the union rule is applied to No. 1 and No. 2 NDE systems and the intersection rule is employed for the No. 3 NDE system. The resulting POD curve from the application of No. 1 and No. 2 NDE systems, $POD(a;1U2)$, is given by Equation 2. Hence, it follows from Equation 4 that

$$POD[a;(1U2)\cap 3] = POD(a;3)POD(a;1U2) \quad (6)$$

Substituting Equation 2 into Equation 6, one obtains

$$\begin{aligned} POD[a;(1U2)\cap 3] &= POD(a;3)[POD(a;1) + POD(a;2) \\ &\quad - POD(a;1)POD(a;2)] \end{aligned} \quad (7)$$

The inspection procedure for three NDE systems, presented in Equation 7, is shown by a flow chart in Figure 7 and explained as follows. After the first inspection by the No. 1 NDE system, components are divided into two populations: an accepted one and a rejected one. The accepted population is further inspected by the No. 2 NDE system (to reduce Type I error) and the accepted components are returned to service. The components rejected by the No. 2 NDE system along with the components rejected by the No. 1 NDE system are then inspected by the No. 3 NDE system (to reduce Type II error). Then the rejected components (by No. 3 NDE system) are replaced or repaired and the accepted components are returned to service. It should be mentioned that $POD(a;3)$ for the third NDE system should be very close to 1.0 (such as 0.99) at $a=a_{NDE}$, so that the adverse effect on the Type I error is minimal. Likewise, the bandwidth of $POD(a;3)$ should be as narrow as possible to reduce the Type II error effectively. Inspections using such an NDE system may be expensive and time consuming, but the number of components to be inspected by the No. 3 NDE system may be small. This will be discussed later.

If m NDE systems are employed, then there are many different combinations of union and intersection rules that can be investigated. However, the basic mathematical approach to derive the resulting POD curve is the same as that described previously. For instance, for a

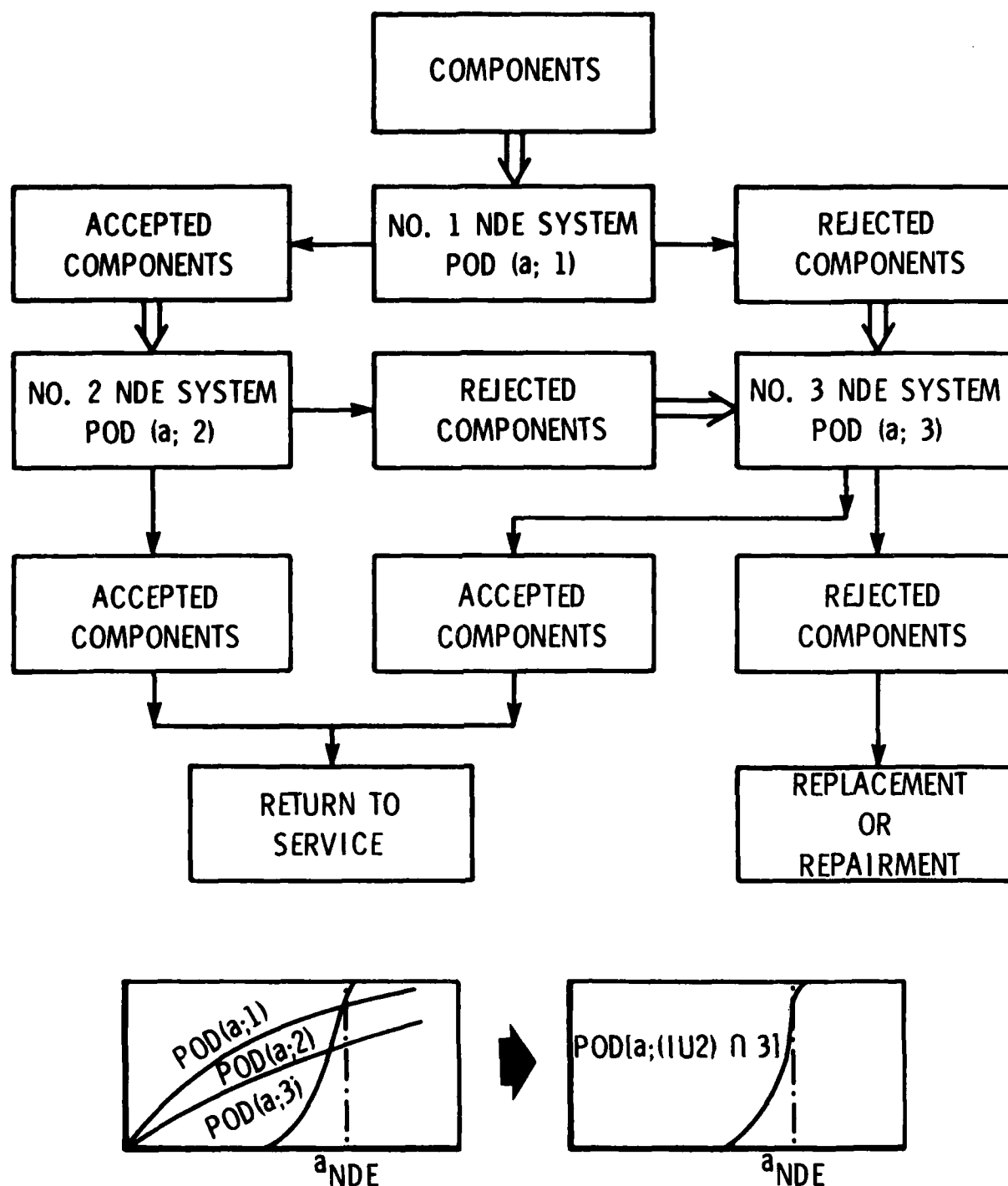


Figure 7. Inspection Procedure for Three NDE Systems with Union-Intersection Rule.

special case in which $POD(a;1)=POD(a;2)=POD(a;3)$, then the resulting POD curve using the union rule is given by

$$POD(a; \bigcup_{j=1}^3 j) = 1 - [1-POD(a;1)]^3 \quad (8)$$

When the fourth NDE system with $POD(a;4)$ is further applied to inspect those rejected components using the intersection rule, the resulting POD curve is given by

$$POD[a; (\bigcup_{j=1}^3 j) \cap 4] = POD(a;4)POD(a; \bigcup_{j=1}^3 j) \quad (9)$$

in which $POD(a; \bigcup_{j=1}^3 j)$ is given by Equation 8.

4. INSPECTION SEQUENCE FOR MINIMUM NUMBER AND COST OF INSPECTIONS

The resulting POD curves under multiple inspections derived in the previous sections are independent of the sequence (or order) of applications of multiple NDE systems. However, the number of inspections required for components and hence the cost of inspection is indeed influenced by the sequence of inspections. For the case of two inspections with the union rule as shown in Figure 5, $POD(a;1)$ should be better than $POD(a;2)$ such that fewer components will be accepted by the No. 1 NDE system. Therefore, the number of components to be inspected by the No. 2 NDE system is minimal. In general, for multiple inspections with the union rule, the NDE system with the highest resolution capability should be applied first in order to minimize the subsequent number of inspections. However, the minimization of the number of inspections implies the minimization of the inspection cost only when the cost per inspection for both No. 1 and No. 2 NDE system is almost the same. If there is a difference in the inspection cost for two NDE systems, then the system with the lower inspection cost should be the No. 1 NDE system. This is because the No. 1 NDE system has to inspect all the components whereas only those components accepted by the No. 1 NDE system will be inspected by the No. 2 NDE system.

On the other hand, for the case of two inspections using the intersection rule, as shown in Figure 6, $POD(a;2)$ should be better than $POD(a;1)$,

so that the number of components rejected by the No. 1 NDE system, which should be inspected by the No. 2 NDE system, will be minimal. For the case of three inspections using the union-intersection rule, the number of components to be inspected by the No. 3 NDE system is independent of the inspection sequence. However, for the first two inspections using the union rule, $POD(a;1)$ should be better than $POD(a;2)$ to achieve a minimum number of inspections.

Again, depending on the cost of inspection for each NDE system, the rationale described previously can be applied to minimize the inspection cost.

5. CORRELATED MULTIPLE INSPECTIONS

The solutions obtained previously for the resulting POD curves under multiple inspection procedures are based on the assumption that inspection results from multiple NDE systems are statistically independent. This assumption is consistent with the current practice for establishing the POD curve for each NDE system in which independent sampling has been assumed, i.e., each inspection result from the same NDE system is assumed to be statistically independent.

It is more economical to perform multiple inspections using the same NDE system. However, the question of whether the results of multiple inspections using the same NDE system, but under different inspection conditions, will be independent or correlated has not yet been fully resolved. Take eddy-current inspection for instance. The following conditions may be different in multiple inspections; inspector, gain of NDE signal, scanning speed for inspection, position of probe, signal data processing, surface preparation of inspected parts, loading condition of parts, the same system at different locations or facilities, etc.

For a fully automated NDE system currently under development for the RFC system, it is anticipated that the error or uncertainty due to human operation and others will be greatly reduced, and the systematic error or uncertainty of the NDE system itself will prevail. Thus, multiple inspections using such a fully automated NDE system alone for a single location may be highly correlated if the preparation for the surface condition of the location is identical.

The mathematical solutions for correlated inspections are presented in Appendix A. With correlated inspection systems, however, additional POD information is needed. For instance, the conditional probability of detecting the crack length, a , by the No. 2 NDE system under the condition that the crack has been detected by the No. 1 NDE system is required. The procedure to establish such a conditional POD curve is described in Appendix B.

6. APPLICATION OF INDEPENDENT INSPECTIONS

One of the motivations of the present investigations is the application to the Retirement-For-Cause of gas turbine engine components, such as disks. A disk usually contains many holes, such as bolt holes, cooling holes and rim holes, in which cracks may occur. Since the crack in each hole may have a different length, orientation and geometry, the inspection of one hole can be assumed to be statistically independent of the inspection of another hole. Likewise, in order to reduce Type II error, the rejected holes may be cleaned, polished or even replicated, in which case a high resolution capability for the POD curve can be achieved. It may be reasonable to assume that the inspection for a hole with replication is statistically independent of the inspection for the same hole without replication even when the same NDE system is used. The application of the present results to RFC of engine components will be presented in later sections.

7. TYPE I AND TYPE II ERRORS

The effect of multiple inspections on the POD curve, Type I and Type II errors, and the inspection limit a_{NDE} will be demonstrated later. While the capability of a particular NDE system is defined by its POD curve, the Type I and Type II errors depend not only on the POD curve itself but also on the pre-inspection distribution of the flaw length in the component. For instance, if all the crack lengths in the component prior to inspection are smaller than a_{NDE} , then the Type I error is zero.

Let $F(a)$ and $f(a)$ be the distribution function and the probability density function, respectively, of the flaw length in the component prior

to inspection. Then the Type I and Type II errors, denoted by P_I and P_{II} , respectively, are given by

$$P_I = \int_{a_{NDE}}^{\infty} f(x)[1-POD(x)]dx \quad (10)$$

$$P_{II} = \int_0^{a_{NDE}} f(x)POD(x)dx \quad (11)$$

in which

P_I = probability of missing (or accepting) a crack length longer than a_{NDE} ,

P_{II} = probability of detecting (or rejecting) a crack length smaller than a_{NDE} ,

and $POD(a)$ is the POD curve of a particular NDE system.

Both P_I and P_{II} , given by Equations 10 and 11, are the quantitative measures of Type I and Type II errors. Two qualitative measures of Type I and Type II errors which depend exclusively on the POD curve, may also be appealing,

$$A_I = \int_{a_{NDE}}^{\infty} [1-POD(x)]dx \quad (12)$$

$$A_{II} = \int_0^{a_{NDE}} POD(x)dx \quad (13)$$

It is apparent from Equations 12 and 13 that A_I is the area above the POD curve from a_{NDE} to infinity, and A_{II} is the area under the POD curve from zero to a_{NDE} , as shown in the shaded areas of Figure 3. While A_I and A_{II} are not the quantitative measures of Type I and Type II errors, they may serve for qualitative comparisons between the capability of various NDE systems when the value of the inspection limit, a_{NDE} , is fixed.

When multiple inspections are employed, the $POD(a)$ function appearing in Equations 10-13 represents the resulting POD curve derived in Equations 1-9. Hence, it should be replaced by the appropriately corresponding POD curve resulting from multiple inspections.

8. DISTRIBUTION OF PRE-INSPECTION FLAW LENGTH

Theoretically, the distribution of the flaw length for a component prior to inspection can be derived from the distributions of times to crack initiation (or equivalent initial flaw length), crack growth rates in service, and service loads. Such an approach, however, is very complex. From the NDE standpoint, it is reasonable to assume the Weibull distribution for pre-inspection flaw lengths for illustration. Information on the statistical variabilities of the equivalent initial flaw length, the crack propagation rate and the service loads for engine disks indicates that the statistical dispersion (coefficient of variation) of the crack length in service is of the order of 100%. The Weibull distribution with a 100% coefficient of variation degenerates into a special case of the negative exponential distribution. As a result, the distribution of the pre-inspection flaw length may be assumed to follow the negative exponential distribution, i.e.,

$$\begin{aligned} f(a) &= \lambda e^{-\lambda a} \quad ; \quad a \geq 0 \\ F(a) &= 1 - e^{-\lambda a} \quad ; \quad a \geq 0 \end{aligned} \tag{14}$$

in which $f(a)$ and $F(a)$ are, respectively, the probability density function and the distribution function of the pre-inspection flaw length. In Equation 14, $1/\lambda$ represents the average flaw length.

The lognormal distribution may also be used for the pre-inspection flaw length distribution as follows;

$$\left. \begin{aligned} f(a) &= \frac{\log e}{\sqrt{2\pi} a \sigma} \exp \left\{ -\frac{1}{2} \left(\frac{\log a - \mu}{\sigma} \right)^2 \right\} \\ F(a) &= \Phi \left(\frac{\log a - \mu}{\sigma} \right) \end{aligned} \right\} \tag{15}$$

in which μ and σ are the mean value and the standard deviation, respectively, of the logarithm of the flaw length, and $\Phi(\)$ is the standardized normal distribution function.

SECTION III

NUMERICAL EXAMPLES

1. EXAMPLE NO. 1

Eddy current inspection data for fastener holes in skin and stringer wing assembly, referred to as HAVE CRACK, were available in Reference 3 and analyzed by the binomial method. The same data set was further analyzed in Reference 8 using the regression method with the assumed functional form for the POD curve as follows;

$$POD(a;1) = \frac{\exp(\alpha + \beta \ln a)}{1 + \exp(\alpha + \beta \ln a)} \quad (16)$$

in which $\alpha = -2.9$ and $\beta = 1.7$ (Figure 8). This POD curve is replotted in Figure 9(a) as Curve 1. The crack length associated with 90% and 96% detection probabilities are, respectively, 20.05 mm and 35.7 mm.

The data set used to establish the POD curve was generated using the same cracked specimens but inspected by different inspectors and NDE systems at different locations. If the components are inspected twice at different locations, i.e., $POD(a;1) = POD(a;2)$, the resulting POD curve, i.e., $POD(a;1 \cup 2)$, with the union rule is shown as Curve 2 (Equation 2) in Figure 9(a). One can further improve the Type I error by performing a third inspection using the union rule. With $POD(a;1) = POD(a;2) = POD(a;3)$, the resulting $POD(a;1 \cup 2 \cup 3)$, Equation 3, is displayed in Figure 9(a) as Curve 3. If the inspection limit, a_{NDE} , is required to be 12.4 mm, i.e., $a_{NDE} = 12.4$ mm, then, A_I and A_{II} (Equations 12 and 13) are computed and shown in Table 1. It is observed from Table 1 that A_I reduces and A_{II} increases as the number of inspections increases.

The distribution of the flaw length prior to inspection is given by Equation 14 in which the average flaw length is assumed to be 5 mm, i.e., $\lambda = 0.2/\text{mm}$. The probability density function given by Equation 14 is displayed in Figure 9(a) as a dashed curve. With such a pre-inspection flaw length distribution, the probability that the crack length will exceed $a_{NDE} = 12.4$ mm is 8.37%, i.e., on the average there are 8.37% of the

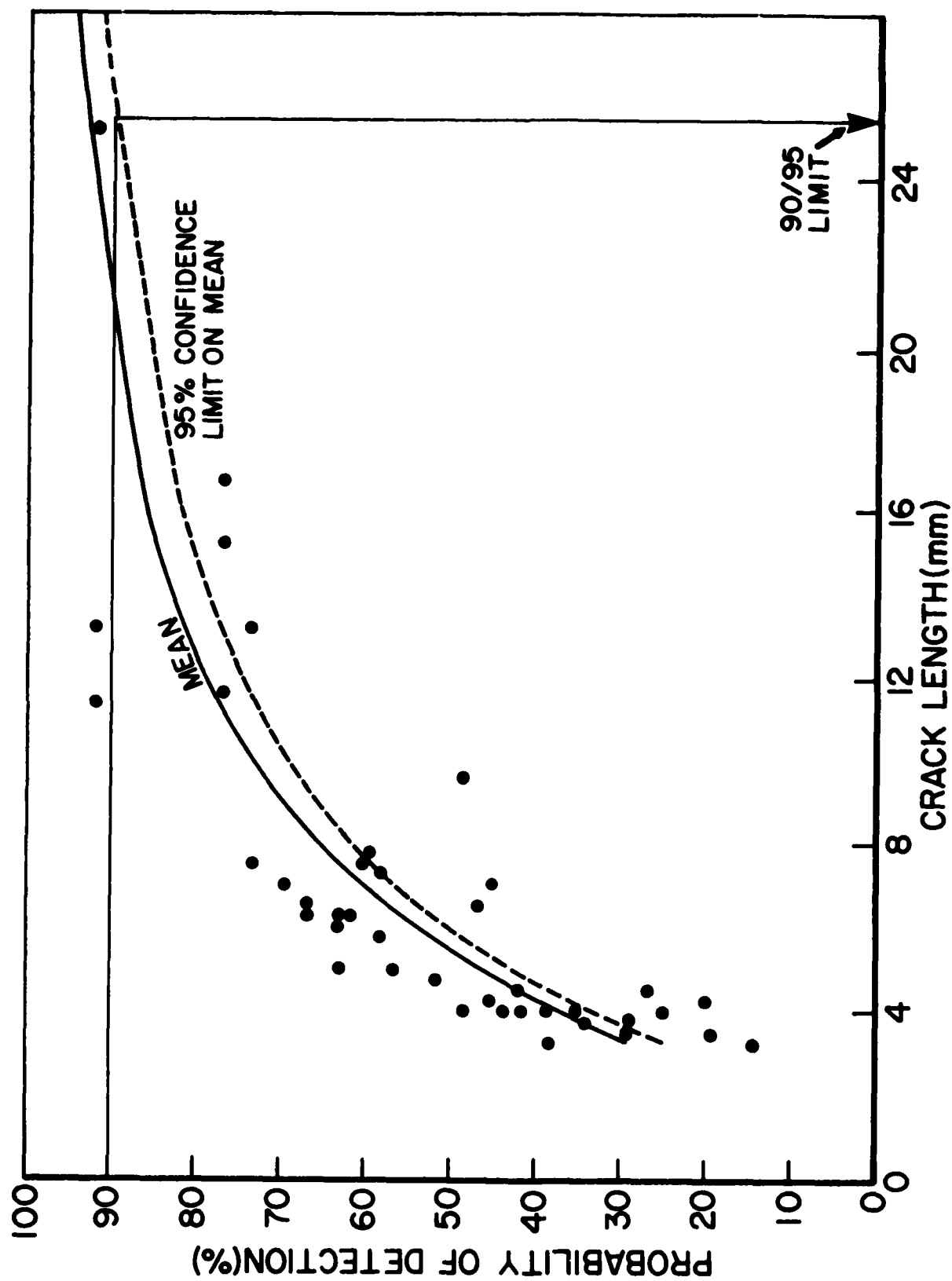


Figure 8. Eddy Current Inspections of Skin and Stringer Wing Assembly, 60 Inspections Per Fastener Hole (from References 3 and 8).

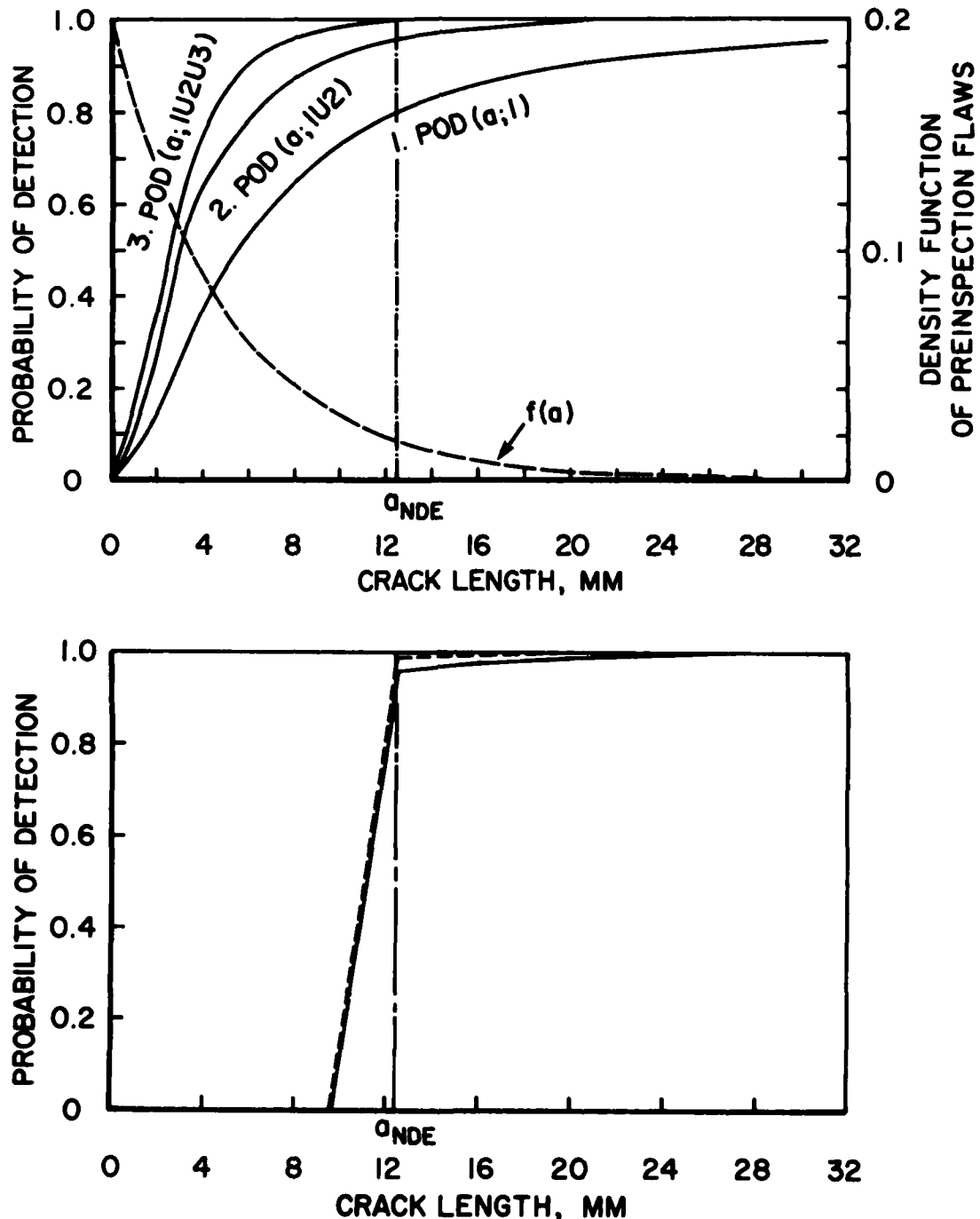


Figure 9. Resulting POD Curves Under Multiple Inspections;
(a) Union Rule and (b) Union-Intersection Rule.

components that will have a crack length longer than 12.4 mm.

Therefore, the average percentage of good components, P_G , prior to inspection is 91.63%, i.e., $P_G=91.36\%$.

The Type I and Type II errors, P_I and P_{II} , are computed from Equations 10 and 11 in which $POD(x)$ is replaced by $POD(x;1)$, $POD(x;1U2)$ and $POD(x;1U2U3)$, respectively. The results are shown in Table 1. It is observed from Table 1 that the Type I error reduces drastically as the number of inspections with the union rule increases. However, the Type II error increases simultaneously.

TABLE 1

TYPE I AND TYPE II ERRORS; $a_{NDE} = 12.4$ mm, $P_G = 91.63\%$

TABLE 1

No. of Inspections Type	A_I (mm)	A_{II} (mm)	P_I	P_{II}
1 POD(a;1)	2.5	5.99	1.15×10^{-2}	28.6%
2 POD(a;1U2)	0.24	8.30	1.72×10^{-3}	42.7%
3 POD[a;(1U2) $\Omega 3^*$]	0.24	1.1	1.72×10^{-3}	5.9%
3 POD(a;1U2U3)	0.03	9.36	2.74×10^{-4}	50.8%
4 POD[a;(1U2U3) $\Omega 3^*$]	0.03	1.38	2.74×10^{-4}	6.2%

To reduce the Type II error, an additional inspection with a high resolution capability is used in conjunction with the intersection rule. For illustrative purposes, the POD curve of the NDE system for the

additional inspection using the intersection rule is assumed to resemble that of the x-ray system shown in Figure 1, i.e.,

$$\left. \begin{aligned} \text{POD}(a;3^*) &= 0 && \text{for } a < 9.6 \text{ mm} \\ &= \frac{a-9.6}{2.8} && \text{for } 9.6 \leq a \leq 12.4 \\ &= 1 && \text{for } a > 12.4 \text{ mm} \end{aligned} \right\} \quad (17)$$

It is obvious that the POD curve given above is a straight line between 9.6 mm and 12.4 mm (Figure 1).

The resulting POD curve, denoted by $\text{POD}[a;(1U2)\Omega 3^*]$ and $\text{POD}[a;(1U2U3)\Omega 3^*]$, are presented in Figure 9(b) as solid and dashed curves, respectively. Note that $\text{POD}[a;(1U2)\Omega 3^*]$ is the resulting POD curve under two inspections with the union rule, i.e., $\text{POD}(a;1)=\text{POD}(a;2)$, as well as the third inspection with the POD curve given by Equation 17. Likewise, $\text{POD}[a;(1U2U3)\Omega 3^*]$ is the resulting POD curve under three inspections with the union rule, and an additional inspection with the intersection rule, where the POD curve is given by Equation 17. Both $\text{POD}[a;(1U2)\Omega 3^*]$ and $\text{POD}[a;(1U2U3)\Omega 3^*]$ are computed from Equations 7 and 9, respectively.

The Type I and Type II errors (P_I and P_{II}), as well as A_I and A_{II} , are computed from Equations 10-13 and the results are shown in Table 1. It is observed from Table 1 and Figure 9(b) that multiple inspections can reduce both Type I and Type II errors simultaneously.

2. EXAMPLE NO. 2

Eddy current inspections of etched fatigue cracks in 2219-T87 aluminum plates are available from Reference 2, in which the optimized probability method along with the binomial approach was used to establish the 95% confidence POD curve shown in Figure 10. For situations in which both Type I and Type II errors are important, such as the Retirement-For-Cause of engine components, the mean POD curve should be used. For the purpose of illustration, the mean POD curve is approximated by

$$\text{POD}(a;1) = 1 - e^{-\beta a}; \quad a \geq 0 \quad (18)$$

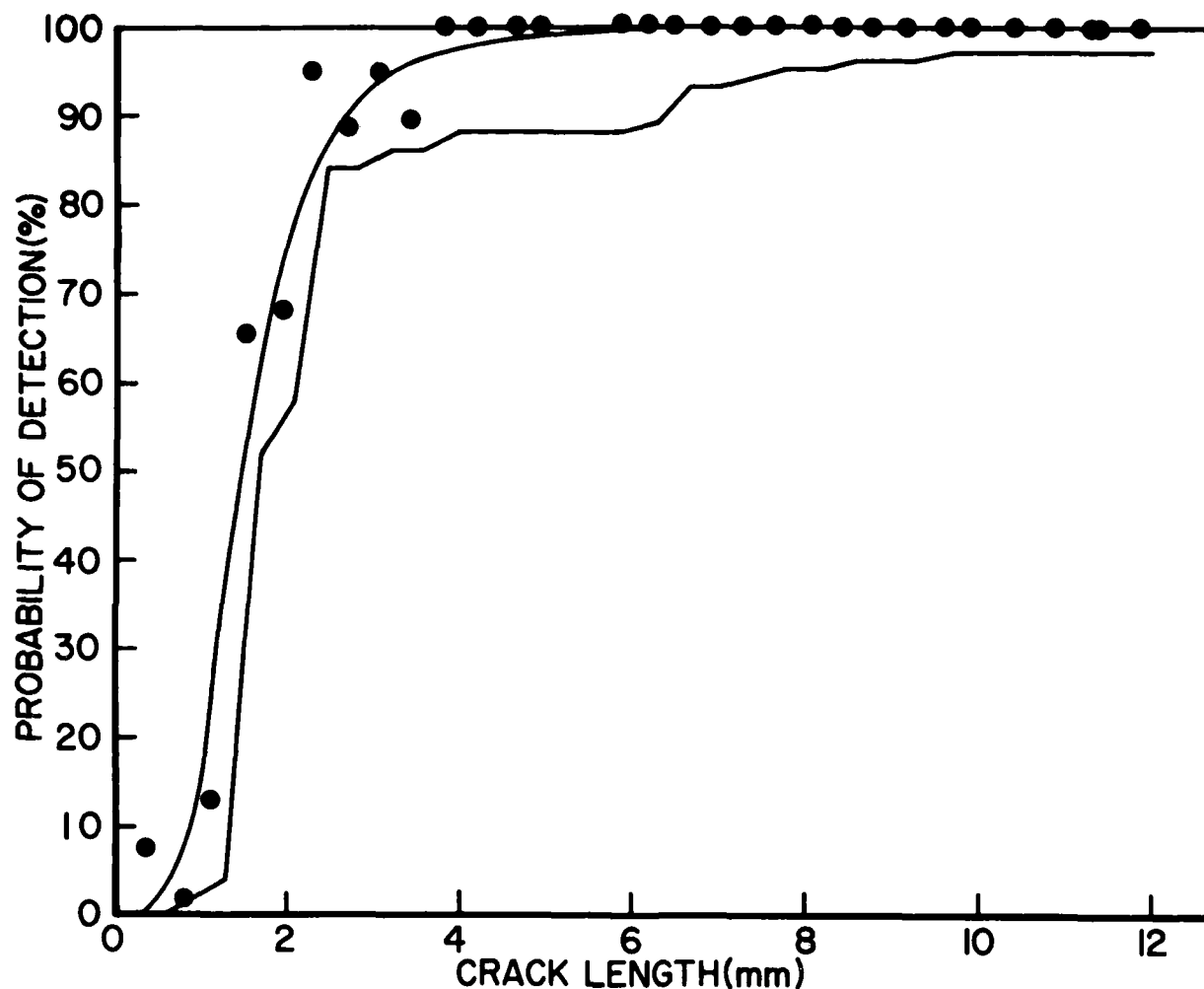


Figure 10. Optimized Probability Method - 361 Eddy Current Inspections of Etched Fatigue Cracks in 2219-T87 Aluminum Plates (from Reference 2).

with $\beta_1 = 0.46/\text{mm}$ as shown in Figure 11 (Curve 1). From Curve 1 it is observed that the inspection limit corresponding to a 90% detection probability is 5 mm, i.e., $a_{\text{NDE}} = 5 \text{ mm}$. In what follows, 5 mm will be used as the inspection limit or the reset crack length, a_{NDE} .

Suppose the POD curve for the second NDE system is given by

$$\text{POD}(a;2) = 1 - e^{-\beta_2 a} \quad ; \quad a \geq 0 \quad (19)$$

with $\beta_2=0.198/\text{mm}$. The $\text{POD}(a;2)$ given by Equation 19 is plotted in Figure 11 as Curve 2. It is obvious that the second NDE system has a worse detection capability than the first one.

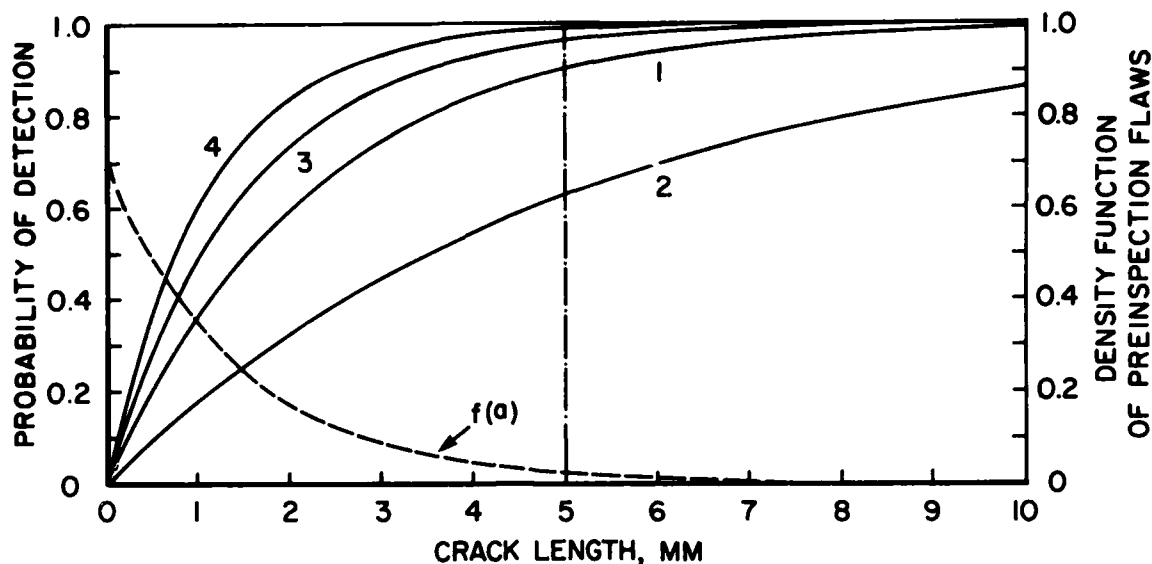


Figure 11. POD Curves (1 and 2) and Resulting POD Curves Using the Union Rule.

With the application of the second NDE system using the union rule, the resulting POD curve, i.e., $\text{POD}(a;1\cup 2)$, is shown in Figure 11 as Curve 3. Now the inspection limit, $a_{\text{NDE}}=5 \text{ mm}$, for the resulting POD curve corresponds to a 96% detection probability. Thus, it is shown that even with a poor NDE system, a second inspection using the union rule can reduce the Type I error. The measures A_I and A_{II} for Type I and Type II errors defined in Equations 12 and 13 are obtained as follows;

$$A_I = \exp[-(\beta_1 + \beta_2)a_{\text{NDE}}]/(\beta_1 + \beta_2) \quad (20)$$

$$A_{II} = a_{\text{NDE}} - \{1 - \exp[-(\beta_1 + \beta_2)a_{\text{NDE}}]\}/(\beta_1 + \beta_2) \quad (21)$$

Assuming that the second NDE system has the same resolution capability as the first one, i.e., $\beta_1=\beta_2=0.46/\text{mm}$, the resulting POD curve, i.e., $\text{POD}(a;1\cup 2)$, is plotted in Figure 11 as Curve 4. Now the detection probability at the inspection limit $a_{\text{NDE}}=5 \text{ mm}$ increases to 99%.

The distribution of the pre-inspection flaw length is assumed to follow the negative exponential distribution given by Equation 14 with $\lambda=0.7/\text{mm}$ which is also shown in Figure 11 (dashed curve). The probability that a crack length will exceed $a_{\text{NDE}}=5 \text{ mm}$ is computed as 3%. In other words, on the average, 3% of the components should be repaired or replaced if an ideal NDE system is used, i.e., $P_G=97\%$. The Type I and Type II errors given in Equations 10 and 11 are obtained as

$$P_I = \frac{\lambda}{\lambda + \beta_1 + \beta_2} \exp \left[- (\lambda + \beta_1 + \beta_2) a_{\text{NDE}} \right] \quad (22)$$

$$P_{II} = \left[1 - e^{-\lambda a_{\text{NDE}}} \right] - \frac{\lambda}{\lambda + \beta_1 + \beta_2} \left[1 - \exp \left\{ - (\lambda + \beta_1 + \beta_2) a_{\text{NDE}} \right\} \right] \quad (23)$$

Values of A_I , A_{II} , P_I and P_{II} are shown in Tables 2 and 3.

As expected, the Type I error is reduced under two inspections using the union rule whereas the Type II error increases. From Tables 2 and 3, the Type II error, either under single or double inspections, may not be acceptable from an economical standpoint. As a result, a third inspection is applied using the intersection rule as follows.

The third NDE system should have a high detection probability at the inspection limit, $a_{\text{NDE}}=5 \text{ mm}$, and it should also be narrow-banded to be effective for reducing the Type II error. Such a high quality POD curve may be achieved using the first NDE system if the cracked locations are cleaned, polished or replicated. For illustrative purposes, the POD curve, $\text{POD}(a;3)$, is assumed to be of the following forms;

$$\left. \begin{aligned} \text{POD}(a;3) &= 0 & a < a_1 \\ &= \frac{a - a_1}{a_2 - a_1} & a_1 \leq a \leq a_2 \\ &= 1 & a > a_2 \end{aligned} \right\} \quad (24)$$

or

$$\text{POD}(a;3) = 1 - \exp \left\{ -(a/\beta_0)^{\alpha_0} \right\} ; \quad a \geq 0 \quad (25)$$

TABLE 2

TYPE I AND TYPE II ERRORS; $\beta_1 = 0.46/\text{mm}$, $\beta_2 = 0.198/\text{mm}$,
 $a_{\text{NDE}} = 5 \text{ mm}$, $P_G = 97\%$

No. of Inspections	Rule	A_I (mm)	A_{II} (mm)	P_I	P_{II}
1		0.218	3.04	1.83×10^{-3}	36%
2	U	0.066	3.54	0.57×10^{-3}	45%
3*	U-1	0.066	1.16	0.57×10^{-3}	4.7%
3**	U-1	0.069	1.04	0.59×10^{-3}	3.84%
*: POD(a;3) given by Equation 24 with $a_1=2.5 \text{ mm}$, $a_2=5.0 \text{ mm}$					
**: POD(a;3) given by Equation 25 with $\alpha_0=8.0$, $\beta_0=4.13 \text{ mm}$					

TABLE 3

TYPE I AND TYPE II ERRORS; $\beta_1 = 0.46/\text{mm}$, $\beta_2 = 0.46/\text{mm}$,
 $a_{\text{NDE}} = 5 \text{ mm}$, $P_G = 97\%$

No. of Inspections	Rule	A_I (mm)	A_{II} (mm)	P_I	P_{II}
1		0.218	3.04	1.83×10^{-3}	36%
2	U	0.011	3.92	0.13×10^{-3}	54%
3*	U-1	0.011	1.22	0.13×10^{-3}	5%
3**	U-1	0.0112	1.09	0.15×10^{-3}	4%
*: POD(a;3) given by Equation 24 with $a_1=2.5 \text{ mm}$, $a_2=5.0 \text{ mm}$					
**: POD(a;3) given by Equation 25 with $\alpha_0=8.0$, $\beta_0=4.13 \text{ mm}$					

The POD curve, $POD(a;3)$, given by Equation 25 is a Weibull function whereas the curve given by $POD(a;3)$ in Equation 24 is a straight line between a_1 and a_2 which resembles the curve for the x-ray system shown in Figure 1. Both Equations 25 and 24 are plotted in Figure 12 as Curve 1 and Curve 2, respectively, with $\alpha_0=8$ and $\beta_0=4.13$ mm, $a_1=2.5$ mm and $a_2=5.0$ mm.

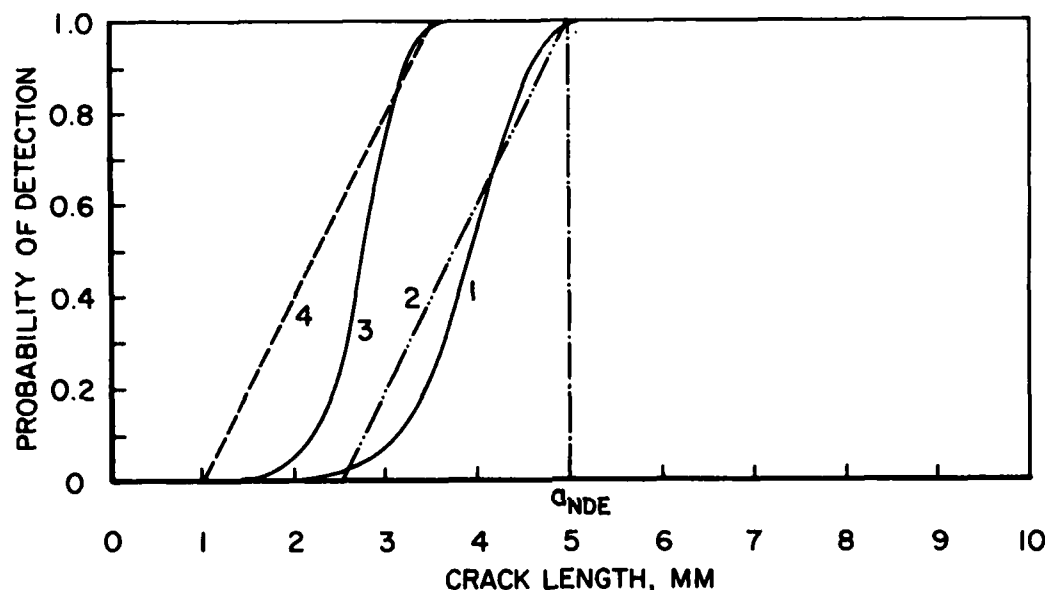


Figure 12. POD Curves for the Third Inspection System $POD(a;3)$.

The resulting POD curves, i.e., $POD[a;(1U2)\Omega3]$ given by Equation 9, are plotted in Figures 13(a)-13(d) for different combinations of $POD(a;1)$, $POD(a;2)$ and $POD(a;3)$, given by Equations 18, 19, 24 and 25. These figures demonstrate a significant improvement of the POD curve using three inspections with the union-intersection rule described previously. The corresponding A_I , A_{II} , P_I and P_{II} values are shown in Tables 2 and 3. As observed from these tables, both Type I and Type II errors have been reduced significantly through multiple inspections. It is further noticed that the values of A_I and A_{II} serve only as qualitative measures of Type I and Type II errors, since they are not directly proportional to P_I and P_{II} .

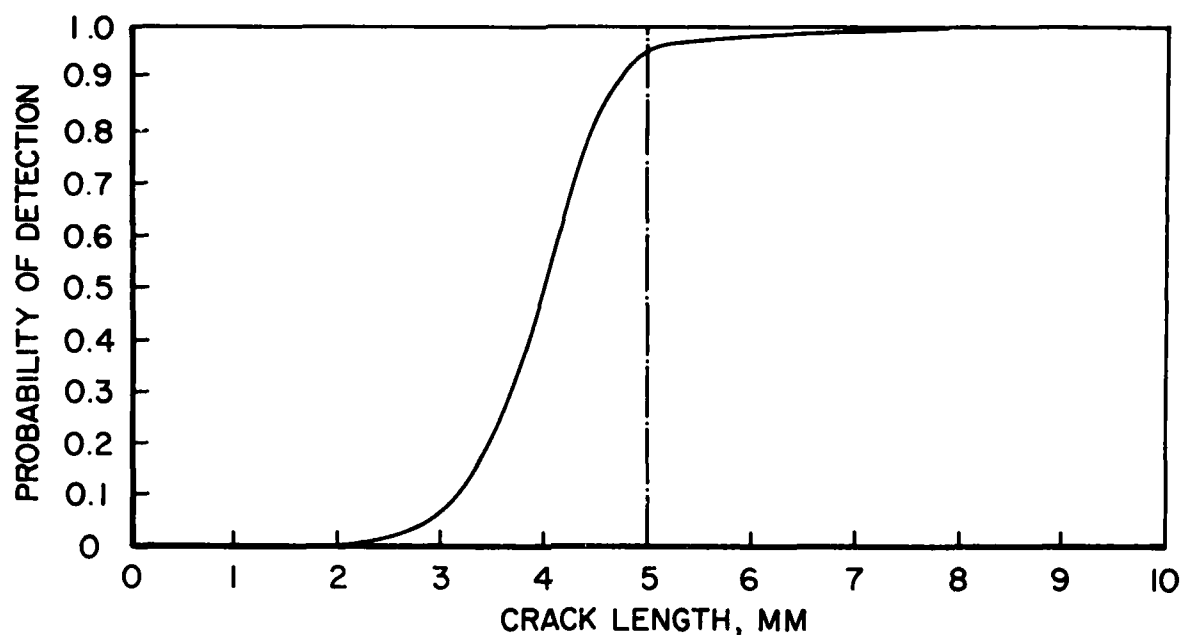


Figure 13(a). Resulting POD Curves Under Three Inspections Using the Union-Intersection Rule: (a) $POD[a; (1U2) \cap 3]$, Weibull $POD(a; 3)$.

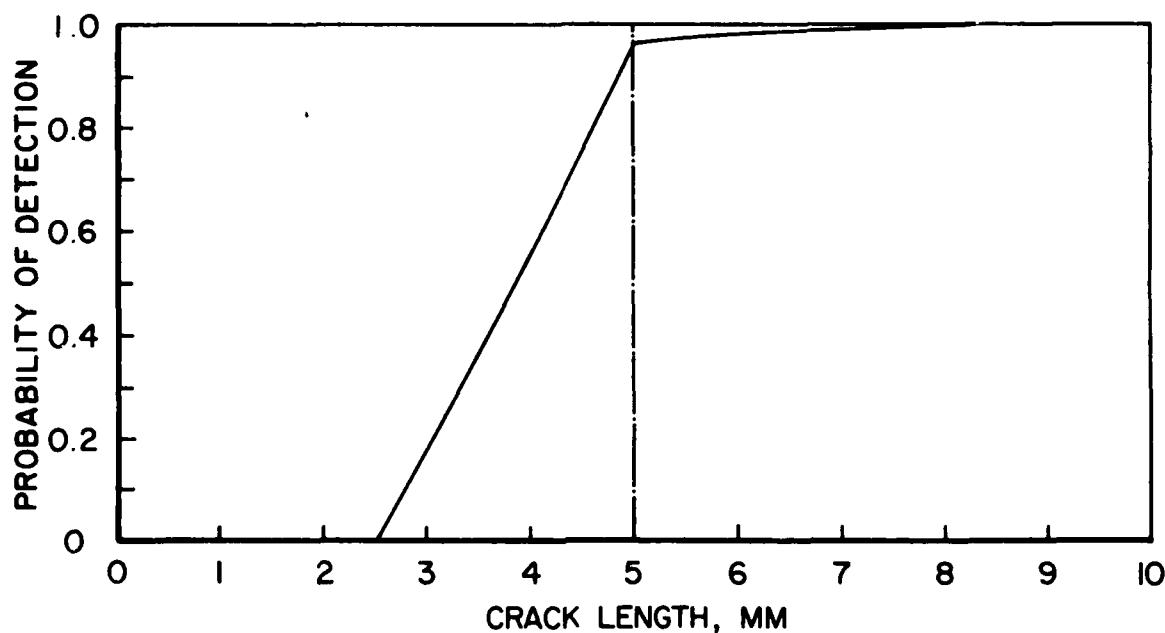


Figure 13(b). Resulting POD Curves Under Three Inspections Using the Union-Intersection Rule: (b) $POD[a; (1U2) \cap 3]$, Straight Line $POD(a; 3)$.

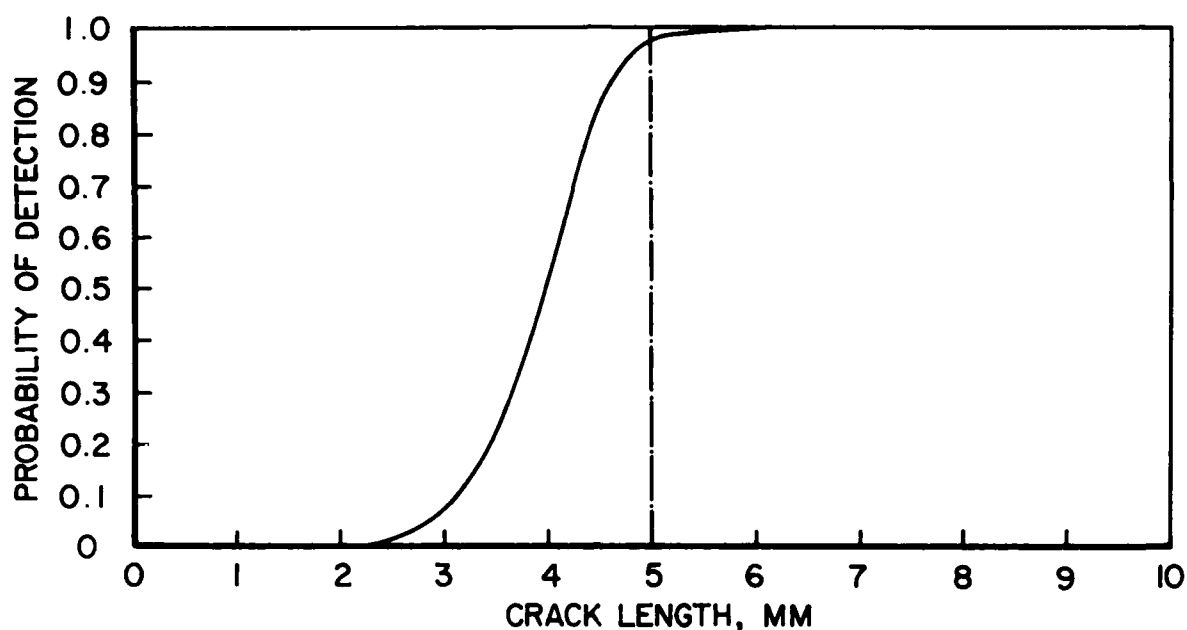


Figure 13(c). Resulting POD Curves Under Three Inspections Using the Union-Intersection Rule: (c) $POD[a; (1U1)\Omega 3]$, Weibull $POD(a; 3)$.

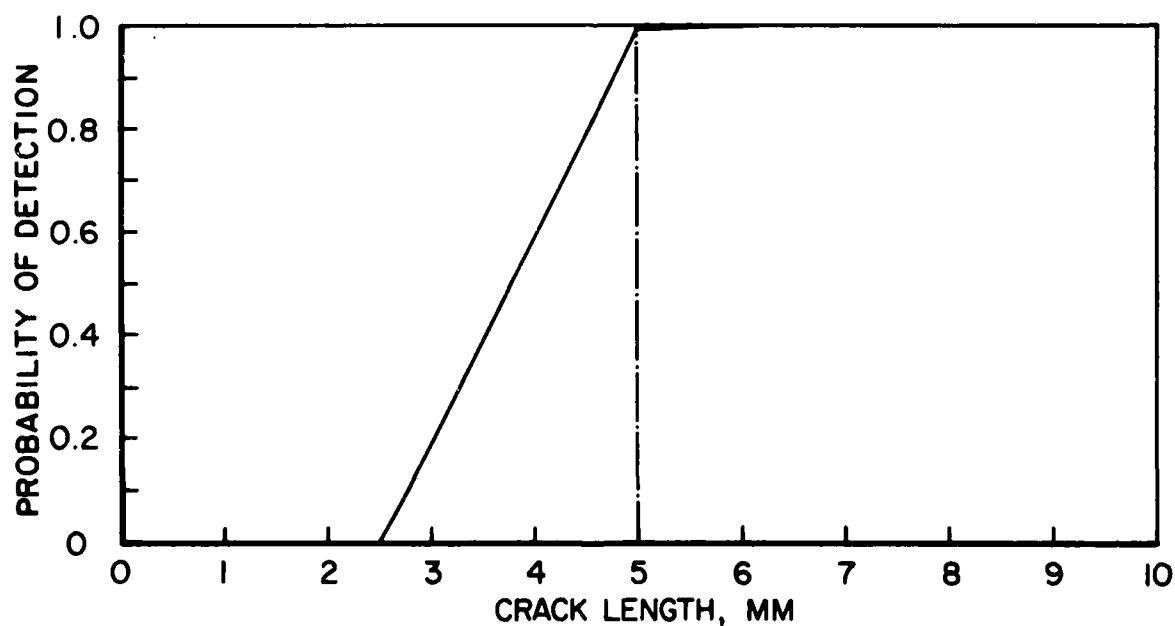


Figure 13(d). Resulting POD Curves Under Three Inspections Using the Union-Intersection Rule: (d) $POD[a; (1U1)\Omega 3]$, Straight Line $POD(a; 3)$.

Tables 2 and 3 indicate a slight increase in the Type I error when the Weibull POD function is applied, (Equation 25) for the third inspection. This is because the detection probability at the inspection limit, a_{NDE} , in Equation 25 is slightly less than 1.0.

Because of the reduction in Type I error using the union rule for $POD(a;1)$ and $POD(a;2)$ it is possible to reduce the inspection limit a_{NDE} . Suppose the inspection limit is reduced to 3.5 mm which corresponds to a 96% detection probability as shown by Curve 4 of Figure 11. Then the average percentage of good components is $P_G=91.4\%$. The $POD(a;3)$ function should be chosen such that it is close to unity at $a=3.5$ mm. Again, Equations 25 and 24 are used with $\alpha_0=8.0$ and $\beta_0=2.89$ mm, $a_1=1.0$ mm, and $a_2=3.5$ mm. These POD curves are shown in Figure 12 as Curve 3 and Curve 4, respectively. The results of A_I , A_{II} , P_I and P_{II} are presented in Table 4. As indicated by Table 4, multiple inspection procedures are capable of reducing both Type I and Type II errors.

TABLE 4

TYPE I AND TYPE II ERRORS; $\beta_1 = 0.46/\text{mm}$, $\beta_2 = 0.46/\text{mm}$,
 $a_{NDE} = 3.5$ mm, $P_G = 91.4\%$

No. of Inspections	Rule	A_I (mm)	A_{II} (mm)	P_I	P_{II}
1		0.435	1.76	1.0×10^{-2}	32.1%
2	U	0.043	2.56	1.49×10^{-3}	48.3%
3*	U-I	0.043	1.124	1.49×10^{-3}	12.9%
3**	U-I	0.044	0.724	1.53×10^{-3}	6.37%
*: $POD(a;3)$ given by Equation 24 with $a_1=1.0$ mm, $a_2=3.5$ mm					
**: $POD(a;3)$ given by Equation 25 with $\alpha_0=8.0$, $\beta_0=2.89$ mm					

As a final example, the $POD(a;1)$ given by Equation 18 is used whereas the $POD(a;2)$ has a lower bound at $a_0=1.5$ mm, i.e.,

$$\begin{aligned} POD(a;2) &= 0 && \text{for } a < a_0 \\ &= 1 - e^{-\beta_1(a-a_0)} && \text{for } a \geq a_0 \end{aligned} \quad (26)$$

where $\beta_1=0.46/\text{mm}$. Both $POD(a;1)$ and $POD(a;2)$ given by Equations 18 and 26 are plotted in Figure 14 as Curves 1 and 2, respectively. The resulting POD curve using the union rule, $POD(a;1 \cup 2)$, is also shown in Figure 14 as Curve 3 (dashed curve). Note that $POD(a;1 \cup 2)$ is identical to $POD(a;1)$ in the region $a < a_0=1.5$ mm.

Then, the same $POD(a;3)$ given by Equations 24 and 25, respectively, are used in conjunction with the intersection rule. The Type I and Type II errors resulting from multiple inspections are shown in Table 5. Table 5 clearly indicates the advantage of multiple inspections in terms of Type I and Type II errors.

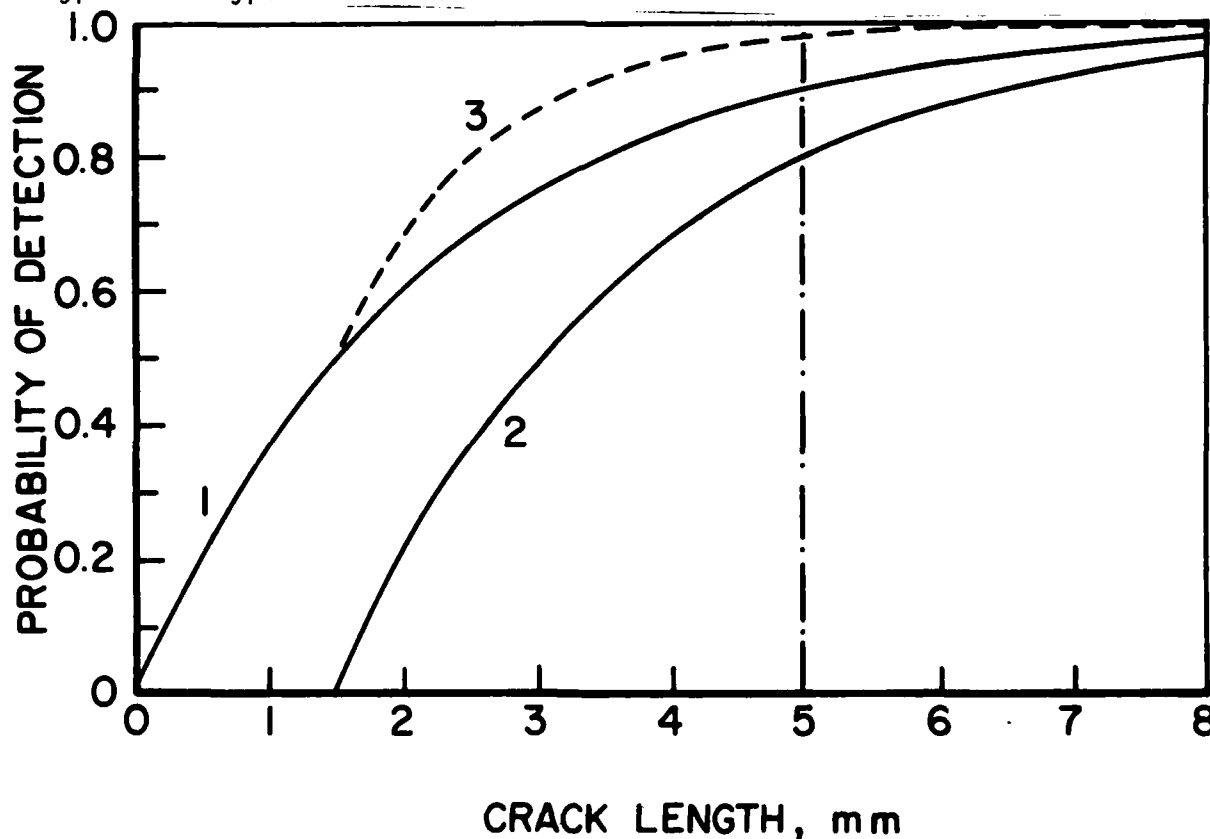


Figure 14. POD Curves for NDE Systems (Curves 1 and 2) and Resulting POD Curve (Curve 3) Under Multiple Inspections.

TABLE 5

TYPE I AND TYPE II ERRORS; $\beta_1 = 0.46/\text{mm}$, $\beta_2 = 0.46/\text{mm}$,
 $a_0 = 1.5 \text{ mm}$, $a_{\text{NDE}} = 5 \text{ mm}$

No. of Inspections	Rule	A_I	A_{II}	P_I	P_{II}
1		0.218	3.04	1.83×10^{-3}	36%
2	U	0.022	3.39	0.26×10^{-3}	39.7%
3*	U-I	0.022	1.12	0.26×10^{-3}	4.6%
3**	U-I	0.023	1.06	0.28×10^{-3}	3.9%
*: POD(a;3) given by Equation 24 with $a_1=2.5 \text{ mm}$, $a_2=5.0 \text{ mm}$					
**: POD(a;3) given by Equation 25 with $\alpha_0=8.0$, $\beta_0=4.13 \text{ mm}$					

SECTION IV

INSPECTION RELIABILITY OF ENGINE DISKS

For gas turbine engine components, such as disks, inspections are performed for each critical location, including bolt holes, cooling holes, rim holes, etc. A disk which consists of a large number of holes is normally retired if at least one hole is rejected by the NDE system. The POD curve established for any one particular NDE system applies to one hole only. Thus, the POD curve for a disk containing a large number of holes differs significantly from that of the NDE system. As a result, one important task in the Retirement-For-Cause analysis is to establish, if possible, the POD curve for a disk from the POD curve for a given NDE system. An exploratory analytical study of this subject follows.

For simplicity of presentation, the analysis is limited to one type of hole (such as bolt holes) to examine the relation between the POD curve of the NDE system and that of a disk. The general approach in dealing with a disk containing bolt holes, cooling holes, rim holes, and other critical locations which are subject to inspection will be presented in a future report.

The acceptance or rejection of a disk depends not only on the POD curve of the NDE system employed but also on the distribution of the flaw length in each hole prior to inspection. In this connection, two extreme cases will be investigated. Both cases are mathematically simple.

Case 1 - Completely Correlated Crack Length: At one extreme, the crack length in a bolt hole is completely correlated with that in other bolt holes in the same disk. Thus, the crack length in each bolt hole of a given disk is identical. However, the crack length varies from disk to disk and it is a random variable across the ensemble of disks as schematically shown in Figure 15(a).

Case 2 - Completely Uncorrelated Crack Length: At another extreme, the crack length varies from one bolt hole to another in the same disk. The crack length in each bolt hole is a statistically independent and identically distributed random variable as schematically shown in Figure 15(b).

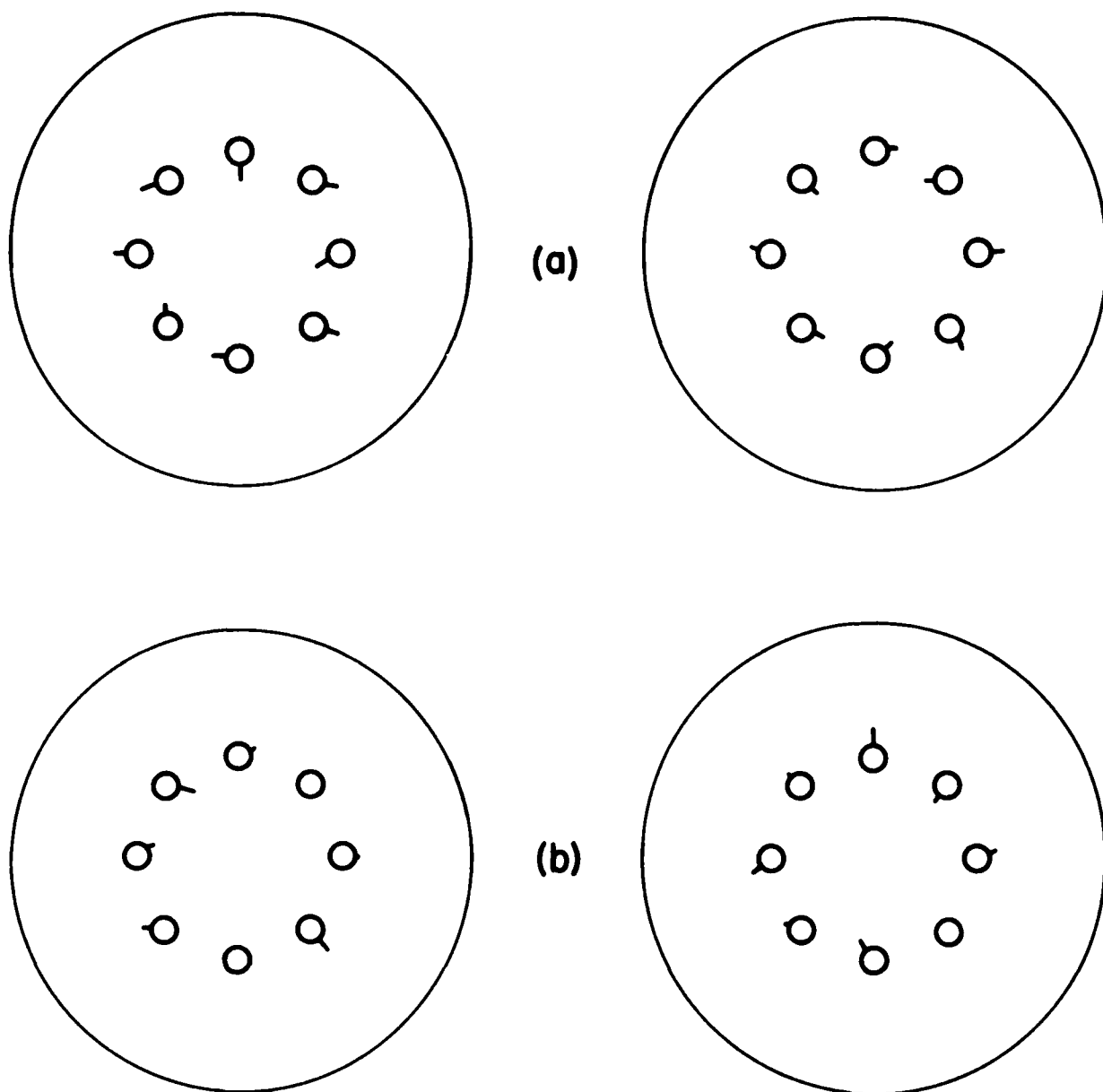


Figure 15. Schematic Distribution of Flaw Length in Bolt Holes; (a) Totally Correlated Crack Length and (b) Totally Uncorrelated Crack Length.

Basically, the statistical variability of the crack length in each bolt hole is contributed to by two major elements; (i) the statistical variability of service loads and (ii) the statistical variability of material properties, including the time to crack initiation, the initial flaw length and the crack propagation. While the service load is a statistical variable, it varies from engine (or disk) to engine (disk) and the loading applied to each bolt hole in the same disk is almost identical. The material properties, however, vary from one bolt hole to another not only in the same disk but also among different disks. Thus, at one extreme, if the statistical variability of material properties is insignificant compared to that of the service load, then the crack length in each bolt hole of the same disk is almost completely correlated as described in Case 1. At the other extreme, if the scatter of the service load is very small compared to the statistical variability of material properties, then the crack length in each hole will be statistically independent, as described in Case 2.

In reality, however, depending on the mission characteristics of a particular type of aircraft, the true situation will lie between the two extreme cases described previously. Theoretically, the exact distribution of the crack length in each bolt hole of a disk prior to inspection can be derived from the statistical distributions of the time to crack initiation, the equivalent defect size, the crack growth rate and the service loads. However, such an approach is analytically complex. A separate report on an analytical RFC approach will be presented later. From the standpoint of NDE reliability for engine components as well as the possible improvement of NDE capability through multiple inspections, these two extreme cases outlined herein are investigated because of their mathematical simplicity. Likewise, a greater insight into the influence of NDE capability on the RFC of engine disks can be achieved from the present investigation. Analytical solutions for the two extreme cases are obtained in the following.

1. COMPLETELY CORRELATED CRACK LENGTH

When the crack length in each bolt hole is identical in the same disk, but varies from disk to disk, the inspection of a disk containing

m holes is equivalent to inspecting a crack length m times (one time for each hole) independently, using the union rule. This is because the disk will be retired if any hole is rejected by the NDE system.

Let $POD(a;1)$ be the POD curve associated with the particular NDE system employed for inspection. Then the POD curve for a disk containing m bolt holes, denoted by $POD(a;Um)$, is obtained from $POD(a;1)$ using the union rule,

$$POD(a;Um) = 1 - [1 - POD(a;1)]^m \quad (27)$$

A good disk is defined as a disk in which the crack length in each bolt hole is smaller than the inspection limit a_{NDE} . If $F(a)$ and $f(a)$ denote the distribution function and the probability density function, respectively, of the pre-inspection flaw length in the bolt hole, then the probability that a disk is good is given by

$$P_G = P[a \leq a_{NDE}] = \int_0^{a_{NDE}} f(x) dx = F(a_{NDE}) \quad (28)$$

in which $F(a_{NDE})$ is the distribution function of the pre-inspection flaw length in the hole evaluated at a_{NDE} . Note that $F(a_{NDE})$ can also be interpreted as the average percentage of good disks prior to inspection.

The Type I and Type II errors, P_I and P_{II} , of a disk are given by

$$\left. \begin{aligned} P_I &= \int_{a_{NDE}}^{\infty} f(x) [1 - POD(x;1)]^m dx \\ P_{II} &= \int_0^{a_{NDE}} f(x) \left\{ 1 - [1 - POD(x;1)]^m \right\} dx \end{aligned} \right\} \quad (29)$$

Numerical examples will be given to demonstrate the inspection reliability in terms of Type I and Type II errors for engine disks. Since Type I and Type II errors depend on both the POD curve of the NDE system and the distribution of the pre-inspection flaw length, various types of POD functions will be investigated. Thus, one can determine the direction in which the POD curve of the NDE system should be improved to achieve a maximum benefit from the inspection.

It should be emphasized that the numerical examples given in Sections IV and V are mainly for illustration. The range of the flaw length for POD curves employed is far from the current gas turbine engine inspection technology, although the POD curves are obtained from available data. Furthermore, the flaw length in disk holes is not realistic. However, the conclusions and trends obtained for both Type I and Type II errors will not be altered. This is because when the flaw length in holes and the flaw length for POD curves are reduced by the same factor γ , not only the Type I and Type II errors remain the same, but also the average percentage of good holes at the time of inspection maintenance remains identical. Realistic examples for the current state of technology in engine disk inspections will be presented in Section VI.

2. EXAMPLE NO. 3

a. Exponential POD Function

The exponential-type POD curve associated with the eddy-current inspection of aluminum plate given by Equation 18 with $\beta_1=0.46/\text{mm}$ is considered, i.e.,

$$\text{POD}(a;1) = 1 - e^{-\beta_1 a} \quad ; \quad a \geq 0 \quad (30)$$

From Equation 30, the detection probability for the inspection limit $a_{\text{NDE}}=5 \text{ mm}$ is 90%.

The same pre-inspection density function, $f(a)$, for the flaw length in each hole as given by Equation 14 with $\lambda=0.7/\text{mm}$ is used herein. With such a pre-inspection flaw length distribution, there are, on the average, 3% of disks that will have a crack length exceeding the inspection

limit $a_{NDE}=5$ mm, i.e., $P_G=97\%$ in Equation 28. The resulting POD curve for the disk, $POD(a;U10)$, containing ten bolt holes, i.e., $m=10$ given by Equation 27, is plotted in Figure 16. Also shown in Figure 16 are the $POD(a;1)$ of the NDE system and the pre-inspection density function of the flaw length $f(a)$. It is observed that the bandwidth of the POD curve for a disk, $POD(a;U10)$, is much smaller than that of the POD curve of the NDE system, $POD(a;1)$. With the inspection limit $a_{NDE}=5$ mm, the Type I and Type II errors (P_I and P_{II}), as well as the average percentage of good disks, P_G , are presented in Table 6.

In the first row of Table 6, the disk is assumed to consist of only one hole whereas the second row represents the results for ten bolt holes in one disk (e.g., TF 33 disk). A comparison between the results in the first and the second rows of Table 6 indicates that the Type I error reduces drastically from 1.83×10^{-3} for one bolt hole to 4.1×10^{-13} for a disk with ten bolt holes. However, the Type II error increases from 36.8% to 83%.

Since the Type I error is extremely small for the disk, one can reduce the inspection limit a_{NDE} in order to reduce the Type II error while keeping the Type I error at an acceptable level. The results using different values of the inspection limit, a_{NDE} , are presented in Table 6. As expected, the Type II error reduces and the Type I error increases as the inspection limit a_{NDE} decreases.

Note that the Type II error is the probability of rejecting a disk that is a good disk, i.e.,

$$P_{II} = P[R \cap G] = P[R, G] \quad (31)$$

in which $\{R\}$ =the event of rejecting a disk and $\{G\}$ =the event that the disk is good. As the values of the inspection limit, a_{NDE} , vary, the average percentage of good disks changes accordingly. Therefore, another measure of the Type II error, referred to as the conditional Type II error, may be of interest. The conditional Type II error, denoted by P_{II}^* , is the probability of rejecting a disk under the condition (or

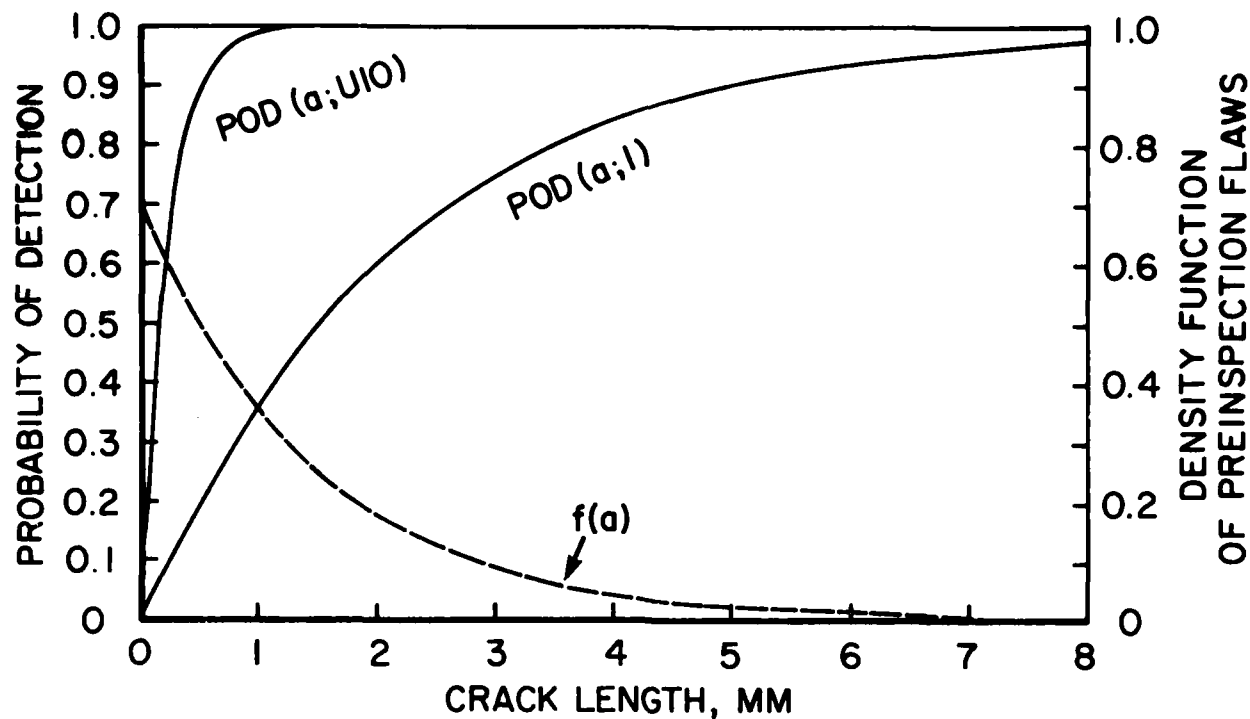


Figure 16. Exponential POD Curves for the NDE System and Disk.

TABLE 6

TYPE I AND TYPE II ERRORS FOR DISK; EXPONENTIAL POD CURVE
WITH $\beta_1 = 0.46/\text{mm}$

No. of Holes	a_{NDE} (mm)	P_G	P_I	P_{II}	P_{II}^* (P_{II}/P_G)
1	5	97.0%	1.83×10^{-3}	36.8%	37.9%
10	5	97.0%	4.1×10^{-13}	83.0%	85.5%
10	4	94.0%	8.2×10^{-11}	80.7%	85.8%
10	3	87.8%	1.64×10^{-8}	74.5%	85.1%
10	2	75.3%	3.3×10^{-6}	62.0%	82.3%
10	1.5	65.0%	4.7×10^{-5}	51.0%	78.4%
10	1.0	50.0%	6.6×10^{-4}	37.2%	74.4%

given) that the disk is good. Hence, we have from Equations 28 and 31 that

$$P_{II}^* = P_{II}/P_G \quad (32)$$

The conditional Type II error, P_{II}^* , is also given in Table 6.

The results shown in Table 6 are striking. It appears that the Type I error for a disk is insignificant whereas the Type II error may be a serious problem. Likewise, the inspection limit a_{NDE} should be determined by the POD curve for the disk rather than the POD curve of the NDE system.

b. Weibull POD Function

The sensitivity of Type I and Type II errors for disks with respect to different types of POD function is studied herein. Let us consider a Weibull-type POD function for the NDE system as follows;

$$POD(a;1) = 1 - \left\{ \exp \left(\frac{a}{\beta_0} \right)^{\alpha_0} \right\} ; \quad a \geq 0 \quad (33)$$

in which α_0 is the shape parameter representing the bandwidth of the POD curve and β_0 is the scale parameter representing the central location of the POD curve. To be consistent with the previous example, we choose $\alpha_0=3.0$ and $\beta_0=3.79$ mm such that the inspection limit, $a_{NDE}=5$ mm, corresponds to a 90% detection probability. The distribution of the pre-inspection flaw length is identical to that considered in the previous example.

The Weibull POD curve (Equation 33), the POD curve for the disk $POD(a;U10)$ (Equation 27), and the density function of the pre-inspection flaw length are shown in Figure 17. Unlike the exponential POD function given by Equation 30, the Weibull function is an S shaped function; hence the areas A_I and A_{II} are smaller.

The results of Type I and Type II errors, conditional Type II error, and the average percentage of good disks before inspection, are shown in Table 7 for different values of the inspection limit a_{NDE} . The

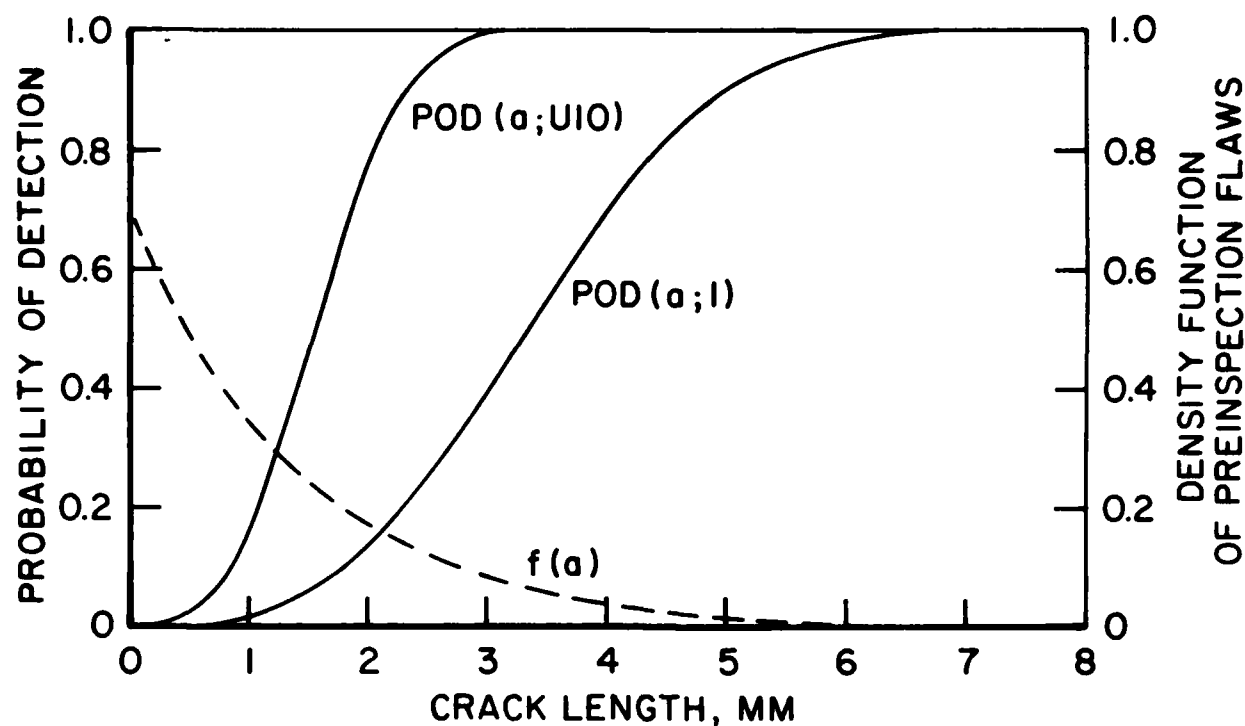


Figure 17. Weibull POD Curves for the NDE System and Disk.

TABLE 7

TYPE I AND TYPE II ERRORS FOR DISK: WEIBULL POD CURVE WITH
 $\alpha_0 = 3.0$, $\beta_0 = 3.79$ mm

No. of Holes	a_{NDE} (mm)	P_G	P_I	P_{II}	P_{II}^* (P_{II}/P_G)
1	5	97.0%	9.2×10^{-4}	10.3%	10.6%
10	5	97.0%	1.5×10^{-13}	32.0%	32.9%
10	4	94.0%	3.4×10^{-8}	30.0%	31.9%
10	3	87.8%	9.7×10^{-5}	23.8%	27.1%
10	2.5	82.6%	1.4×10^{-3}	18.76%	22.7%
10	2	75.3%	1.1×10^{-2}	12.5%	16.6%
10	1	50.0%	1.54×10^{-1}	1.76%	3.5%

same phenomenon is observed in Table 7 that the Type I error for a disk is about ten orders of magnitude smaller than that for a hole for $a_{NDE}=5$ mm. Such a difference will be manifested drastically as the number of bolt holes increases. A comparison between Tables 6 and 7 indicates that the Weibull POD curve is more beneficial in terms of the Type II error. This is because its bandwidth is smaller. However, the Type I error increases more rapidly as the value of the inspection limit a_{NDE} reduces.

c. Exponential POD Function with a Lower Bound

During the first few inspection maintenances, the majority of flaws are still very small, and the rejection of good disks (Type II error) is of main concern, as demonstrated in the previous two examples. Therefore, we shall consider a POD function having a lower bound below which the crack length can not be detected. Let the POD curve be of the exponential type with a lower bound a_0 ,

$$\begin{aligned} \text{POD}(a;l) &= 0 & a < a_0 \\ &= 1 - \exp\{-\beta_1(a-a_0)\} & a > a_0 \end{aligned} \quad (34)$$

in which $a_1 = 1$ mm and $\beta_1=0.46/\text{mm}$. Such a POD curve is identical to the one considered in the first example except that the curve is shifted 1 mm to the right-hand side. The pre-inspection flaw distribution is identical to that of the previous example.

The POD curve for the NDE system (Equation 34), the resulting POD curve for a disk, and the pre-inspection density function of the flaw length are displayed in Figure 18. The inspection limit corresponding to a 90% detection probability is $a_{NDE}=6$ mm. The results of Type I and Type II errors, the conditional Type II error, and the average percentage of good disks are presented in Table 8 for different values of the inspection limit a_{NDE} . A comparison between Tables 6 and 8

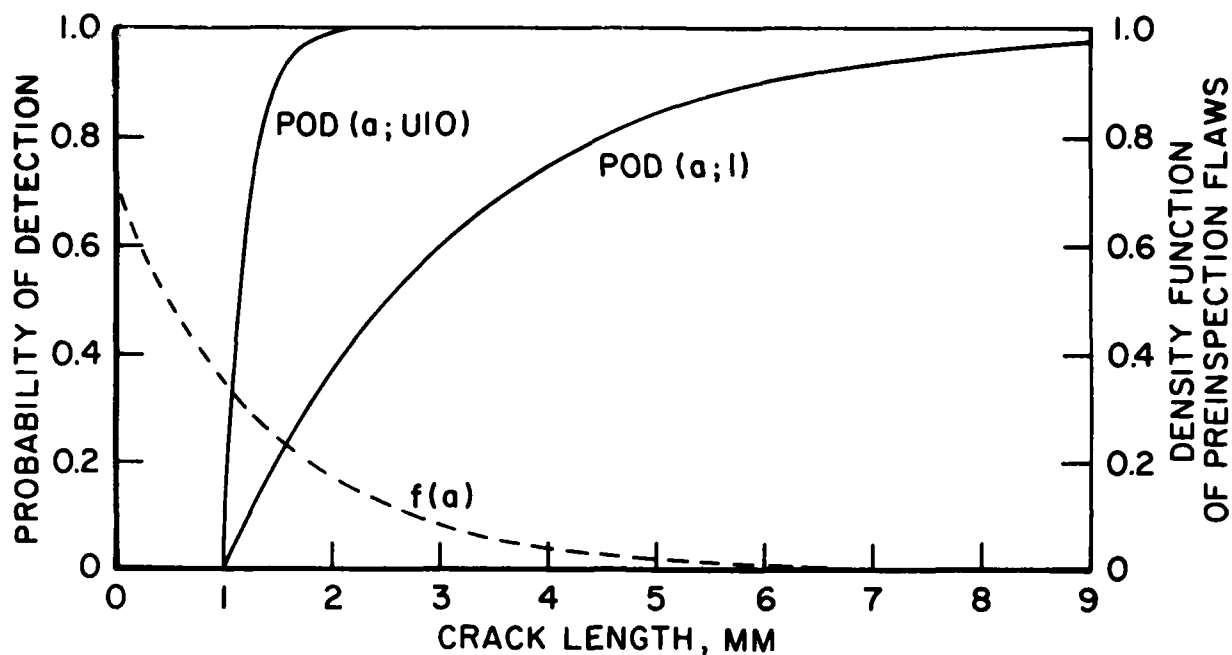


Figure 18. Exponential POD Curves with Lower Bound at 1 mm for the NDE System and Disk.

TABLE 8

TYPE I AND TYPE II ERRORS: EXPONENTIAL POD CURVE WITH LOWER
BOUND AT $a_0 = 1$ mm, $\beta_1 = 0.46/\text{mm}$

No. of Holes	a_{NDE} (mm)	P_G	P_I	P_{II}	P_{II}^* (P_{II}/P_G)
1	6	98.5%	9.1×10^{-4}	18.3%	18.5%
10	6	98.5%	2.0×10^{-13}	41.6%	42.3%
10	5	97.0%	4.1×10^{-11}	40.0%	41.2%
10	4	94.0%	8.15×10^{-9}	37.9%	39.3%
10	3	87.8%	1.6×10^{-6}	30.8%	35.0%
10	2	75.3%	3.2×10^{-4}	18.4%	24.4%
10	1.5	65.0%	4.6×10^{-3}	8.6%	13.2%

indicates that the POD curve with a lower bound does improve the Type II error for disks whereas the Type I error is still insignificant.

d. Narrow-Banded Weibull POD Function

For the purpose of illustration, an hypothetical Weibull POD curve for an NDE system with a narrow bandwidth is considered,

$$\text{POD}(a;1) = 1 - \exp \left[-\left(\frac{a}{\beta_0} \right)^{\alpha_0} \right] ; \quad a \geq 0 \quad (35)$$

in which $\alpha_0=8.0$ and $\beta_0=2.48$ mm. Such a narrow-banded POD curve may be achieved by an NDE system when the bolt hole is replicated. The POD curve in Equation 35 and the $\text{POD}(a;U10)$ for a disk are displayed in Figure 19. The pre-inspection flaw distribution is identical to that of the previous example. The results of Type I and Type II errors and the average percentage of good disks are presented in Table 9. Again, the Type I error reduces drastically for a disk as compared to that for a hole. The Type II error, however, is significantly smaller than all the previous cases, and it may be acceptable for the RFC system.

e. Conclusions

The conclusions obtained from the previous examples are summarized below: (1) The difference in the Type I error is dramatic between inspecting a disk with ten bolt holes and inspecting a single bolt hole. The difference becomes more radical as the number of bolt holes in a disk increases. (2) The Type I error for disks containing many bolt holes appears to be insignificant. (3) The Type II error for disks may be of practical concern. However, if the bandwidth of the POD curve of the NDE system is narrow, as indicated by the last example, the Type II error may be acceptable. (4) The direction for improving the NDE system in applications to RFC of engine components appears to be the bandwidth of the POD curve rather than the value of the inspection limit that corresponds to a 90% detection probability and a 95% confidence level as specified by damage tolerance requirements.

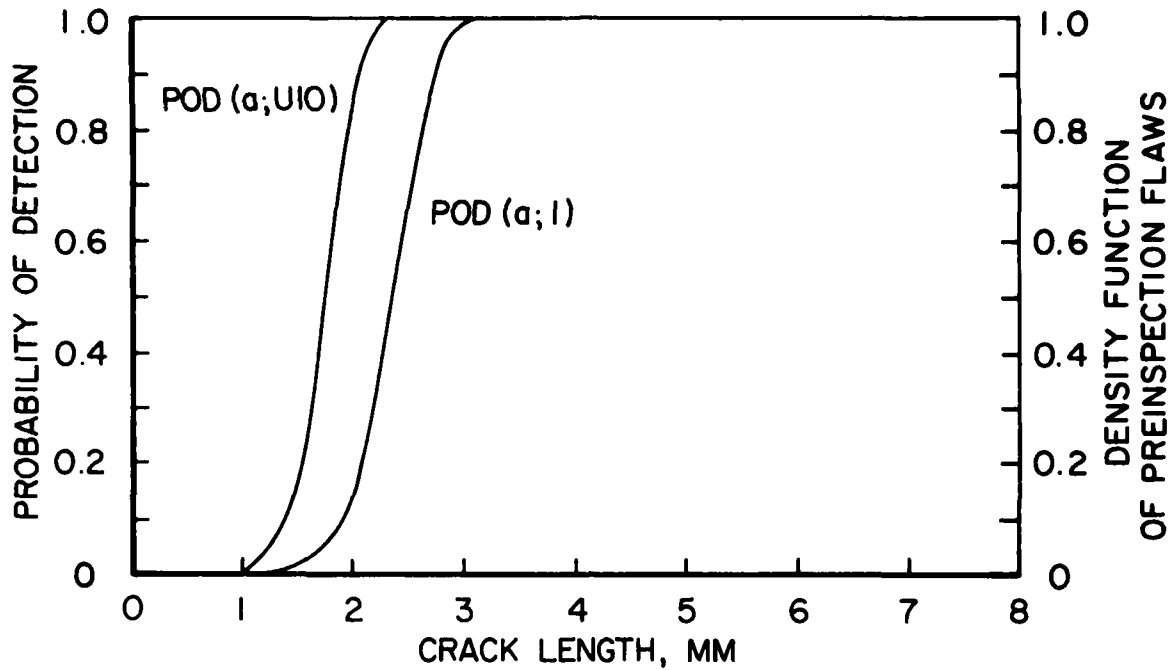


Figure 19. Narrow-Banded Weibull POD Curves for the NDE System and Disk.

TABLE 9

TYPE I AND TYPE II ERRORS: NARROW-BANDED WEIBULL POD CURVE WITH
 $\alpha_0 = 8.0$, $\beta_0 = 2.48$ mm

No. of Holes	a_{NDE} (mm)	P_G	P_I	P_{II}	P_{II}^* (P_{II}/P_G)
1	2.75	85.4%	4.4×10^{-2}	3.8%	4.4%
10	2.75	85.4%	1.77×10^{-13}	15.3%	17.9%
10	2.5	82.6%	7.69×10^{-8}	12.5%	15.1%
10	2.25	79.3%	7.53×10^{-5}	9.2%	11.0%
10	2.15	77.8%	4.23×10^{-4}	7.7%	9.9%
10	2.05	76.2%	1.6×10^{-3}	6.2%	8.1%
10	2.0	75.3%	2.8×10^{-3}	5.5%	7.3%

3. TOTALLY UNCORRELATED CRACK LENGTH

At another extreme, the crack length varies from one bolt hole to another not only within the same disk but also across the ensemble of disks. The crack length in each bolt hole is a statistically independent and identically distributed random variable as shown in Figure 15(b). In the case of totally correlated crack length, the average percentage of good disks is identical to the average percentage of good holes. However, for the case of totally uncorrelated crack length, the average percentage of good disks is significantly smaller than that of the bolt holes. To appreciate the difference, consider 100 bolt holes, each with a random crack length, in which ten of them are bad holes, i.e., 90% good holes. If a disk contains ten bolt holes and the 100 bolt holes are randomly distributed into ten disks, then the number of good disks ranges from nine (all the bad holes are put into one disk) to zero (one bad hole in each disk). Therefore, the percentage of good disks ranges from 0% to 90%. As a result, given the same pre-inspection distribution of the flaw length, the return-to-service interval should be shorter (or the inspection limit a_{NDE} should be larger) to maintain the same level of Type I error as the previous case.

Let a_j be the crack length in the j th bolt hole of a disk. Then the probability, P_G , that a disk consisting of m bolt holes is a good disk is given by

$$P_G = P \left[\bigcap_{j=1}^m \{a_j \leq a_{NDE}\} \right] \quad (36)$$

Since a_j ($j=1,2,\dots,m$) are statistically independent and identically distributed random variables, Equation 36 becomes

$$P_G = \prod_{j=1}^m P[a_j \leq a_{NDE}] = [F(a_{NDE})]^m \quad (37)$$

in which $F(a)$ is the distribution function of the crack length in a hole prior to inspection.

If $f(a)$ denotes the probability density function of the crack length in a hole, the Type I error, P_I , for a disk is the probability of accepting a bad disk, and it can be expressed as

$$P_I = \left\{ \int_0^{\infty} f(x)[1-POD(x;1)]dx \right\}^m - \left\{ \int_0^{a_{NDE}} f(x)[1-POD(x;1)]dx \right\}^m \quad (38)$$

in which the first integral term is the probability of accepting a bolt hole (regardless of good or bad hole), and hence, the first term represents the probability of accepting a disk or m bolted holes (again regardless of good or bad disk). The second integral term of Equation 38 is the probability of accepting a good hole, and hence, the second term indicates the probability of accepting a good disk or m good holes.

If the NDE system is able to detect all the cracks larger than the inspection limit a_{NDE} , i.e., $POD(a;1)=1$ for $a \geq a_{NDE}$, then it follows from Equation 38 that the Type I error is zero (i.e., $P_I=0$). A schematic flow chart presented in Figure 20 will help to explain Equations 38 and 39.

The Type II error for a disk is the probability of rejecting a good disk, which can be expressed as follows;

$$P_{II} = P_G - \left\{ \int_0^{a_{NDE}} f(x)[1-POD(ax;1)]dx \right\}^m \quad (39)$$

in which $P_G = [F(a_{NDE})]^m$ given by Equation 37 is the probability that the disk is good. The second term on the right-hand side of Equation 39 is the probability of accepting a good disk (Figure 20). If the NDE system cannot detect any crack length below the inspection limit a_{NDE} , i.e., $POD(a;1)=0$ for $a \leq a_{NDE}$, then it follows from Equation 39 that the Type II error is zero, i.e., $P_{II}=0$.

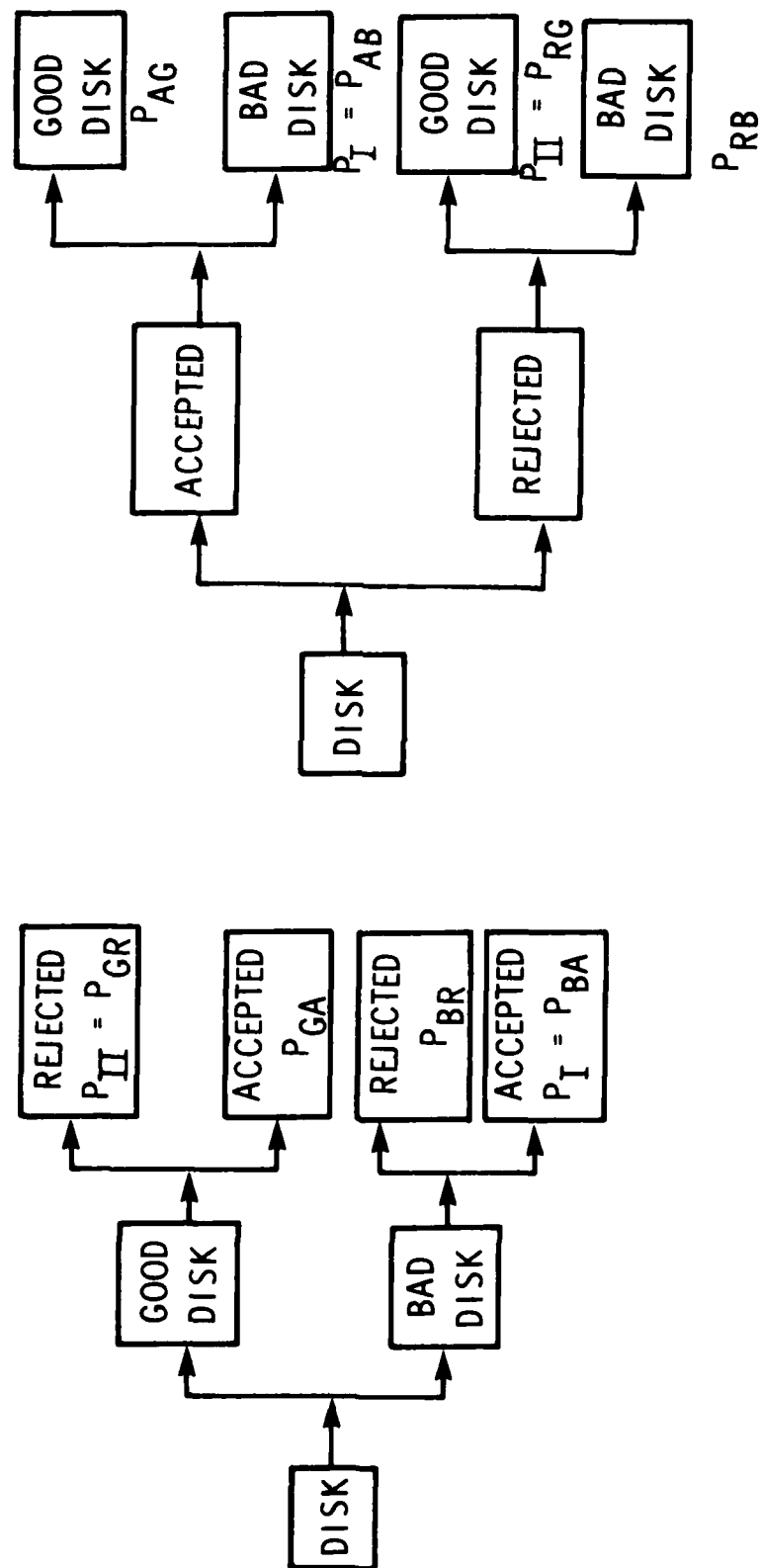


Figure 20. Schematic Description of Type I and Type II errors for Independent Flaw Length.

Since the acceptance of a disk implies the acceptance of all m bolt holes in a disk, the crack length of a disk, denoted by a_m , can be described by the maximum crack length of m holes, i.e.,

$$a_m = \max_{1 \leq j \leq m} (a_j) \quad (40)$$

Thus, a disk is good if its crack length a_m is smaller than the inspection limit a_{NDE} . The distribution function, $F_m(a)$, of the crack length a_m of a disk can be derived from that of the crack length of a hole, $F(a)$, using the extreme value distribution,

$$F_m(a) = P[a_m \leq a] = P \left[\bigcap_{j=1}^m \{a_j \leq a\} \right] = [F(a)]^m \quad (41)$$

The probability density function of the crack length a_m of a disk is given by $f_m(a) = dF_m(a)/da$ and it follows from Equation 41 that

$$f_m(a) = m[F(a)]^{m-1} f(a) \quad (42)$$

in which $f(a)$ is the probability density function of the crack length in the bolt hole.

Therefore, the probability that the disk is good is given by

$$P_G = P[a_m \leq a_{NDE}] = [F(a_{NDE})]^m \quad (43)$$

in which Equation 41 has been used. As expected, P_G derived in Equation 43 is identical to Equation 37.

While it is possible to describe the crack length of a disk, a_m , the POD curve for a disk loses its meaning in the present case because of the following reasons: (1) The inspection of a disk implies the

inspections of m bolt holes in which the crack length varies independently from one hole to another; and (2) The inspection of a disk is not identical to the inspection of the crack length a_m of the disk. As a result, the POD curve for a disk does not exist. Consequently, both the capability of an NDE system and the inspection reliability for a disk should be described in terms of Type I and Type II errors.

4. EXAMPLE No. 4

a. Various POD Functions

For the purpose of comparison between the two extreme cases investigated previously, the same numerical example for the case of totally correlated crack length with the exponential POD curve, and the distribution of the pre-inspection flaw length in each hole displayed in Figure 16, are considered. Both curves are also shown in Figure 21 as the dotted curve and Curve 1, respectively, along with the distribution of the pre-inspection flaw length of a disk (Equation 42) shown as Curve 2. It can be observed from Figure 21 that the distribution of the pre-inspection flaw length for a disk is shifted to the right-hand side, indicating a larger percentage of bad disks than that of bad holes.

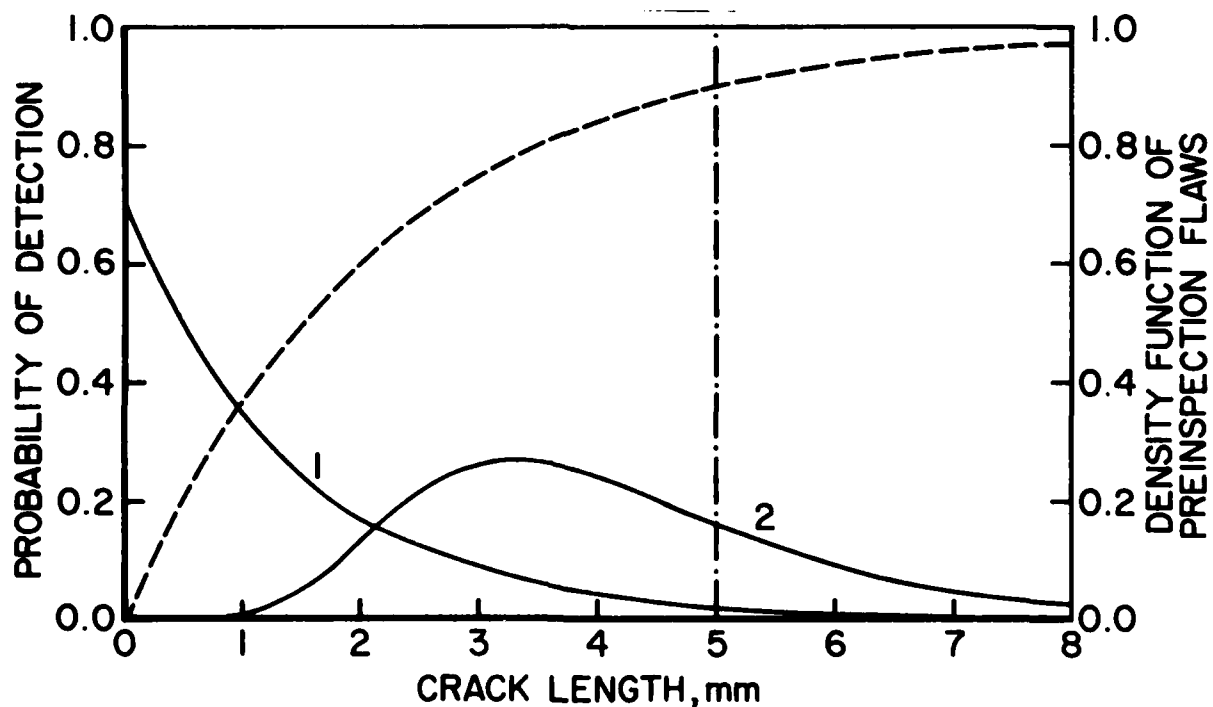


Figure 21. Distributions of Pre-inspection Flaw Length for Bolt Hole and Disk; $\lambda = 0.7/\text{mm}$.

The average percentage of good disks, P_G , is obtained by substituting Equation 14 into Equation 43,

$$P_G = [1 - \exp(-\lambda a_{NDE})]^m \quad (44)$$

and the results are given in Table 10 for different values of the inspection limit a_{NDE} . A comparison between Tables 6 and 10 indicates a substantial reduction of the average percentage of good disks prior to inspection, when the crack length in each hole is statistically independent.

TABLE 10

TYPE I AND TYPE II ERRORS FOR TOTALLY UNCORRELATED CRACK LENGTH;
EXPONENTIAL POD CURVE WITH $\beta_1 = 0.46/\text{mm}$ and $\lambda = 0.7/\text{mm}$

No. of Holes	a_{NDE} (mm)	P_G	P_I	P_{II}	P_{II}^* (P_{II}/P_G)
1	5	97.0%	1.830×10^{-3}	36.8%	37.9%
10	5	73.6%	0.190×10^{-3}	72.9%	99.0%
10	4	53.4%	0.592×10^{-3}	52.8%	98.9%
10	3	27.1%	1.720×10^{-3}	26.6%	98.2%
10	6	86.0%	0.605×10^{-4}	85.3%	99.2%
10	7	92.8%	0.190×10^{-4}	92.2%	99.4%
10	8	96.4%	0.597×10^{-5}	95.72%	99.3%
10	9	98.2%	0.187×10^{-5}	97.5%	99.29%

The Type I and Type II errors can be obtained by substituting Equations 14 and 30 into Equations 38 and 39; with the results

$$P_I = \left(\frac{\lambda}{\lambda + \beta_1} \right)^m \left\{ 1 - \left[1 - e^{-(\lambda + \beta_1)a_{NDE}} \right]^m \right\} \quad (45)$$

$$P_{II} = P_G - \left(\frac{\lambda}{\lambda + \beta_1} \right)^m \left[1 - e^{-(\lambda + \beta_1)a_{NDE}} \right]^m \quad (46)$$

in which P_G is given in Equation 44.

The results of Type I and Type II errors as well as the conditional Type II error are presented in Table 10 for different values of the inspection limit a_{NDE} .

Although the Type I error at $a_{NDE} = 5$ mm for a disk is smaller than that for a hole in Table 10, the improvement is by no means as significant as that shown in Table 6. It is impossible to achieve the kind of Type I error shown in Table 6, even when the inspection limit a_{NDE} is increased to 9 mm. While the Type II error, P_{II} , for a disk at $a_{NDE} = 5$ mm is 72.9%, the conditional Type II error, P_{II}^* , is 99% because the average percentage of good disks is only 73.6%. In other words, if we know that the disk is good, the probability of rejecting it is 99%. The last column of Table 10 indicates that the Type II error is extremely bad when the POD curve of the NDE system is the exponential function and the pre-inspection crack length in each hole is statistically independent.

In the first few inspection maintenances, the average percentage of bad disks is usually very small because of safety considerations. Thus, the example considered previously may be more representative when the disk is in service for a longer period of time. We shall investigate the situation in which the pre-inspection flaw length at holes is reduced. In this connection, the same exponential distribution, Equation 14, will

be used, but with a smaller average flaw length, i.e., $1/\lambda = 1.0$ mm or $\lambda = 1.0/\text{mm}$, as shown in Figure 22 by Curve 1. Also plotted in Figure 22 as Curve 2 is the distribution of the pre-inspection flaw length for a disk. The average percentage of good disks for $a_{\text{NDE}} = 5$ mm prior to inspection is computed from Equation 44 as 93.46%. The same POD curve employed in the previous example is used herein and plotted as a dashed curve in Figure 22.

The results of the average percentage of good disks, Type I and Type II errors, and conditional Type II error are presented in the upper part of Table 11 for different values of the inspection limit a_{NDE} . Unlike Table 6, the Type I error in Table 11 improves only slightly at $a_{\text{NDE}} = 5$ mm for a disk and then deteriorates as the inspection limit reduces. Likewise, both the Type II error and the conditional Type II error are too high for practical applications.

Instead of the exponential POD curve employed above, the Weibull-type POD curve shown in Figure 17 as $\text{POD}(a;1)$, i.e., $\alpha_0 = 3.0$ and $\beta_0 = 3.79$ mm, is considered. The results of Type I error, Type II error, and conditional Type II error are presented in the lower part of Table 11. It is observed that the Type I error for a disk is worse than that for a hole at $a_{\text{NDE}} = 5$ mm, and it becomes much worse as the inspection limit a_{NDE} reduces. However, the Type II error improves over that of the previous example, although it is still quite significant.

Finally, let us consider a narrow-banded Weibull-type POD curve as shown by Curve 1 of Figure 12, i.e., $\alpha_0 = 8.0$ and $\beta_0 = 4.13$ mm. The results are shown in Table 12. Table 12 demonstrates a significant improvement over Table 11, indicating the importance of the bandwidth of the POD curve. In Table 12, both Type I and Type II errors may be acceptable. In reality, the narrow-band POD curve used in this example, i.e., $\alpha_0 = 8.0$ and $\beta_0 = 4.13$ mm, may not be achieved by an NDE system. Fortunately, however, such a narrow-banded POD curve can be established by two inspections using the intersection rule described previously in which the rejected holes may be cleaned up, polished or even replicated before the second inspection, as described in the next section.

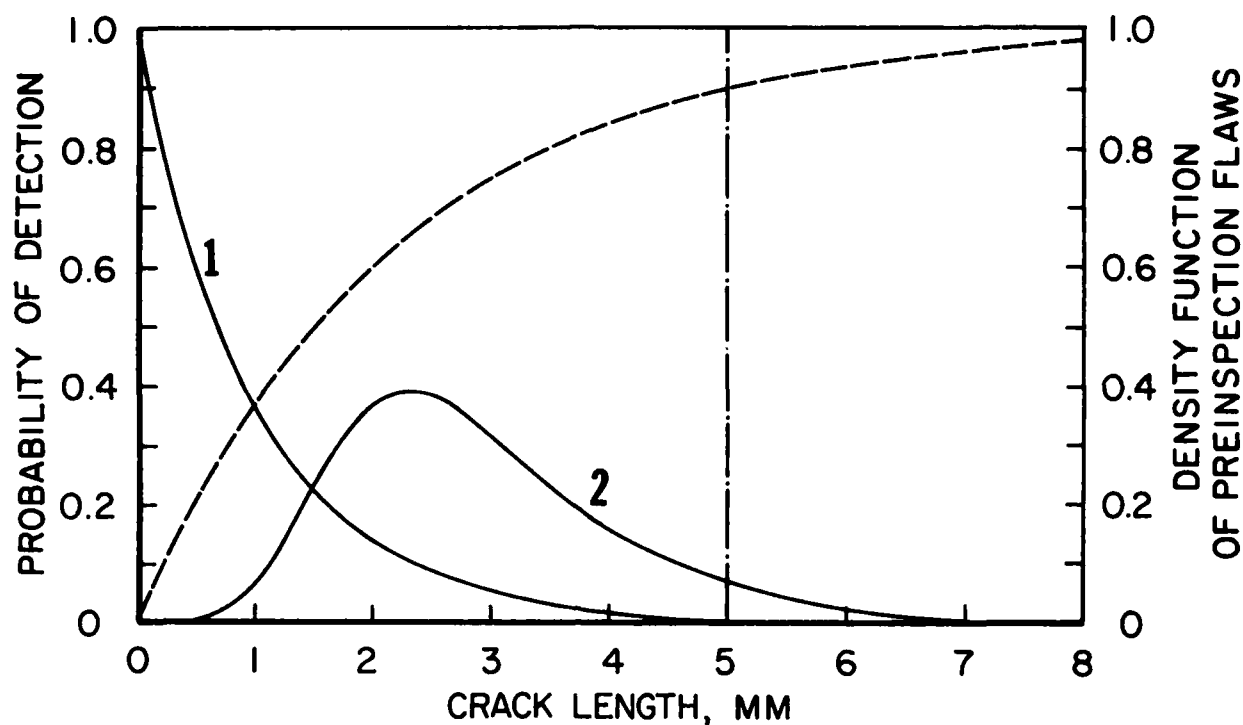


Figure 22. Distribution of Pre-inspection Flaw Length for Bolt Hole and Disk; $\lambda = 1.0/\text{mm}$.

TABLE 11
TYPE I AND TYPE II ERRORS FOR TOTALLY UNCORRELATED CRACK LENGTH
WITH $\lambda = 1.0/\text{mm}$

EXPONENTIAL TYPE POD CURVE; $\beta_1 = 0.46/\text{mm}$

No. of Holes	a_{NDE} (mm)	P_G	P_I	P_{II}	P_{II}^* (P_{II}/P_G)
1	5	99.33%	4.60×10^{-4}	30.9%	31.1%
10	5	93.46%	1.53×10^{-4}	91.2%	97.6%
10	4	83.12%	6.50×10^{-4}	80.9%	97.3%
10	3	60.00%	2.60×10^{-3}	58.0%	97.0%
WEIBULL TYPE POD CURVE; $\alpha_0 = 3.0$, $\beta_0 = 3.79 \text{ mm}$					
1	5	99.33%	2.60×10^{-4}	6.1%	6.14%
10	5	93.46%	1.40×10^{-3}	43.7%	46.76%
10	4	83.12%	1.42×10^{-2}	34.6%	41.6%
10	3	60.00%	8.90×10^{-2}	18.9%	31.5%

TABLE 12

TYPE I AND TYPE II ERROR FOR TOTALLY UNCORRELATED CRACK LENGTH
 WITH $\lambda = 1.0/\text{mm}$ AND NARROW-BANDED WEIBULL-TYPE POD CURVE
 FOR $\alpha_0 = 8.0$ AND $\beta_0 = 4.13$ mm

No. of Holes	a_{NDE} (mm)	P_G	P_I	P_{II}	P_{II}^* (P_{II}/P_G)
1	5	99.33%	7.00×10^{-6}	1.79%	1.8%
10	5	93.46%	5.63×10^{-5}	15.50%	16.6%
10	4.8	92.07%	3.09×10^{-4}	14.20%	15.4%
10	4.6	90.39%	1.22×10^{-3}	12.6%	13.9%
10	4.4	88.38%	3.71×10^{-3}	10.8%	12.2%

b. Conclusions

The conclusions obtained previously for the totally uncorrelated crack length are summarized as follows: (1) The average number of bad disks is much higher than the average number of bad holes prior to inspection. This is of practical importance because in the Retirement-For-Cause analysis, the distribution of the flaw length at each hole is simulated. (2) Both Type I and Type II errors are more serious than those in the case of totally correlated crack length. (3) Depending on the pre-inspection flaw length in holes or equivalently the length of service life for disks prior to inspection, both Type I and Type II errors may be of concern, if the bandwidth of the POD curve is not narrow enough. (4) When the POD curve is narrow-banded, both Type I and Type II errors may be acceptable, as demonstrated in the last numerical example.

SECTION V

MULTIPLE INSPECTIONS FOR ENGINE DISKS

It was explained in the previous section, that if the bandwidth of the POD curve of the NDE system is not narrow enough, then the Type II error may be of great concern in the RFC system. Should this be the case, a redundant NDE system for a second inspection of rejected disks is highly desirable, as will be demonstrated in this section. Mathematical results for engine disks are presented, in which each hole rejected by the No. 1 NDE system is further inspected by the No. 2 NDE system (intersection rule). Numerical examples are given to illustrate quantitatively the advantage of multiple inspections for engine disks.

To effectively reduce the Type II error, it is assumed that the POD curve of the No. 2 (or redundant) NDE system is narrow-banded, representing the inspection of holes with polishment or replication. Again, two extreme cases will be investigated; totally correlated flaw length and totally uncorrelated flaw length.

1. TOTALLY CORRELATED FLAW LENGTH

When a hole is inspected by two NDE systems with $POD(a;1)$ and $POD(a;2)$, respectively, using the intersection rule, the resulting POD curve for a hole follows from Equation 4 as

$$POD(a;1 \cap 2) = POD(a;1)POD(a;2) \quad (47)$$

The POD curve for a disk consisting of m holes, denoted by $POD(a;Um)$, follows from Equations 27 and 47 as

$$POD(a;Um) = 1 - [1 - POD(a;1)POD(a;2)]^m \quad (48)$$

Hence, the Type I and Type II errors for disks is given by

$$P_I = \int_{a_{NDE}}^{\infty} f(x) [1 - POD(x;1)POD(x;2)]^m dx \quad (49)$$

and

$$P_{II} = \int_0^{a_{NDE}} f(x) \left\{ 1 - [1 - \text{POD}(x;1)\text{POD}(x;2)]^m \right\} dx \quad (50)$$

in which $f(a)$ is the probability density function of the pre-inspection flaw length in holes. The probability, P_G , that a disk is good (or the average percentage of good disks) is given by Equation 28.

2. TOTALLY UNCORRELATED FLAW LENGTH

Both Type I and Type II errors as well as the average percentage of good disks are derived in Equations 38, 39 and 37, respectively, in which $\text{POD}(x;1)$ should be replaced by $\text{POD}(x;1)\text{POD}(x;2)$, i.e.,

$$P_G = [F(a_{NDE})]^m \quad (51)$$

$$P_I = \left\{ \int_0^\infty f(x) [1 - \text{POD}(x;1)\text{POD}(x;2)] dx \right\}^m - \left\{ \int_0^{a_{NDE}} f(x) [1 - \text{POD}(x;1)\text{POD}(x;2)] dx \right\}^m \quad (52)$$

$$P_{II} = P_G - \left\{ \int_0^{a_{NDE}} f(x) [1 - \text{POD}(x;1)\text{POD}(x;2)] dx \right\}^m \quad (53)$$

A flow chart explaining the procedures of two inspections using the intersection rule for disks derived above is given in Figure 23. It should be mentioned that only those holes rejected by the No. 1 NDE system are further inspected by the No. 2 NDE system (Figure 23). Therefore, the probability, P_{R1} , that a hole will be rejected by the No. 1 NDE system is given by

$$P_{R1} = \int_0^\infty f(x) \text{POD}(x;1) dx \quad (54)$$

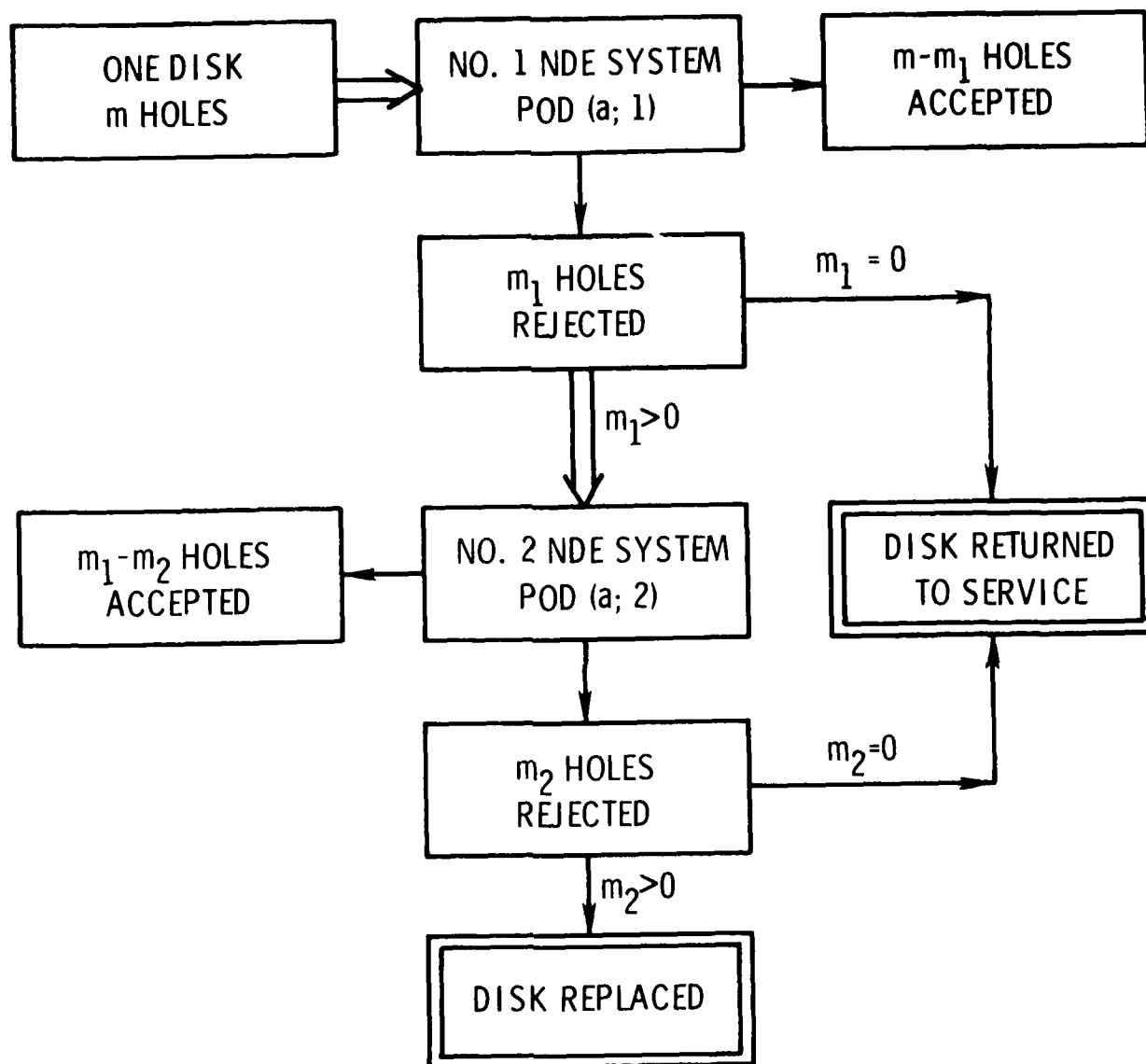


Figure 23. Procedures for Two Inspections for Disks.

Furthermore, P_{R_1} also represents the average percentage of holes to be inspected by the No. 2 NDE system. Indeed, P_{R_1} is an important quantity in determining the cost benefit for two inspections. It is interesting to observe from Equation 54 that the average percentage of holes to be inspected by the No. 2 NDE system is independent of the inspection limit a_{NDE} .

3. NUMERICAL EXAMPLES

As mentioned previously, the redundant system has a high resolution capability, representing the inspection of holes with polishment or replication. Therefore, a narrow-banded Weibull POD curve is considered

$$POD(a;2) = 1 - \exp[-(a/\beta)^\alpha] \quad ; \quad a \geq 0 \quad (55)$$

in which $\alpha=8.0$ and $\beta=4.13$ mm. Such a POD curve was shown in Figure 12 as Curve 1.

The exponential distribution for the pre-inspection flaw length given by Equation 14 is considered,

$$f(a) = \lambda e^{-\lambda a} \quad ; \quad a \geq 0 \quad (56)$$

a. Examples for Totally Correlated Flaw Length

For the case of totally correlated flaw length, we choose $\lambda=0.7/\text{mm}$ in Equation 56. Such a distribution of the pre-inspection flaw length was shown in Figure 16. For the purpose of comparison between the results of single inspection and that of two inspections, the same $POD(a;1)$ shown in Figure 16 is considered, i.e., $POD(a;1) = 1 - \exp(-\beta_1 a)$ with $\beta_1=0.46/\text{mm}$.

The results of Type I error, Type II error and conditional Type II error for disks are presented in Table 13. The corresponding results under a single inspection were shown in Table 6. A comparison between Tables 6 and 13 indicates a drastic reduction for the Type II error resulting from the second inspection, whereas the Type I error remains insignificant. For instance, with the inspection limit $a_{NDE}=4.0$ mm, the

TABLE 13

TYPE I AND TYPE II ERRORS FOR TOTALLY CORRELATED CRACK
 LENGTH USING TWO INSPECTIONS; $\lambda = 0.7/\text{mm}$, $\beta_1 = 0.46/\text{mm}$,
 $\alpha = 8.0$, $\beta = 4.13 \text{ mm}$

No. of Holes	a_{NDE} (mm)	P_G	P_I	P_{II}	P_{II}^*
1*	5	97.00%	1.80×10^{-3}	36.8%	37.9%
1	5	97.00%	1.90×10^{-3}	3.5%	3.6%
10	5	97.00%	6.04×10^{-13}	9.6%	9.9%
10	4.5	95.70%	1.22×10^{-9}	8.3%	8.7%
10	4.0	94.00%	7.45×10^{-6}	6.5%	6.9%
10	3.5	91.37%	1.10×10^{-3}	4.1%	4.5%
10	3.0	87.80%	1.36×10^{-2}	1.7%	1.9%
*One Inspection For One Hole					

Type II error under a single inspection is 80.7%, whereas it is reduced to 6.5% using two inspections. Likewise, the Type I errors for both cases are acceptable.

The average percentage of holes, P_{R_1} , to be inspected by the No. 2 NDE systems is computed from Equation 54 as 40%. Thus, by inspecting 40% of the holes using the No. 2 NDE system, one can reduce the Type II error for disks from 80.7% to 6.5%.

As a second example, the Weibull-type $\text{POD}(a;1)$ function given by Equation 33 with $\alpha_0=3.0$ and $\beta_0=3.79 \text{ mm}$ is considered. Such a POD curve was shown in Figure 17. The results of Type I error, Type II error and conditional Type II error for disks are shown in Table 14.

It is observed from Table 14 that the Type I error is insignificant and the Type II error is acceptable. The corresponding results under a single inspection were given in Table 7. A comparison between Tables 7 and 14 indicates that a significant reduction of Type II error

can be achieved by the second inspection. The average percentage of holes to undergo the second inspection is computed from Equation 54 as 13%. For instance, with the inspection limit $a_{NDE}=4.0$ mm, the Type II error is reduced from 30% (Table 7) to 4.7% (Table 14) by inspecting 13% of holes (on the average) for a second time.

TABLE 14

TYPE I AND TYPE II ERRORS FOR TOTALLY CORRELATED CRACK LENGTH USING TWO INSPECTIONS; $\lambda = 0.7/\text{mm}$, $\alpha_0 = 3.0$, $\beta_0 = 3.79$ mm, $\alpha = 8.0$, $\beta = 4.13$ mm

No. of Holes	a_{NDE} (mm)	P_G	P_I	P_{II}	P_{II}^*
1*	5	97.00%	9.20×10^{-4}	10.30%	10.60%
1	5	97.00%	9.40×10^{-4}	2.87%	2.96%
10	5	97.00%	2.83×10^{-13}	7.82%	8.06%
10	4.5	95.70%	8.38×10^{-9}	6.55%	6.84%
10	4.0	94.00%	3.28×10^{-5}	4.76%	5.06%
10	3.5	91.37%	2.61×10^{-3}	2.47%	2.70%
10	3.0	87.80%	2.16×10^{-2}	0.70%	0.80%
*One Inspection For One Hole.					

b. Examples for Totally Uncorrelated Flaw Length

For the case of totally uncorrelated flaw length, $\lambda=1.0/\text{mm}$ is chosen for Equation 56 to compare the results with those under a single inspection. The distribution of the pre-inspection flaw length was shown in Figure 22 as Curve 1. The same POD curves used in two previous examples, i.e., $\text{POD}(a;1) = 1 - \exp(-\beta_1 a)$ with $\beta_1=0.46/\text{mm}$ and $\text{POD}(a;1) = 1 - \exp[-(a/\beta_0)^{\alpha_0}]$ (Equation 33) with $\alpha_0=3.0$ and $\beta_0=3.79/\text{mm}$ are considered. The results for Type I error, Type II error and conditional Type II error are shown in Table 15. The corresponding results using a single inspection were given in Table 11. A comparison between Tables 11 and 15

demonstrates a significant reduction for the Type II error using a second inspection (Equation 55).

TABLE 15

TYPE I AND TYPE II ERRORS FOR TOTALLY UNCORRELATED CRACK LENGTH USING TWO INSPECTIONS; $\lambda = 1.0$, $\alpha = 8.0$, $\beta = 4.13$ mm

EXPONENTIAL TYPE POD(a;l); $\beta_1 = 0.46/\text{mm}$					
No. of Holes	a_{NDE} (mm)	P_G	P_I	P_{II}	P_{II}^*
1*	5	99.33%	4.60×10^{-4}	30.9%	31.10%
1	5	99.33%	4.62×10^{-4}	1.5%	1.50%
10	5	93.46%	3.80×10^{-3}	13.0%	13.90%
10	4	83.12%	3.30×10^{-2}	5.6%	6.70%
WEIBULL TYPE POD(a;l); $\alpha_0 = 3.0$, $\beta_0 = 3.79$ mm					
1*	5	99.33%	2.60×10^{-4}	6.1%	6.14%
1	5	99.33%	2.68×10^{-4}	1.1%	1.11%
10	5	93.46%	2.20×10^{-3}	10.5%	11.24%
10	4	83.12%	3.80×10^{-2}	3.7%	4.45%
*One Inspection For One Hole.					

4. CONCLUDING REMARKS

When the bandwidth of the POD curve is not narrow enough, the second inspection, using an NDE system having a narrow-banded POD curve, will reduce the Type II error substantially. This conclusion holds for both cases when the flaw length in each hole of the same disk is completely correlated or completely independent. The second inspection may be expensive and time consuming, for instance, the replication of holes. However, the average percentage of holes to undergo the second inspection is reasonably small and therefore the second inspection may be economically beneficial.

Although the flaw length in disk holes and that for the POD curves used in the numerical examples are not close to the situation for gas turbine engine disks, the conclusions and trends obtained for both Type I and Type II errors remain the same. This is because both Type I and Type II errors, as well as the average percentage of good holes prior to inspection, remain identical when the flaw length for POD curves and that in disk holes are reduced by a factor of γ (e.g., $\gamma = 5.0$).

SECTION VI

INSPECTION RELIABILITY OF ENGINE DISKS USING P&W POD CURVE

The numerical examples presented in the previous two sections are intended only to illustrate the effect of various types of POD curves on the inspection reliability as well as the effect of multiple inspections. While the POD curves used are obtained from the literature, they are far from current engine inspection technology, although the trends and conclusions regarding both types of errors will not be altered. Recently, a laboratory POD curve was established by the Pratt and Whitney Aircraft Company, as shown in Figure 24. Such a POD curve may be representative of future inspection technology for RFC inspection systems, and it is used in this section. Therefore, examples are given to demonstrate the magnitude of Type I and Type II errors for engine disks under a single inspection, but using different distribution functions for the pre-inspection flaw length. The application of multiple inspections is not given due to lack of a POD curve for holes with polishment or replication.

The POD curve shown in Figure 24 can be fitted by the three-parameter Weibull distribution very well,

$$\begin{aligned} \text{POD}(a;1) &= 0 && \text{for } a \leq a_0 \\ &= 1 - \exp \left\{ - \left(\frac{a-a_0}{\beta_2} \right)^{\alpha_2} \right\} && \text{for } a > a_0 \end{aligned} \quad (57)$$

in which a_0 is the lower bound below which the crack length can not be detected. The best-fitted parameter values are obtained as follows: $a_0 = 1.4$ mils (10^{-3} inch), $\beta_2 = 4.05$ mils and $\alpha_2 = 2.0$. With this set of parameter values, the plot of Equation 57 cannot be distinguished from the POD curve shown in Figure 24.

The negative exponential distribution for the pre-inspection flaw length given by Equation 14 is employed. Currently, the target for the inspection limit, a_{NDE} , of advanced engine disks is about 5 mils (5×10^{-3} inches). Consequently, the average pre-inspection flaw length is assumed to be $1/\lambda = 1.429$ mils, or $\lambda = 0.7/\text{mil}$, indicating that at the time of

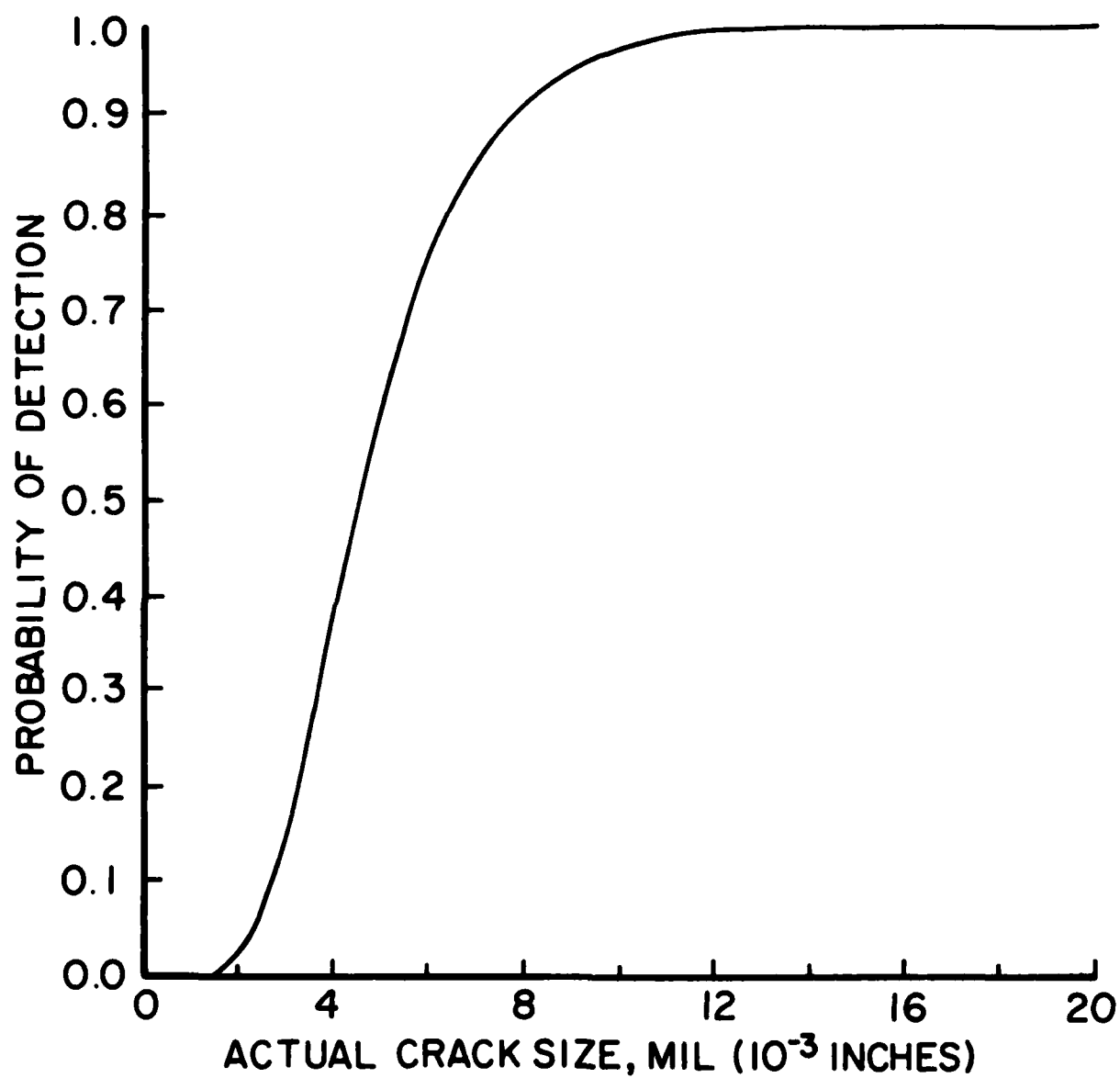


Figure 24. POD Curve for Second Turbine Disk Radial Cooling Hole.

inspection, 3% of holes will have a flaw length longer than 5 mils, i.e., $P_G = 0.97$. The density function $f(a)$ of the pre-inspection flaw length is shown in Figure 25 as Curve 1.

The results of Type I and Type II errors are presented in Table 16, in which "+" represents the case for totally correlated flaw length in each hole of the same disk and "++" denotes the case for totally independent flaw length in each hole. Table 16 indicates similar trends already shown in Tables 6-12, as follows.

(1) For the case of completely correlated flaw length, the Type I error is very small. The Type II error, however, is moderate (e.g., at $a_{NDE} = 5$ mils, $P_{II} = 15.3\%$). This is so because the POD curve has a lower bound at $a_0 = 1.4$ mils where 62.5% of the flaws are shorter than 1.4 mils. The beneficial effect resulting from a POD curve which has a lower bound has been discussed previously.

(2) For the case of totally independent flaw length, the Type I error requires a serious consideration and the Type II error is also higher in the range where $a_{NDE} \geq 5$ mils. For instance, at $a_{NDE} = 5$ mils, we have $P_{II} = 23.4\%$ and $P_{II}^* = 31.8\%$.

Suppose the return to service interval is increased, or the safety factor is reduced, such that at the time of inspection, there are 8.2% of flaws exceeding 5 mils, i.e., $\lambda = 0.5/\text{mil}$ or the average flaw length $= 1/\lambda = 2$ mils. Such a distribution is shown in Figure 25 as Curve 2. The results of Type I and Type II errors are presented in Table 17. For the case of totally correlated flaw length, the Type I error is always small but the Type II error increases over the previous example, as expected, because of more large flaws. For the case of totally independent flaw length, the Type I error requires considerable attention. Although the Type II error at $a_{NDE} = 5$ mils is $P_{II} = 19.4\%$, the conditional Type II error increases to $P_{II}^* = 45.7\%$. This is because we have only 42.5% of good disks at the time of inspection, i.e., $P_G = 42.5\%$.

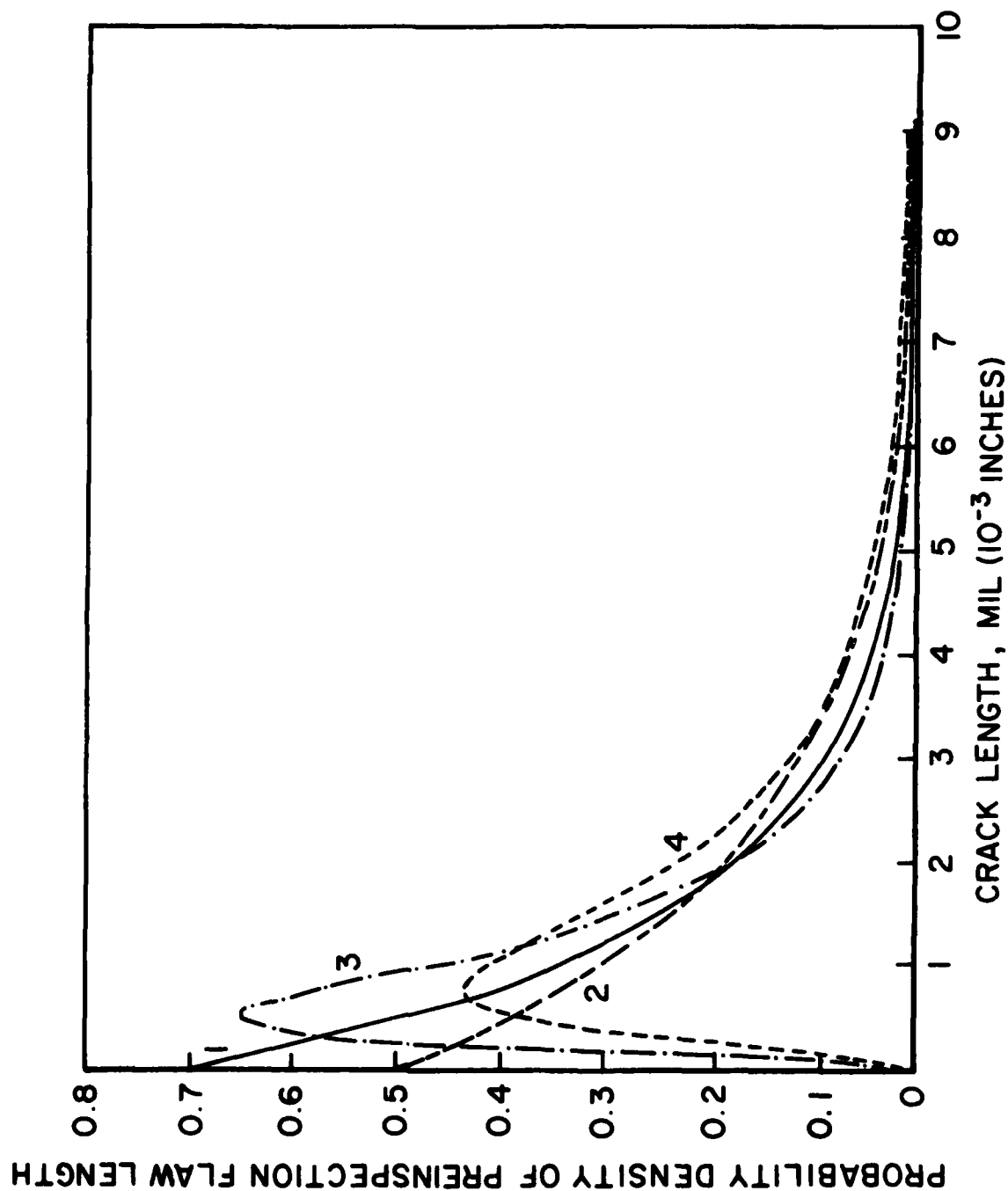


Figure 25. Probability Density Functions of Pre-inspection Flaw Length with 100% Coefficient of Variation.

TABLE 16

TYPE I AND TYPE II ERRORS FOR DISK USING P&W POD CURVE AND AVERAGE FLAW LENGTH 1.429 mils ($\lambda=0.71/\text{mil}$); EXPONENTIAL DISTRIBUTION FOR PRE-INSPECTION FLAW LENGTH, + TOTALLY CORRELATED FLAW LENGTH, ++ TOTALLY INDEPENDENT FLAW LENGTH.

a_{NDE} MIL	NO. OF HOLES	P_G	P_I	P_{II}	P_{II}^*
4	1	93.9%	2.52×10^{-2}	2.3%	2.5%
	10^+	93.9%	1.67×10^{-4}	12.3%	13.1%
	10^{++}	53.4%	1.30×10^{-1}	11.8%	22.1%
5	1	97.0%	7.79×10^{-3}	3.6%	3.7%
	10^+	97.0%	1.47×10^{-6}	15.3%	15.8%
	10^{++}	73.6%	4.35×10^{-2}	23.4%	31.8%
6	1	98.5%	2.15×10^{-3}	4.6%	4.7%
	10^+	98.5%	4.04×10^{-9}	16.9%	17.2%
	10^{++}	86.0%	1.23×10^{-2}	32.7%	38.0%
7	1	99.3%	5.27×10^{-4}	5.2%	5.2%
	10^+	99.3%	3.38×10^{-12}	17.6%	17.7%
	10^{++}	92.8%	3.04×10^{-3}	38.6%	41.6%
8	1	99.6%	1.15×10^{-4}	5.5%	5.5%
	10^+	99.6%	8.53×10^{-16}	17.9%	18.0%
	10^{++}	96.4%	6.67×10^{-4}	41.9%	43.5%
9	1	99.8%	2.24×10^{-5}	5.7%	5.7%
	10^+	99.8%	6.49×10^{-20}	18.2%	18.2%
	10^{++}	98.2%	1.29×10^{-4}	43.7%	44.5%

TABLE 17

TYPE I AND TYPE II ERRORS FOR DISK USING P&W POD CURVE AND AVERAGE FLAW LENGTH 2.0 mils ($\lambda=0.5$ mil); EXPONENTIAL DISTRIBUTION FOR PRE-INSPECTION FLAW LENGTH, + TOTALLY CORRELATED FLAW LENGTH, ++ TOTALLY INDEPENDENT FLAW LENGTH.

a_{NDE} MIL	NO. OF HOLES	P_G	P_I	P_{II}	P_{II}^*
4	1	86.5%	4.79×10^{-2}	3.1%	3.6%
	10^+	86.5%	2.77×10^{-4}	15.8%	18.3%
	10^{++}	23.4%	1.21×10^{-1}	7.2%	20.8%
5	1	91.8%	1.78×10^{-2}	5.4%	5.9%
	10^+	91.8%	2.97×10^{-6}	21.2%	23.0%
	10^{++}	42.5%	5.23×10^{-2}	19.4%	45.7%
6	1	95.0%	5.90×10^{-3}	7.5%	7.9%
	10^+	95.0%	9.87×10^{-9}	24.4%	25.7%
	10^{++}	60.0%	1.84×10^{-2}	33.5%	55.8%
7	1	97.0%	1.75×10^{-3}	9.0%	9.3%
	10^+	97.0%	1.00×10^{-11}	26.3%	27.1%
	10^{++}	73.6%	5.58×10^{-3}	45.8%	62.2%
8	1	98.2%	4.63×10^{-4}	10.1%	10.3%
	10^+	98.2%	3.09×10^{-15}	27.5%	28.0%
	10^{++}	83.1%	1.49×10^{-3}	55.0%	66.2%
9	1	98.9%	1.09×10^{-4}	10.8%	10.9%
	10^+	98.9%	2.86×10^{-19}	28.2%	28.5%
	10^{++}	89.4%	3.50×10^{-4}	61.2%	68.5%

For all cases considered so far, including those of the previous sections, the conditional Type II error P_{II}^* for the case of completely independent flaw length is always higher than that for the case of totally correlated flaw length.

As mentioned previously, the negative exponential distribution for the pre-inspection flaw length given by Equation 14 is a special case of the Weibull distribution in which the coefficient of variation (dispersion) is 100%. It may be interesting to examine the sensitivity of Type I and Type II errors with respect to the variation of the distribution function used for the pre-inspection flaw length. In this connection, the log-normal distribution given by Equation 14(b), is considered. The coefficient of variation, V , of the lognormal distribution is related to σ through

$$V = \left\{ \exp[(\sigma \ln 10)^2] - 1 \right\}^{1/2} \quad (58)$$

To be consistent with the previous examples, V is chosen to be 100%, resulting in $\sigma = 0.3616$. Two cases corresponding to the previous examples, for $\lambda = 0.7/\text{mil}$ and $\lambda = 0.5/\text{mil}$, respectively, are considered: (1) a median flaw length of 1.045 mils (i.e., $\mu = 0.019$), that results in 3% of flaws exceeding $a_{NDE} = 5$ mils, and (2) a median flaw length of 1.57 mils (i.e., $\mu = 0.1963$), that results in 8.2% flaws exceeding $a_{NDE} = 5$ mils. These two lognormal probability density functions are shown in Figure 25 as Curve 3 ($\mu = 0.019$) and Curve 4 ($\mu = 0.1963$), respectively, for comparison.

The results of Type I and Type II errors are presented in Tables 18 and 19, respectively, for $\mu = 0.019$ and $\mu = 0.1963$. A comparison between Tables 16 and 18 as well as Tables 17 and 19 indicates that the difference is very small. This is expected from Figure 24, since the main difference between the exponential and lognormal distributions lies in the small flaw size region, $a < a_0 = 1.4$ mil, in which the NDE system cannot detect any flaw. Consequently, when the number of bad holes is within 8% at the time of inspection, the functional form for the distribution function of the pre-inspection flaw length is not important, as long as the

statistical dispersion is identical and there is a reasonable lower bound for the POD curve.

TABLE 18

TYPE I AND TYPE II ERRORS FOR DISK USING P&W POD CURVE AND MEDIAN FLAW LENGTH 1.045 mils ($\mu=0.019$); LOGNORMAL DISTRIBUTION FOR PRE-INSPECTION FLAW LENGTH, + TOTALLY CORRELATED FLAW LENGTH, ++ TOTALLY INDEPENDENT FLAW LENGTH.

a_{NDE} MIL	NO. OF HOLES	P_G	P_I	P_{II}	P_{II}^*
4	1	94.7%	1.98×10^{-2}	2.0%	2.1%
	10^+	94.7%	1.27×10^{-4}	10.7%	11.3%
	10^{++}	57.7%	1.10×10^{-1}	10.9%	18.9%
5	1	97.0%	6.50×10^{-3}	3.0%	3.1%
	10^+	97.0%	1.15×10^{-6}	13.0%	13.4%
	10^{++}	73.7%	3.86×10^{-2}	19.7%	26.7%
6	1	98.2%	2.01×10^{-3}	3.7%	3.8%
	10^+	98.2%	3.45×10^{-9}	14.2%	14.5%
	10^{++}	83.5%	1.22×10^{-2}	26.8%	32.1%
7	1	98.9%	5.82×10^{-4}	4.3%	4.4%
	10^+	98.9%	3.33×10^{-12}	14.9%	15.1%
	10^{++}	89.3%	3.55×10^{-3}	31.7%	35.5%
8	1	99.3%	1.56×10^{-4}	4.6%	4.6%
	10^+	99.3%	1.02×10^{-15}	15.3%	15.4%
	10^{++}	93.0%	9.53×10^{-4}	35.2%	37.9%
9	1	99.5%	3.84×10^{-5}	4.8%	4.8%
	10^+	99.5%	9.72×10^{-20}	15.5%	15.6%
	10^{++}	95.2%	2.35×10^{-4}	37.4%	39.3%

TABLE 19

TYPE I AND TYPE II ERRORS FOR DISK USING P&W POD CURVE AND MEDIAN FLAW LENGTH 1.57 mils ($\mu=0.1963$); LOGNORMAL DISTRIBUTION FOR PRE-INSPECTION FLAW LENGTH, + TOTALLY CORRELATED FLAW LENGTH, ++ TOTALLY INDEPENDENT FLAW LENGTH.

a_{NDE} MIL	NO. OF HOLES	P_G	P_I	P_{II}	P_{II}^*
4	1	86.9%	4.34×10^{-2}	3.3%	3.8%
	10^+	85.9%	2.57×10^{-4}	17.0%	19.6%
	10^{++}	24.5%	1.11×10^{-1}	7.8%	31.8%
5	1	91.8%	1.59×10^{-2}	5.4%	5.9%
	10^+	91.8%	2.63×10^{-6}	21.9%	23.9%
	10^{++}	42.4%	4.63×10^{-2}	19.2%	45.3%
6	1	94.6%	5.37×10^{-3}	7.2%	7.6%
	10^+	94.6%	8.70×10^{-9}	24.7%	26.1%
	10^{++}	57.5%	1.65×10^{-2}	31.3%	54.4%
7	1	96.4%	1.68×10^{-3}	8.5%	8.8%
	10^+	96.4%	9.16×10^{-12}	26.4%	27.4%
	10^{++}	69.0%	5.26×10^{-3}	41.7%	60.4%
8	1	97.5%	4.82×10^{-4}	9.5%	9.7%
	10^+	97.5%	3.02×10^{-15}	27.5%	28.2%
	10^{++}	77.4%	1.52×10^{-3}	49.7%	64.2%
9	1	98.2%	1.26×10^{-4}	10.2%	10.4%
	10^+	98.2%	3.08×10^{-19}	28.3%	28.8%
	10^{++}	83.3%	3.99×10^{-4}	55.5%	66.6%

Instead of assuming a 100% coefficient of variation (dispersion) for the pre-inspection flaw length, a 50% coefficient of variation is considered in conjunction with the lognormal distribution given by Equation 14(b). The parameter σ is then computed from Equation 58 with $V = 50\%$ as 0.2052, i.e., $\sigma = 0.2052$. For the purpose of comparison with the previous example, the same percentage of flaws smaller than $a_{NDE}=5$ mils at the time of inspection is considered, i.e., $P_G = 97\%$. Then μ is calculated from Eq. 14(b) as 0.3133, indicating that the median flaw length is $(10)^{0.3133} = 2.06$ mils. Such a lognormal probability density function for the pre-inspection flaw length is displayed in Figure 26.

A comparison between Curve 3 of Figure 25 and Figure 26 shows that when the statistical dispersion of the pre-inspection flaw length is reduced, the peak of the density function is shifted to the right-hand side (large crack size region) in order to maintain the same percentage of good holes. As a result, it is expected that the Type II error will increase.

The Type I and Type II errors, the percentage of good disks, and the conditional Type II error are shown in Table 20. A comparison between Tables 18 and 20 indicates that the Type II error increases substantially for the inspection limit $a_{NDE} \geq 4$ mils. For instance, with $a_{NDE}=5$ mils, the Type I error is almost the same whereas the Type II error increases from the range of 13.0% - 19.7% (Table 18) to the range of 33.5% - 40.3% (Table 20). The Type II error becomes more serious when the statistical dispersion of the flaw length prior to inspection is smaller.

Consequently, it is concluded that even with the advanced inspection technology currently available, the Type II error may be of practical concern, depending on the location of the central portion of the pre-inspection flaw length.

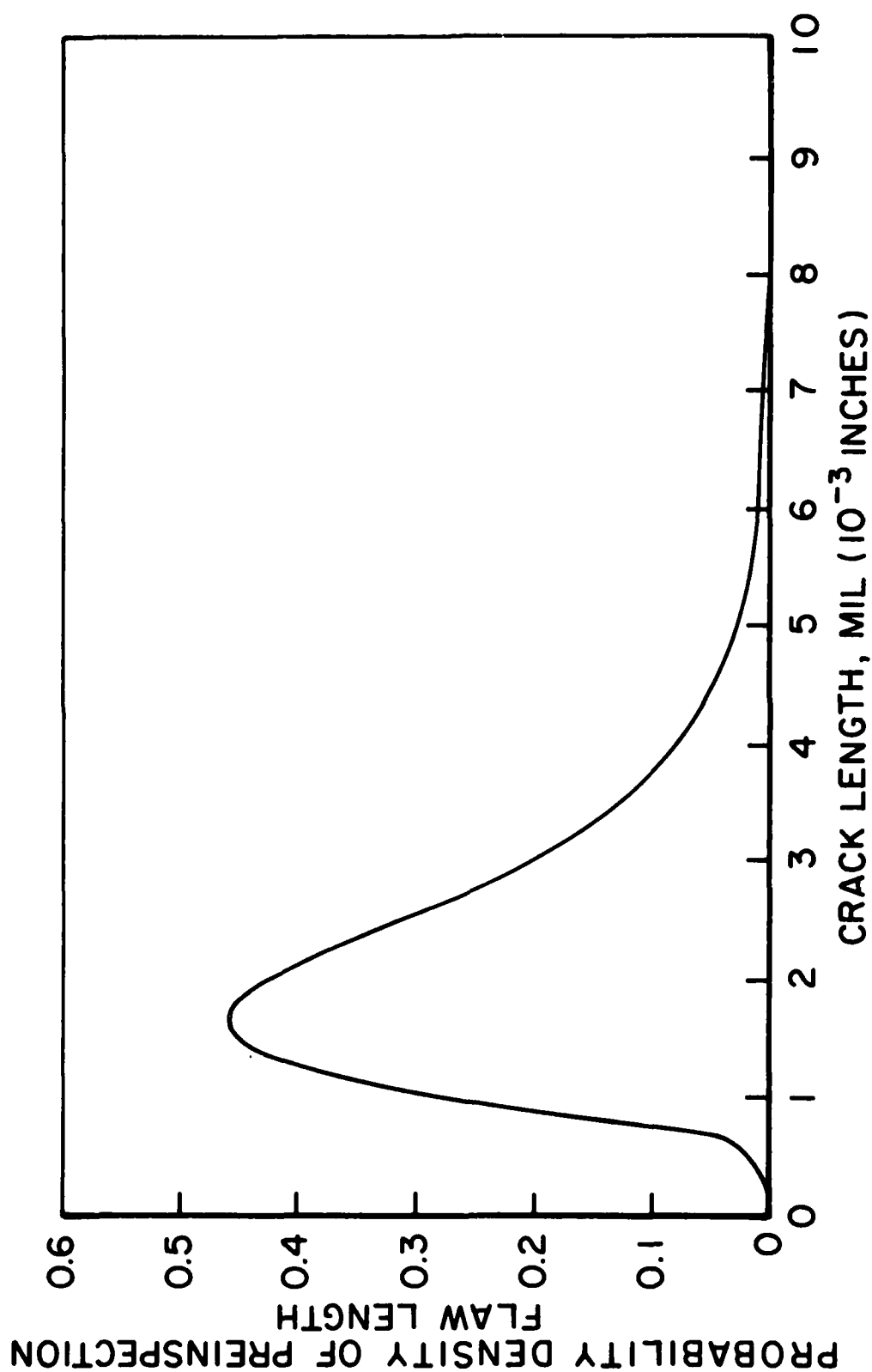


Figure 26. Lognormal Probability Density Function for Pre-inspection Flaw Length with 50% Coefficient of Variation.

TABLE 20

TYPE I AND TYPE II ERRORS FOR DISKS USING P&W POD CURVE AND MEDIAN FLAW LENGTH 2.06 mils ($\mu=0.3133$); LOGNORMAL DISTRIBUTION FOR PRE-INSPECTION FLAW LENGTH WITH 50% DISPERSION, + TOTALLY CORRELATED FLAW LENGTH, ++ TOTALLY INDEPENDENT FLAW LENGTH.

a _{NDE} MIL	NO. OF HOLES	P _G	P _I	P _{II}	P _{II} [*]
4	1	92.0%	3.83×10^{-2}	5.20%	5.65%
	10 ⁺	92.0%	2.87×10^{-4}	28.60%	31.10%
	10 ⁺⁺	43.2%	1.27×10^{-1}	19.00%	44.00%
5	1	97.0%	8.77×10^{-3}	7.36%	7.59%
	10 ⁺	97.0%	1.91×10^{-6}	33.50%	34.50%
	10 ⁺⁺	73.7%	3.42×10^{-2}	40.30%	54.70%
6	1	98.8%	1.89×10^{-3}	8.51%	8.61%
	10 ⁺	98.8%	4.00×10^{-9}	35.30%	35.70%
	10 ⁺⁺	88.8%	7.62×10^{-3}	52.70%	59.30%
7	1	99.5%	3.74×10^{-4}	9.06%	9.11%
	10 ⁺	99.5%	2.64×10^{-12}	36.00%	36.20%
	10 ⁺⁺	95.3%	1.52×10^{-3}	58.60%	61.50%
8	1	99.8%	6.86×10^{-5}	9.30%	9.32%
	10 ⁺	99.8%	5.48×10^{-16}	36.30%	36.40%
	10 ⁺⁺	98.0%	2.80×10^{-4}	61.20%	62.40%
9	1	99.9%	1.16×10^{-5}	9.41%	9.42%
	10 ⁺	99.9%	3.56×10^{-20}	36.40%	36.40%
	10 ⁺⁺	99.1%	4.73×10^{-5}	62.20%	62.80%

SECTION VII

CONCLUSIONS AND DISCUSSION

An exploratory study has been made of the possible application of multiple inspection procedures and its potential pay-offs. The solutions are obtained for both independent NDE systems and dependent NDE systems. The resulting POD curve under multiple inspections is derived quantitatively from the POD curves of individual NDE systems when the union rule, the intersection rule and the combination thereof are used. Thus, researchers and practicing engineers can play with different combinations of NDE systems and procedures to arrive at an optimum strategy for their particular purpose.

Numerical examples are given using available POD curves from certain NDE systems to illustrate the basic idea and the application of multiple inspection strategy. It is shown that multiple inspections using the union rule alone, in general, reduce Type I error but increase Type II error, and the effect is reversed if the intersection rule is employed alone. It is further shown that both Type I and Type II errors can be simultaneously reduced significantly by the combined use of union and intersection rules. However, caution should be exercised in selecting the third NDE system (or POD curve) to minimize possible adverse effects. The sequence of inspections to minimize the inspection cost has also been discussed.

The multiple inspection procedures presented include multiple inspections using the same NDE system or the identical redundant NDE system as a special case, in which the second or subsequent inspections are performed under different inspection environments. In particular, the same NDE system (or the identical redundant NDE system) may be used for the second inspection of the rejected holes of gas turbine engine disks, with those holes being polished or replicated.

An exploratory study has been made for the inspection reliability of engine disks containing many holes. Because of mathematical simplicity, two extreme cases for the correlation between the flaw length in each hole of the same disk have been studied in Sections IV-V: (1) Totally

correlated flaw length and (2) Totally independent flaw length. For the case of totally correlated flaw length, the Type I error is insignificant whereas the Type II error may be serious and therefore of practical concern, if the bandwidth of the POD curve of the NDE system is not narrow enough. For the case of totally independent flaw length, not only the Type I error warrants special attention, but also the Type II error is worse than that for the case of totally correlated flaw length.

In reality, however, the exact solutions for Type I and Type II errors lie between these two extreme cases. Nevertheless, from the NDE standpoint, the present results for these two extreme cases provide important information for a greater insight into the influence of the NDE inspection system on RFC/NDE results. One of the important and significant conclusions obtained from the present study is that for the RFC system, the bandwidth of the mean POD curve of the NDE system is the most important controlling factor rather than a single value of the flaw length associated with a 90% detection probability and 95% confidence level.

The bandwidth of the POD curve, fortunately, can be reduced to a desirable level by multiple inspection procedures usually using two inspections with the intersection rule; thus significantly reducing the Type II error. As a result, for the RFC/NDE system in which both Type I and Type II errors are of practical importance, redundant NDE systems for performing a second inspection of the rejected holes by polishment or replication may be worthwhile to consider.

The present investigation allows for a quantitative description of the inspection reliability of engine disks in terms of Type I and Type II errors. The mathematical solutions obtained herein provide tools for NDE engineers to manipulate various POD curves and the inspection limits a_{NDE} in order to achieve the most beneficial RFC inspection procedures for engine disks. Although the range of the crack length and POD curves used in the numerical examples of Sections IV and V are not realistic for gas turbine engine disks, the trends and conclusions obtained will not be altered, as explained in those sections.

For the damage tolerant analysis in which the structural safety is of primary concern, the inspection limit a_{NDE} has been specified to be the crack length corresponding to a 90% detection probability and 95% confidence level. As a result, many of the POD curves appearing in the literature are associated with a 95% confidence level. It should be emphasized, however, that in the Retirement-For-Cause analysis, the life cycle cost (LCC) is the objective function to be minimized, and hence both Type I and Type II errors are of practical importance. Consequently, the POD curve used in the RFC analysis should be the mean POD curve, i.e., the POD curve associated with a 50% confidence level. If a POD curve with a 95% confidence level is used, the estimation of the Type I error will be too conservative, whereas the Type II error estimate will be overly unconservative. The trend will be reversed if a POD curve with a low level of confidence is employed.

It has been shown previously that the distribution of the pre-inspection flaw length has a significant effect on both Type I and Type II errors. An obvious example is that the Type I error will be zero if all the flaw lengths prior to inspections are smaller than the inspection limit a_{NDE} . In fact, the distribution of the pre-inspection flaw length is a function of service time (i.e., time dependent), and owing to crack propagation it is shifting continuously to the large crack size region (e.g., to the right-hand side of Figure 11) as the service time increases. The numerical results shown in this report may represent the situation for the first few inspection maintenances in service. Both Type I and Type II errors will increase rapidly as the central portion of the distribution of the pre-inspection flaw length (i.e., a majority of the flaw lengths) is shifted into the large flaw size region close to a_{NDE} , at a later service time. Unfortunately, such a situation is unavoidable, because the philosophy of the RFC system is to exhaust the fatigue life of every individual component. Thus, during the inspection maintenance at a later service time, both Type I and Type II errors will be much higher (or more serious) than those examples presented herein. As a result, multiple inspection procedures proposed may be even more beneficial as the service time increases. Further study is needed in this regard.

While the Type I error is directly related to the safety and reliability of engine disks in service, the structural reliability can be alleviated or safeguarded by a safety factor incorporated in the return to service interval. Therefore, there is a remedy available for the Type I error. However, if the bandwidth of the POD curve is not narrow enough, the only alternative to cope with the Type II error, that rejects good disks during the inspection maintenance, appears to be the multiple inspection procedures, in particular when a fleet of disks is in service for a long time.

The inspection reliability of gas turbine engine disks using advanced eddy-current laboratory inspection technology (recently reported by Pratt & Whitney Aircraft) has been investigated. Such an inspection system is capable of detecting a 5 mils (5×10^{-3} inches) flaw with a 55% probability and its POD curve is assumed to have a lower bound at 1.4 mils below which no flaw can be detected. The results for the Type II error may be of practical concern, depending on the location of the central portion of the distribution of the flaw length prior to inspection. When the Type II error is not acceptable, the multiple inspection procedures proposed herein should be considered.

APPENDIX A

MULTIPLE INSPECTIONS WITH CORRELATED NDE SYSTEMS

Let R_j be the event that the crack length, a , is rejected (detected) by the j th NDE system. Then, we have $POD(a;j) = P[R_j]$.

(1) Intersection Rule: The probability of detecting the crack length, a , by both No. 1 and No. 2 NDE systems is given by

$$\begin{aligned} POD(a;1\cap 2) &= P[R_1 \cap R_2] = P[R_1]P[R_2|R_1] \\ &= POD(a;1)POD(a;2|1) \end{aligned} \quad (A-1)$$

in which $POD(a;2|1)$ = conditional probability that the crack length, a , is detected by the No. 2 NDE system under the condition that it has been detected by the No. 1 NDE system. The experiments to be performed to establish such a conditional POD curve is described in Appendix B.

If both NDE systems are statistically independent, then $POD(a;2|1) = POD(a;2)$ and Equation A-1 reduces to Equation 4, i.e.,

$$POD(a;1\cap 2) = POD(a;1)POD(a;2) \quad (A-2)$$

In a similar fashion, the resulting POD curve for m dependent NDE systems can be derived, except that there will involve more conditional POD functions.

(2) Union Rule: The probability of detecting the crack length, a , by either the No. 1 NDE system or the No. 2 NDE system, or both, is given by

$$\begin{aligned} POD(a;1\cup 2) &= P[R_1 \cup R_2] = P[R_1] + P[R_2] - P[R_1 \cap R_2] \\ &= P[R_1] + P[R_2] - P[R_1]P[R_2|R_1] \end{aligned}$$

or

$$POD(a;1\cup 2) = POD(a;1) + POD(a;2) - POD(a;1)POD(a;2|1) \quad (A-3)$$

where $POD(a;2|1)$ has been described before.

If both NDE systems are statistically independent, we have $POD(a;2|1) = POD(a;2)$ and Equation A-3 reduces to Equation 2,

$$POD(a;1 \cup 2) = POD(a;1) + POD(a;2) - POD(a;1)POD(a;2) \quad (A-4)$$

Similar procedures can be applied to m correlated NDE systems.

(3) Combination Rule: The POD curve resulting from the application of three inspections with union-intersection rule shown in Figure 7 can be expressed as

$$\begin{aligned} POD[a;(1 \cup 2) \cap 3] &= P[(R_1 \cup R_2) \cap R_3] = P[R_3]P[R_1 \cup R_2 | R_3] \\ &= P[R_3]\{P[R_1 | R_3] + P[R_2 | R_3] - P[R_1 \cap R_2 | R_3]\} \\ &= P[R_3]\{P[R_1 | R_3] + P[R_2 | R_3] - P[R_1 | R_3]P[R_2 | R_1 \cap R_3]\} \end{aligned}$$

or

$$\begin{aligned} POD[a;(1 \cup 2) \cap 3] &= POD(a;3)\{POD(a;1|3) + POD(a;2|3) \\ &\quad - POD(a;1|3)POD[a;2|(1 \cap 3)]\} \end{aligned} \quad (A-5)$$

in which $POD(a;1|3)$ = conditional probability that the crack length, a , is detected by the No. 1 NDE system under the condition that it has been detected by the No. 3 NDE system, and $POD[a;2|(1 \cap 3)]$ = conditional probability that the crack length, a , is detected by the No. 2 NDE system under the condition that it has been detected by both No. 1 and No. 3 NDE systems.

Usually the No. 3 NDE system is required to have a high resolution capability. If the No. 3 NDE system is statistically independent of No. 2 and No. 1 NDE systems, then Equation A-5 is simplified as

$$\begin{aligned} POD[a;(1 \cup 2) \cap 3] &= POD(a;3)\{POD(a;1) + POD(a;2) \\ &\quad - POD(a;1)POD(a;2|1)\} \end{aligned} \quad (A-6)$$

in which $POD(a;2|1)$ has been explained before.

If both No. 1 and No. 2 NDE systems are also statistically independent, then Equation A-6 reduces to Equation 7 as follows

$$\begin{aligned} \text{POD}[a;(1U2)\Omega 3] &= \text{POD}(a;3)\{\text{POD}(a;1) + \text{POD}(a;2) \\ &\quad - \text{POD}(a;1)\text{POD}(a;2)\} \end{aligned} \quad (\text{A-7})$$

APPENDIX B

EXPERIMENTAL PROCEDURES FOR ESTABLISHING CONDITIONAL POD CURVE

The conditional probability of detection $POD(a;2|1)$ by the No. 2 NDE system under the condition that the crack has been detected by the No. 1 NDE system can be established by the following procedures. (1) N specimens with the same crack length are manufactured and inspected by the No. 1 NDE system. (2) After inspection, N_1 specimens are rejected (or detected) and $N - N_1$ specimens are accepted (not detected). (3) Only the N_1 specimens rejected by the No. 1 NDE system are further inspected by the No. 2 NDE system; with N_2 specimens being rejected and $N_1 - N_2$ specimens being accepted by the No. 2 NDE system. (4) The conditional probability, $POD(a;2|1)$, is the ratio of N_2 to N_1 as $N \rightarrow \infty$, i.e., $POD(a;2|1) = \lim_{N \rightarrow \infty} (N_2/N_1)$. (5) Procedures (1) through (4) are repeated for different crack length. A flow chart is shown schematically in Figure 27.

The procedure described above is straightforward but may be tedious. It is expected that more efficient procedures can be established in a further research.

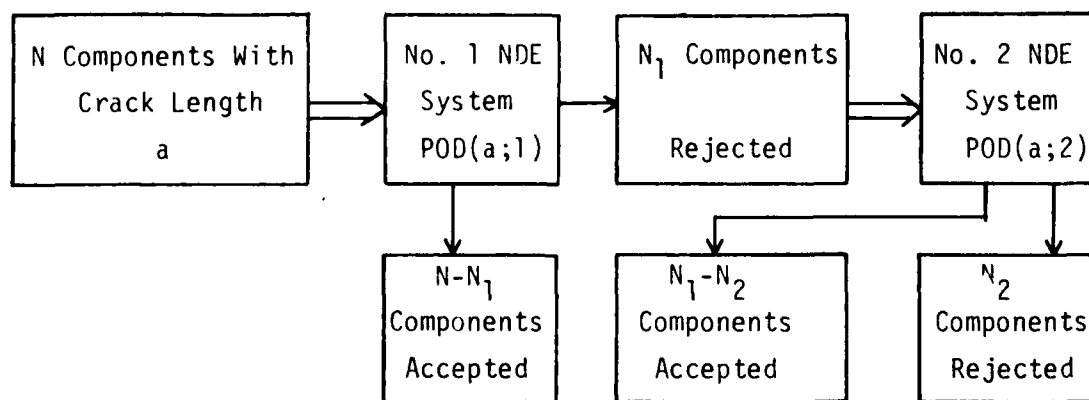


Figure 27. Procedures for Establishing Conditional POD Curve.

REFERENCES

1. P. F. Packman, S. J. Klima, R. L. Davies, J. Malpani, J. Moyzis, W. Walker, B. G. W. Yee, and D. P. Johnson, "Reliability of Flaw Detection by Nondestructive Inspection," ASM Metal Handbook, Vol. 11, 8th Edition, Metals Park, Ohio, pp. 214-224, 1976.
2. B. G. W. Yee, F. H. Chang, J. C. Coughman, G. H. Lemon, and P. F. Packman, "Assessment of NDE Reliability Data," NASA CR-134991, National Aeronautics and Space Administration, Lewis Research Center, Cleveland, Ohio, 1976.
3. W. H. Lewis, B. D. Dodd, W. H. Sproat, and J. M. Hamilton, "Reliability of Nondestructive Inspections - Final Report," Report No. SA-ALC/MEE 76-6-38-1, United States Air Force, San Antonio Air Logistics Center, Kelly Air Force Base, Texas, 1978.
4. "Aircraft Structural Integrity Program, Airplane Requirements," Military Standard MIL-STD-1530A, 1975.
5. "Airplane Damage Tolerance Requirements," Military Specifications MIL-A-83444, 1974.
6. R. J. Hill, W. H. Reimann, and J. S. Ogg, A Retirement-For-Cause Study of an Engine Turbine Disk, AFWAL-TR-81-2094, Nov. 1981.
7. C. G. Annis, Jr., M. C. Van Wanderham, J. A. Harris, Jr., and D. L. Sims, "Gas Turbine Engine Disk Retirement for Cause: An Application of Fracture Mechanics and NDE," Journal of Engineering for Power, ASME, Vol. 103, No. 1, 1981.
8. A. P. Berens and P. W. Hovey, Evaluation of NDE Reliability Characterization, AFWAL TR-81-4160, Air Force Wright Aeronautical Laboratories, Wright-Patterson Air Force Base, Ohio, Nov. 1981.

FWA